TRIPLE QUANTUM IMAGING OF SODIUM IN INHOMOGENEOUS FIELDS

by

Costin Tanase

BS, University of Bucharest, 1996

Submitted to the Graduate Faculty of

Arts and Sciences in partial fulfillment

of the requirements for the degree of

Doctor of Philosophy

University of Pittsburgh

2004

UNIVERSITY OF PITTSBURGH

FACULTY OF ARTS AND SCIENCES

This dissertation was presented

by

Costin Tanase

It was defended on

11/23/2004

and approved by

Dr. Robert Coalson - Committee member

Dr. Hrvoje Petek - Committee member

Dr. Frank Tabakin - Committee member

Dr. Fernando Boada - Committee co-chairperson

Dr. Irving Lowe - Committee chairperson

TRIPLE QUANTUM IMAGING OF SODIUM IN INHOMOGENEOUS FIELDS

Costin Tanase, PhD

University of Pittsburgh, 2004

Triple quantum filtered sodium MRI techniques have been recently demonstrated *in vivo*. These techniques have been previously advocated as a means to separate the sodium NMR signal from different physiological compartments based on the differences between their relaxation rates. Among the different triple quantum coherence transfer filters, the three-pulse coherence transfer filter has been demonstrated to be better suited for human imaging than the traditional four-pulse implementation. While the three-pulse structure has distinct advantages in terms of the radiofrequency power efficiency, it is characterized, also, by an increased dependence on the main magnetic field inhomogeneities. In this thesis, we characterize these dependences and introduce a method for their compensation through the acquisition of a field map and the use of a modified phase cycling scheme.

We analyze the dynamics of spin 3/2 systems using the density matrix theory of relaxation. We show that by using the superoperator formalism, we can obtain an algebraic formulation of the density matrix's evolution, in which the contributions from relaxation and radio frequency application are factored out. To achieve this goal, we derive an exact form for the propagator of the density matrix, in the presence of both static quadrupolar couplings and magnetic field inhomogeneities.

Using the algebraic formulation, we derive exact expressions for the behavior of the density matrix in the classical one-, two- and three-pulse NMR experiments. These theoretical

formulas are then used to illustrate the bias introduced on the measured relaxation parameters by the presence of large spatial variations in the B_0 and B_1 fields. This approach is proved useful for the characterization of the spatial variations of the signal intensity in multiple quantum-filtered sodium MRI experiments.

On the imaging applications side, we demonstrate that the conventional on-the-fly triple quantum filtered schemes are affected by the presence of B_0 inhomogeneities in a severe way, which can be described as destructive interference among several coherence pathways. A new class of robust filtering schemes is introduced to avoid the destructive interference. The usefulness of the introduced technique is experimentally illustrated for twisted projection imaging, for human brain imaging.

TABLE OF CONTENTS

LIST OF FIGURES

PREFACE

The finalization of this work benefited greatly from the environments offered by the Physics Department and by the Magnetic Resonance Research Center.

I express my gratitude to the Committee Members Dr. Robert Coalson, Dr. Hrvoje Petek, Dr. Frank Tabakin, Dr. Fernando Boada, and Dr. Irving Lowe for their guidance through the process of graduation. I am especial grateful to Dr. Fernando Boada for his patience while helping me to make the transition from Theoretical to Applied Physics and to Dr. Irving Lowe for offering me the honor of being his student.

Special thanks are addressed to my parents, Aurelia and Pascu Tanase, for their continuous support through this entire journey.

1. INTRODUCTION

Nuclear Magnetic Resonance techniques and Magnetic Resonance Imaging (MRI) in particular, have made significant contributions to the understanding of living systems during the last 50 years. Since the discovery of the NMR phenomena by Felix Bloch and Edward Purcell in 1946, the applications of NMR for the investigation of living systems have flourished. The introduction of the Zeugmatography approach for spatial encoding by Paul Lautenberg, [1], in the 1970's accelerated this pace of discovery and led to the development of MRI and its many applications. Today, MRI is a well-established clinical tool that can provide exquisite images of the soft tissue anatomy in short imaging times.

Extensions of MRI for the study of metabolism and function, however, have progressed at a slower pace than their more anatomical counterparts. This is due in part to the additional demands that such extensions place on the data acquisition and processing methodologies. One such application, with very high potential, was the use of the sodium nucleus for the study of disease conditions in humans. Sodium is one of the most important ions in cell physiology. For example, in the brain, cells maintain a 10-fold trans-membrane sodium gradient as part of the basal physiological function. This gradient is severely disrupted during many pathologies leading to large (>50%) changes in the sodium content of tissues.

The development of sodium MRI techniques has had many challenges that stem from the lower tissue concentration and unfavorable relaxation of this nucleus. Recent developments, however, have provided practical means to address such challenges leading to a renewed interest in the sodium MRI in humans. One of the most desirable features of any sodium MRI technique

would be the ability to sensitize the MRI signal intensity to the changes in sodium content in the intracellular space. The use of triple quantum (TQ) filtered NMR techniques is well suited for the task because of their non-invasive nature and ease of implementation. Indeed, the first demonstrations of the feasibility of such studies in humans have already been published in the literature, and reports have already been presented documenting their use for the study of pathologies such as brain ischemia and cancer.

Characterization and optimization of the TQ signal could therefore enhance the use of these techniques for the study of disease in humans. The TQ signal has a strong dependence on physical quantities that are beyond the control of the operator. Specifically, B_1 and B_0 inhomogeneities could introduce significant variations in the TQ sodium MRI signal that must be corrected for if any quantitative information is to be derived from the studies.

In this thesis, we focus on the optimization of the TQ signal when B_0 inhomogeneities are present. We address this problem by first introducing an algebraic approach for the description of the spin 3/2 dynamics that allows for a more straightforward study of the experiments. Using this formalism, we then illustrate the nature of the signal loss that is introduced by B_0 inhomogeneities and then present a method for their mitigation. This same approach is also used to shed some light into the common pitfalls associated with the experimental measurement of relaxation properties for spin 3/2 systems. The work is also complemented with a related analysis in which these findings are used to provide effective means for the optimization of experimental acquisition parameters such as the preparation time and the readout time.

This thesis is organized to follow the steps involved in the accomplishment of its objectives, as outlined above**.** In Chapter 2, the Liouville representation of quantum mechanics

(QM) is introduced. By using the spherically irreducible tensor operators (SIT) as a basis, the superspace is explicitly constructed as a linear, sixteen dimensional, space. The Liouville superoperators are constructed for each of the relevant interaction, with external magnetic field B_0, with static electric field gradients, and with the applied external radiofrequency field (RF). The evolution of the system under the action of RF, ignoring relaxation effects, is solved. The superoperator describing the system's evolution in this regime is explicitly constructed.

In Chapter 3, the theoretical description of relaxation is constructed in a complete superspace formulation, illustrating the advantages of the superspace formalism. The theory is applied for the relaxation of spin 3/2 particles experiencing quadrupolar fluctuations. The limit of the Redfield theory and the calculation of the relaxation matrix are explicitly offered. The chapter ends with the algebraic calculation of the propagator describing the evolution of spin 3/2 particles when experiencing static magnetic interaction, static quadrupolar interaction, and quadrupolar fluctuations.

In Chapter 4, the core of the theoretical work is presented. It consists of the full construction of the algebraic description for NMR experiments, based on the superspace formalism. The aim of the chapter is to offer algorithms for physical MR signal calculations of a broad range of experiments. The descriptive objective of this thesis is accomplished here, by offering algebraic means for constructing the NMR signal in multiple quantum filtered experiments. Arbitrary B_0, B_1, and static quadrupolar interactions are allowed. The classical one-, two-, and three-pulse experiments are theoretically analyzed and the predictions are verified on both phantom and in-vitro experiments. It is presented the construction of a variety of TQ classes of experiments, in which various combinations of coherence pathways are selected. The phase cycles are predicted and verified experimentally. The theoretical description of the TQ based

determination of T_2 relaxation times is presented. Those methods are proved useful for the measurement of relaxation times *in vivo*.

Chapter 5 offers an introduction to imaging concepts and a simple description of MRI experiments. The four steps process consisting of signal generation, gradient based encoding, signal acquisition, and image reconstruction is described in terms of linear equations. The usefulness of this approach is illustrated for the optimization of SNR in respect with the readout time.

The predictive objective is accomplished in Chapter 6, where the design and the NMR experimental verification of the novel scheme for TQ imaging, insensitive to B_0 inhomogeneities are presented. A TQ imaging protocol is developed. It includes determination of the sample characteristics (based on the TQ NMR experiments), determination of the B_0 distribution (based on field map measurement), and a series of four TQ imaging experiments. Based on this procedure, a final TQ image is obtained, in which the effects of B_0 inhomogeneity are removed. The protocol is demonstrated on an agar gel phantom. The last section of this chapter presents the TQ images acquired on a normal human volunteer with the developed procedure.

The first Appendix presents the linear algebra of the Kronecker product (extensively used in the thesis). The second Appendix presents the formulation of spin 1/2 dynamics in superspace formalism. In this context, the supervector associated with the density matrix is the magnetization vector, while the evolution equations reduce to the standard Bloch equations.

2. SUPERSPACE DESCRIPTION OF 3/2 SPIN SYSTEMS

The construction of the Liouvillian model used for the description of spin 3/2 dynamics is the main objective of this chapter. In Section 2.1, a quantum mechanics introduction for spin 3/2 system is offered. In Section 2.2, the Liouville representation of quantum mechanics (QM) is introduced. In Section 2.3, the spherically irreducible tensor operators (SIT) basis is defined. The procedures for explicitly constructing the supervectors and superoperators, as well as the consequences of axial symmetry are presented. In Section 2.4, the Liouville superoperators describing the interaction with the external magnetic field (B_0) and with the static electric field gradients are offered. In Section 2.5, the evolution of the system under the action of an external radiofrequency (RF) field is described in the approximation of infinitely short duration as a pure rotation operator in superspace. The off-resonance RF pulse is analyzed, and an approximate formula, taking in consideration the effect of finite width, is offered.

2.1. Quantum mechanics of isolated 3/2 spin system

In order to fix notations and conventions we present basic facts about the standard formulation of Quantum Mechanics (QM), the Schroedinger formulation. In the Schroedinger formulation, the states are represented by norm one vectors in a suitable Hilbert space. Taking advantage of the fact that the spin 3/2 systems are described in finite dimensional Hilbert space, the presentation emphasizes the linear algebraic aspect of this formulation. In this way the details of the presentation of the Liouville formulation is made easier. We choose the system of units in

which h/2π=1; in this system of units, the energy and angular frequency have the same units, radians per second.

The quantum mechanical (QM) description of isolated 3/2 spins is constructed in the Hilbert space, H, associated with the j=3/2 irreducible representation of the rotation group. In this space, of dimension N=4, the natural basis is the angular momentum basis, |jm>, with j=3/2. Using this basis, by expressing an arbitrary vector ('ket') as the linear combination

$$|\psi\rangle = \sum_{m=-3/2}^{3/2} \psi_m \, | \, jm\rangle \, , \tag{2.1}$$

the vectors are identified with the four dimensional columns

$$|\psi\rangle = \begin{bmatrix} \psi_{+3/2} \\ \psi_{+1/2} \\ \psi_{-1/2} \\ \psi_{-3/2} \end{bmatrix} . \tag{2.2}$$

The hermitic conjugate, the 'bra', is identified with the four dimensional row obtained by transposition and complex conjugation of the 'ket':

$$\langle\psi| = \left(|\psi\rangle\right)^{\dagger} \quad \langle\psi| = \begin{bmatrix} \psi^*_{3/2} & \psi^*_{1/2} & \psi^*_{-1/2} & \psi^*_{-3/2} \end{bmatrix} . \tag{2.3}$$

All through this thesis, the identifications of vectors with columns and the identification of their hermitic conjugates with rows is systematically made. The set of column vectors representing the angular momentum basis in H is explicitly given by

$$\left|\frac{3}{2}\frac{3}{2}\right\rangle = \begin{pmatrix} 1 \\ 0 \\ 0 \\ 0 \end{pmatrix} = |e_1\rangle, \left|\frac{3}{2}\frac{1}{2}\right\rangle = \begin{pmatrix} 0 \\ 1 \\ 0 \\ 0 \end{pmatrix} = |e_2\rangle, \left|\frac{3}{2}\frac{-1}{2}\right\rangle = \begin{pmatrix} 0 \\ 0 \\ 1 \\ 0 \end{pmatrix} = |e_3\rangle, \left|\frac{3}{2}\frac{-3}{2}\right\rangle = \begin{pmatrix} 0 \\ 0 \\ 0 \\ 1 \end{pmatrix} = |e_4\rangle \tag{2.4}$$

or, in a compact form, $|jm\rangle = |e_{j-m+1}\rangle$.

Consistent with the general principle of QM, the states are identified with 'rays' in Hilbert space, specifying a direction. In order to avoid both ambiguities and occurrences of normalization factors across the formulas, all the vectors describing QM states in this thesis are considered normalized to one

$$\langle \psi \,|\, \psi \rangle = 1 \,. \tag{2.5}$$

The j=3/2 representation of the rotation group is specified in terms of the angular momentum operators. This representation is defined by

$$\begin{aligned} \vec{J}^2 \,|\, jm\rangle &= j\left(j+1\right) |\, jm\rangle \\ J_z \,|\, jm\rangle &= m \,|\, jm\rangle \end{aligned} \,. \tag{2.6}$$

By using the outer product between a bra with a ket, defined as the matrix

$$A = |\, a\rangle\langle b \,| \quad \Rightarrow \quad \left(A\right)_{ij} = a_i^* b_j \,, \tag{2.7}$$

the angular momentum related operators are constructed as four dimensional matrices

$$\begin{aligned} J_z &= \sum_{m=-j}^{j} m \,|\, jm\rangle\langle\, jm \,| \quad \vec{J}^2 = j\left(j+1\right)\mathbf{1}_{2j+1} \\ J^{\pm} &= \sum_{m=-j}^{j} \sqrt{j\left(j+1\right) - m\left(m \pm 1\right)} \,|\, j, m \pm 1\rangle\langle\, jm \,| \\ J_x &= \frac{1}{2}\left(J^+ + J^-\right) \quad J_y = \frac{1}{2i}\left(J^+ - J^-\right) \end{aligned} \tag{2.8}$$

Schroedinger equation describing the time evolution of the vector of state is the four-dimensional linear equation with given initial condition

$$\begin{cases} \dfrac{d}{dt} |\, \psi\left(t\right)\rangle = -iH\left(t\right) |\, \psi\left(t\right)\rangle \\ |\, \psi\left(t = t_0\right)\rangle = |\, \psi\left(t_0\right)\rangle \end{cases} \,. \tag{2.9}$$

The construction can be obtained, for arbitrary initial conditions by making use of the forward propagator, defined by the matrix equation

$$\begin{cases} \dfrac{d}{dt}U(t,t_0) = -iH(t)U(t,t_0) \\ U(t_0,t_0) = 1_H \end{cases}, \tag{2.10}$$

giving the solution of the original Schroedinger equation by

$$|\psi(t)\rangle = U(t,t_0)\,|\psi(t_0)\rangle \tag{2.11}$$

In the case in which the Hamiltonian is time-independent, the forward propagator is the matrix exponential,

$$U(t,t_0) = \exp\left(-i(t-t_0)H\right). \tag{2.12}$$

The physical measurement performed on the system described in the state ψ returns the average value

$$\langle A\rangle = \langle\psi(t)|\,A\,|\psi(t)\rangle = \langle\psi(t_0)|\,U^{\dagger}(t,t_0)\,AU(t,t_0)\,|\psi(t_0)\rangle \tag{2.13}$$

The last equality allows the definition of the Heisenberg representation of the operator, with respect to H, as the time dependent operator $A^H(t)$ given by

$$A^H(t) = U^{\dagger}(t,t_0)\,AU(t,t_0). \tag{2.14}$$

With a given state, we can associate the projector along the one-dimensional subspace spanned by that vector, as the operator

$$P_\psi = |\psi\rangle\langle\psi|, \quad P_\psi^2 = P_\psi \tag{2.15}$$

The measurement of a physical observable Q, for the system in the given state, returns the average value, expressible both as a matrix element and a trace

$$Q_\psi = \langle\psi\,|\,Q\,|\,\psi\rangle = \mathrm{Tr}\left(P_\psi Q\right) \tag{2.16}$$

For one single particle, the description through a state vector is sufficient. For a system of many particles, the quantum state described by a single vector, pure state, is a special particular case

(in which all particles evolve in a totally correlated way). In the situation of a many body system the states that admit a description in terms of a single vector requires a careful preparation, which for complex systems is an unrealistic task.

A general state, in which a partial knowledge of the system is assumed, is a mixed state, and it s described as a superposition of pure states with statistical weights w_i in such a way that the measurement of an observable, Q, is given by the statistical average

$$\langle Q \rangle = \sum_i w_i Q_i = \sum_i w_i \langle \psi_i \,|\, Q \,|\, \psi_i \rangle, \quad \text{where } \sum_i w_i = 1. \tag{2.17}$$

For this (mixed) state, there exist no single vector to describe it; the analog of (2.16) is obtained by constructing the density matrix, that is the hermitic matrix,

$$\begin{gathered} \rho = \sum_i w_i \,|\, \psi_i \rangle\langle \psi_i \,| = \sum_i w_i P_i \\ \rho^\dagger = \rho \end{gathered} \tag{2.18}$$

In a given basis, $|\alpha_i>$, the diagonal elements of the density matrix, $<\alpha_i|\rho|\alpha_i>$, are called the "populations" while the non-diagonal elements are the "coherences" associated with the given basis. This distinction is basis-dependent, what is coherence in a given basis could be population in a different basis.

The knowledge of the density matrix, gives the expectation values of an experiment measuring the observable Q as the trace:

$$\langle Q \rangle = \mathrm{Tr}\left(\rho^\dagger Q\right). \tag{2.19}$$

We just note that the density matrix is a projector if and only if the state is a pure state. The evolution equation for the density matrix is obtained from (2.9) as

$$i\frac{d}{dt}\rho = i\frac{\partial}{\partial t}\rho + \left[H, \rho\right] \tag{2.20}$$

In the case of a stationary statistics (in which the weights associated with the possible individual states, are time independent), we obtain the Liouville- von Neuman equation in the form

$$i\frac{d}{dt}\rho = [H, \rho] \tag{2.21}$$

Using the Schroedinger equation propagator, the time evolution of the density matrix is obtained in the form

$$\rho(t) = U(t, t_0)\rho(t_0)U^{\dagger}(t, t_0). \tag{2.22}$$

2.2. Superspace representation of quantum mechanics

The Liouville representation of quantum mechanics is introduced in order to treat both types of states in a common fashion. In this representation, one starts by describing all the states (pure or mixed) as self-adjoint, positive-defined operators with unit trace [2].

Due to the finite dimensionality of H, both the state space and the observable space (the space of bounded operators acting on H) can be embedded in the linear space of N×N matrices. Following, [3], this N^2 dimensional space is called superspace (or Liouville space) and is denoted S. The elements of S are also referred as supervectors.

In superspace, the double "ket" $|O\rangle\rangle$ and double "bra" $\langle\langle O|$ denote the N^2 dimensional vectors describing the operator O and its hermitic conjugate $O^{\dagger}$, respectively. The explicit construction of supervectors reduces to a one-dimensional labeling of the matrix elements associated with an operator. In this thesis, the consequent choice is made to consider the associated vector as the 'column stacking' of the matrix, while the double "bra" obtained by aligning the rows of the hermitic conjugate, [4]. The properties of those operations are offered in Appendix A. An arbitrary NxN matrix, an NxN set of complex numbers, could be considered as well either as a row of columns, or as a column of rows

$$A=\begin{pmatrix} A_{11} & \cdots & A_{1N} \\ \vdots & & \\ A_{N1} & \cdots & A_{NN} \end{pmatrix}=\left(\mathrm{col}\left(A,1\right),\cdots,\mathrm{col}\left(A,N\right)\right)=\begin{pmatrix} \mathrm{row}\left(A,1\right) \\ \vdots \\ \mathrm{row}\left(A,N\right) \end{pmatrix}, \tag{2.23}$$

The associated supervector and its hermitic conjugate are defined by

$$|A\rangle\rangle=\mathrm{cvec}\left(A\right)=\begin{pmatrix} \mathrm{col}\left(A,1\right) \\ \vdots \\ \mathrm{col}\left(A,N\right) \end{pmatrix} \quad \langle\langle A|=\left(\mathrm{cvec}\left(A\right)\right)^{\dagger}=\left(\mathrm{row}\left(A^{\dagger},1\right),\cdots,\mathrm{row}\left(A^{\dagger},N\right)\right). \tag{2.24}$$

The Liouville space becomes a unitary space when it is equipped with the natural inner product [3]

$$\langle\langle A|B\rangle\rangle\equiv\mathrm{Tr}\left\{A^{\dagger}B\right\}. \tag{2.25}$$

Using the construction presented in (2.24) it becomes obvious that the natural inner product in the space of matrices, when expressed in terms of scalar products of rows and columns,

$$\mathrm{Tr}\left\{A^{\dagger}B\right\}=\sum_{k=1}^{N}\mathrm{row}\left(A^{\dagger},k\right).\mathrm{col}\left(B,k\right) \tag{2.26}$$

is also expressible as the natural scalar product in superspace

$$\sum_{k=1}^{N}\mathrm{row}\left(A^{\dagger},k\right).\mathrm{col}\left(B,k\right)=\left(\mathrm{row}\left(A^{\dagger},1\right),\cdots,\mathrm{row}\left(A^{\dagger},N\right)\right).\begin{pmatrix} \mathrm{col}\left(B,1\right) \\ \vdots \\ \mathrm{col}\left(B,N\right) \end{pmatrix}=\mathrm{cvec}\left(A\right)^{\dagger}.\mathrm{cvec}\left(B\right), \tag{2.27}$$

which is consistent with (2.25).

The linear operators acting on S are called superoperators and to distinguish them, the convention to use bold face letters for the superoperators is followed in this thesis. The simplest examples of superoperators are defined by the left and right multiplication [5]

$$\begin{aligned} \mathbf{A}^{L}\,|\,B\rangle\rangle&\equiv|\,AB\rangle\rangle \\ \mathbf{A}^{R}\,|\,B\rangle\rangle&\equiv|\,AB\rangle\rangle \end{aligned} \tag{2.28}$$

They satisfy obvious properties

$$\mathbf{A}^L\mathbf{B}^R\,|\,C\rangle\rangle = |\,ACB\rangle\rangle = \mathbf{B}^R\mathbf{A}^L\,|\,C\rangle\rangle \quad \Rightarrow \quad \left[\mathbf{A}^L,\mathbf{B}^R\right]=0$$
$$f\left(\mathbf{A}^L\right)|\,B\rangle\rangle = |\,f\left(A\right)B\rangle\rangle \tag{2.29}$$
$$f\left(\mathbf{A}^R\right)|\,B\rangle\rangle = |\,Bf\left(A\right)\rangle\rangle$$

A special class of superoperators is defined by the operation of taking the commutator (the derivation with respect to an operator). Consistent with the previous notations, the commutator superoperator associated with O is denoted using the corresponding bold face $\mathbf{O}^-:\mathsf{H}\to\mathsf{H}$, and is acting on arbitrary operators B as the commutator

$$\mathbf{O}^-\,|\,B\rangle\rangle = |\left[O,B\right]\rangle\rangle = |\,OB-BO\rangle\rangle = \left(\mathbf{O}^L-\mathbf{O}^R\right)|\,B\rangle\rangle\,. \tag{2.30}$$

Similarly, the anti-commutator superoperators are defined by their action as anti-commutators, (with the 1/2 factor included in the definition)

$$\mathbf{O}^+\,|\,B\rangle\rangle = |\,\{O,B\}\rangle\rangle = |\,\frac{1}{2}\left(OB+BO\right)\rangle\rangle = \frac{1}{2}\left(\mathbf{O}^L+\mathbf{O}^R\right)|\,B\rangle\rangle \tag{2.31}$$

Due to their importance, by default the unlabeled bold-faced notation denotes the commutator superoperator. For the particular case of the Hamiltonian, the associated commutator superoperator is the Liouvillian, therefore denoted by **L**.

An illustrative example of the usefulness of superspace description is offered by the derivation of the well-known Baker-Hausdorff-Campbell formula. Starting with the previous observation that left and right superoperators commute (2.29) the exponentiation of the commutator superoperator is written as the product of left and right exponentials

$$\exp\left(\mathbf{A}\right)B = \exp\left(\mathbf{A}^L-\mathbf{A}^R\right)B = \exp\left(\mathbf{A}^L\right)\exp\left(-\mathbf{A}^R\right)B \tag{2.32}$$

the last expression, by definition is

$$\exp\left(\mathbf{A}^L\right)\exp\left(-\mathbf{A}^R\right)B = e^A B e^{-A} \tag{2.33}$$

Expanding in series Taylor the original expression, by the definition **A**

$$\exp(\mathbf{A})B = \sum_{k=0}^{\infty} \frac{1}{k!}(\mathbf{A})^k B = \sum_{k=0}^{\infty} \frac{1}{k!}\Big[A,\Big[\ldots\big[A,B\big]\Big]\Big], \tag{2.34}$$

from where, the BHC formula is recognized:

$$\mathrm{e}^{A} B \mathrm{e}^{-A} = \sum_{k=0}^{\infty} \frac{1}{k!}\Big[A,\Big[\ldots\big[A,B\big]\Big]\Big]. \tag{2.35}$$

The simplest basis in superspace is given by the set of direct products of pure states, $|\, jm\rangle\langle\, jn\,|$, denoted using a convenient notation introduced in, [6] $|\, mn^{\dagger}\rangle\rangle$. The decomposition of the identity in H provides the representation of any operator in terms of its matrix elements

$$O = \sum_{m=-j}^{j}\sum_{n=-j}^{j} |\, jm\rangle\langle\, jm\,|\, O\,|\, jn\rangle\langle\, jn\,| = \sum_{m=-j}^{j}\sum_{n=-j}^{j} \langle\, jm\,|\, O\,|\, jn\rangle\big(|\, jm\rangle\langle\, jn\,|\big) \tag{2.36}$$

which is rewritten in superspace language, as the decomposition of the associated supervector

$$|\, O\rangle\rangle = \sum_{n=-j}^{j} \left(\sum_{m=-j}^{j} \langle\, jm\,|\, O\,|\, jn\rangle\,|\, mn^{\dagger}\rangle\rangle \right). \tag{2.37}$$

This last expression offers another representation of the "cvec" operation, when the summation is understood as an ordered one, and it is the starting point of our symbolic algebraic calculations. By convention, the hermitic conjugate of an operator

$$O^{\dagger} = \sum_{n=-j}^{j}\sum_{m=-j}^{j} \big(\langle\, jm\,|\, O\,|\, jn\rangle\big)^{*} \big(|\, jm\rangle\langle\, jn\,|\big)^{\dagger} \tag{2.38}$$

corresponds to the "bra" in superspace, therefore

$$\langle\langle O\,| \equiv \sum_{m,n=-j}^{j} \langle\langle mn^{\dagger}\,| \big(\langle\, jm\,|\, O\,|\, jn\rangle\big)^{*} . \tag{2.39}$$

This formula re-express the fact that the "bra" is the Liouville space hermitic conjugate of the corresponding "ket". The natural inner product is consistent with the "bra"-"ket" convention

$$\langle\langle mn^{\dagger}\,|\, O\rangle\rangle = \langle\, jn\,|\, O\,|\, jm\rangle \quad \text{and} \quad \langle\langle O\,|\, mn^{\dagger}\rangle\rangle = \big(\langle\, jm\,|\, O\,|\, jn\rangle\big)^{*} . \tag{2.40}$$

2.3. Spherically irreducible tensor operators as natural basis in superspace

From a group theoretical point of view, the superspace is associated with the direct product of two j=3/2 representations of the rotation group. The product reduces to a direct sum of representations labeled with principal quantum numbers l=0,1,2,3. Therefore, the quantum mechanical operators can be expanded in terms of the normalized spherical irreducible tensor (SIT) operators T_{lm}, l=0,1,2,3,m=-l,…,l. [2, 7]

They satisfy the commutation relations with the angular momentum,

$$\begin{aligned} \left[J_z, T_{lk}\right] &= kT_{lk} \\ \left[J^{\pm}, \hat{T}_{lk}\right] &= \sqrt{l(l+1)-k(k\pm 1)}\, T_{l,k\pm 1} \end{aligned}, \tag{2.41}$$

the normalization condition,

$$\mathrm{Tr}\left\{T_{pq}^{\dagger} T_{lk}\right\} = \delta_{pl}\delta_{qk} \tag{2.42}$$

and the hermitic conjugation property

$$T_{lk}^{\dagger} = (-)^{l} T_{l,-k}\,. \tag{2.43}$$

In the superspace notations, using the notations $|lm\rangle\rangle \equiv |T_{lm}\rangle\rangle$ $\langle\langle lm| \equiv \langle\langle T_{lm}^{\dagger}|$, (no confusion with $|mn^{\dagger}\rangle\rangle$ is possible), the SIT's satisfy

$$\begin{aligned} \mathbf{J}_Z\,|lm\rangle\rangle &= m\,|lm\rangle\rangle \\ \langle\langle lm\,|\,\lambda\mu\rangle\rangle &= \delta_{l\lambda}\delta_{m\mu} \\ \sum_{l=0}^{3}\sum_{m=-l}^{l} |lm\rangle\rangle\langle\langle lm| &= \mathbf{1}_{16} \end{aligned}\quad . \tag{2.44}$$

Using the 3j Wigner coefficients, $\begin{pmatrix} j & k & l \\ m & n & p \end{pmatrix}$, the SIT's can be written explicitly in terms of the direct product of basis for H, [8], therefore expressible as a linear combination of 16-dimensional vectors $|mn^{\dagger}\rangle\rangle$.

$$
\begin{aligned}
|kq\rangle\rangle &= \sum_{|m|<j,|m+q|<j} (-1)^{j-(m+q)} \sqrt{2k+1} \begin{pmatrix} k & j & j \\ q & m & -(m+q) \end{pmatrix} |j, m+q\rangle\langle jm| \\
|kq\rangle\rangle &= \sum_{|m|<j,|m+q|<j} (-1)^{j-(m+q)} \sqrt{2k+1} \begin{pmatrix} k & j & j \\ q & m & -(m+q) \end{pmatrix} |m(m+q)^{\dagger}\rangle\rangle
\end{aligned}
\quad . \tag{2.45}
$$

From the Jacobi identity,

$$
\big[A,\big[B,C\big]\big]+\big[B,\big[C,A\big]\big]+\big[C,\big[A,B\big]\big]=0 \tag{2.46}
$$

the fact that the associated superoperator of a commutator is the commutator of the corresponding superoperators is obtained,

$$
\big[\mathbf{A},\mathbf{B}\big]|C\rangle\rangle=\big[A,\big[B,C\big]\big]-\big[B,\big[A,C\big]\big]=\big[\big[A,B\big],C\big]. \tag{2.47}
$$

As a consequence, the SIT superoperators satisfy with the angular momentum superoperators, the same commutation relations as their operator counterparts

$$
\begin{aligned}
\big[\mathbf{J}_Z,\mathbf{T}_{lm}\big] &= m\mathbf{T}_{l,k} \\
\big[\mathbf{J}^{\pm},\mathbf{T}_{lm}\big] &= \sqrt{l(l+1)-m(m\pm1)}\,\mathbf{T}_{l,m\pm1}.
\end{aligned} \tag{2.48}
$$

The structure constants are directly related with the superoperator matrix elements,

$$
\big[T_{lm},T_{\lambda\mu}\big]=\mathbf{T}_{lm}\,|\,\lambda\mu\rangle\rangle=\sum T_{k,m+\mu}\langle\langle k,m+\mu\,|\,\mathbf{T}_{lm}\,|\,\lambda\mu\rangle\rangle \tag{2.49}
$$

and they are shared with their superoperators counterparts,

$$
\big[\mathbf{T}_{lm},\mathbf{T}_{\lambda\mu}\big]=\sum \mathbf{T}_{k,m+\mu}\langle\langle k,m+\mu\,|\,\mathbf{T}_{lm}\,|\,\lambda\mu\rangle\rangle\,. \tag{2.50}
$$

Explicitly, the SIT associated superoperators are then given by the sum

$$
\mathbf{T}_{lm}=\sum_{k=1}^{3}\sum_{q=-k}^{k}\sum_{k'=|m+q|}^{3}(-)^{2j-m-q}\,\Delta(l,k,k')\begin{pmatrix} l & k & k' \\ m & q & -m-q \end{pmatrix}|k',m+q\rangle\rangle\langle\langle kq| \tag{2.51}
$$

where the modified 9j Wigner symbol has been introduced for the sake of simplicity:

$$
\Delta(l,k,k')=\Big[(-)^{l+k+k'}-1\Big]\sqrt{(2l+1)(2k+1)(2k'+1)}\begin{Bmatrix} l & k & k' \\ j & j & j \end{Bmatrix} \tag{2.52}
$$

The |lm>> basis is found more convenient than the original, direct product, basis. The decomposition of general operators and superoperators in terms of SIT's can be written:

$$|B(t)\rangle\rangle = \sum_{l,m} |lm\rangle\rangle\langle\langle lm|B(t)\rangle\rangle,\ \mathbf{B} = \sum_{\lambda,\mu}\sum_{l,m} |lm\rangle\rangle\langle\langle lm|\mathbf{B}|\lambda\mu\rangle\rangle\langle\langle\lambda\mu|, \tag{2.53}$$

with the coefficients being related with the traces:

$$\begin{aligned}\langle\langle lm|B\rangle\rangle &= \mathrm{Tr}\left\{T_{lm}^{\dagger}B\right\}\\ \langle\langle lm|\mathbf{B}|\lambda\mu\rangle\rangle &= \mathrm{Tr}\left\{T_{lm}^{\dagger}\left[B,T_{\lambda\mu}\right]\right\}\end{aligned}. \tag{2.54}$$

The last two relations are the starting point in computer implementation of the superspace algebraic constructions.

The axial symmetry, translated in the commutation of a given superoperator with the superoperator $\mathbf{J}_Z$, has important implications for the matrix elements of the superoperator, and it is used extensively in this thesis

$$\langle\langle lm|\left[\mathbf{B},\mathbf{J}_Z\right]|\lambda\mu\rangle\rangle = 0 \Rightarrow \langle\langle lm|\mathbf{B}|\lambda\mu\rangle\rangle = \delta_{m\mu}\langle\langle lm|\mathbf{B}|\lambda m\rangle\rangle\,. \tag{2.55}$$

From here, the general representation of a superoperator (2.53) is simplified; in terms of its reduced matrix elements $B_{l\lambda}^{m} \equiv \langle\langle lm|\mathbf{B}|\lambda m\rangle\rangle$ it reads

$$\mathbf{B} = \sum_{m=-3}^{3}\sum_{l=|m|}^{3}\sum_{\lambda=|m|}^{3} |lm\rangle\rangle B_{l\lambda}^{m}\langle\langle\lambda m|\,. \tag{2.56}$$

Grouping the terms with the same magnetic quantum number

$$\mathbf{B} = |00\rangle\rangle B_{00}^{0}\langle\langle 00| + \sum_{l=1}^{3}\sum_{\lambda=1}^{3}|l0\rangle\rangle B_{l\lambda}^{0}\langle\langle\lambda 0| + \sum_{m=1}^{3}\sum_{l=m}^{3}\sum_{\lambda=m}^{3}\left(|lm\rangle\rangle B_{l\lambda}^{m}\langle\langle\lambda m| + |l,-m\rangle\rangle B_{l\lambda}^{-m}\langle\langle\lambda,-m|\right) \tag{2.57}$$

one notes that any superoperator, commuting with the Z component of the angular momentum superoperator, has a block diagonal structure in the SIT basis.

$$\mathbf{B} = \text{blockdiag}\left(\left(B_{00}^{0}\right)\ \mathbf{B}^{(0)}\ \ \mathbf{B}^{(1)}\ \ \mathbf{B}^{(2)}\ \ \mathbf{B}^{(3)}\ \ \mathbf{B}^{(-1)}\ \ \mathbf{B}^{(-2)}\ \ \mathbf{B}^{(-3)}\right) \tag{2.58}$$

with the individual blocks having the structure,

$$\begin{aligned}
&\mathbf{B}^{(0)} = \begin{pmatrix} B_{11}^{0} & B_{12}^{0} & B_{13}^{0} \\ B_{21}^{0} & B_{22}^{0} & B_{23}^{0} \\ B_{31}^{0} & B_{32}^{0} & B_{33}^{0} \end{pmatrix}\ \mathbf{B}^{(1)} = \begin{pmatrix} B_{11}^{1} & B_{12}^{1} & B_{13}^{1} \\ B_{21}^{1} & B_{22}^{1} & B_{23}^{1} \\ B_{31}^{1} & B_{32}^{1} & B_{33}^{1} \end{pmatrix}\ \mathbf{B}^{(-1)} = \begin{pmatrix} B_{11}^{-1} & B_{12}^{-1} & B_{13}^{-1} \\ B_{21}^{-1} & B_{22}^{-1} & B_{23}^{-1} \\ B_{31}^{-1} & B_{32}^{-1} & B_{33}^{-1} \end{pmatrix} \\
&\mathbf{B}^{(2)} = \begin{pmatrix} B_{22}^{2} & B_{23}^{2} \\ B_{32}^{2} & B_{33}^{2} \end{pmatrix}\ \mathbf{B}^{(-2)} = \begin{pmatrix} B_{22}^{-2} & B_{23}^{-2} \\ B_{32}^{-2} & B_{33}^{-2} \end{pmatrix}\ \mathbf{B}^{(3)} = \left(B_{33}^{3}\right)\ \mathbf{B}^{(-3)} = \left(B_{33}^{-3}\right)
\end{aligned} \tag{2.59}$$

The component l=m=0 is purposely separated from the larger m=0 subspace because the non-trivial dynamics take place in the fifteen dimensional space spanned by operators with non-vanishing principal quantum number, l≠0. Therefore, from now on, all references to the j=3/2 superspace are restricted to this fifteen dimensional space. The blocks corresponding to a given magnetic number m have dimensions d(m)=4-|m| for nonzero m and d(m)=3, for m=0.

The block decomposition is explicitly revealed if one defines the matrices $\mathbf{e}_m$ which have as columns the SIT supervectors characterized by the given magnetic number m, ordered in the ascending order of principal quantum number l,

$$\begin{aligned}
&\mathbf{e}_m = \left\{|\,|m|, m\rangle\rangle, |\,|m|+1, m\rangle\rangle \cdots, |\,3, m\rangle\rangle\right\} \text{ if } m \neq 0 \\
&\mathbf{e}_0 = \left\{|\,10\rangle\rangle, |\,20\rangle\rangle, |\,30\rangle\rangle\right\}
\end{aligned} . \tag{2.60}$$

In terms of the individual blocks, the decomposition expressed by (2.58) is rewritten

$$\mathbf{B} = \sum_{m=-3}^{3} \mathbf{e}_m \mathbf{B}^{(m)} \mathbf{e}_m^T . \tag{2.61}$$

Based on the multiplication properties of the introduced e_m matrices,

$$\mathbf{e}_m^T \mathbf{e}_m = \mathbf{1}_{d(m)\times d(m)} \quad \mathbf{e}_m^T \mathbf{e}_n = \mathbf{0}_{d(m)\times d(n)} \tag{2.62}$$

the computation of a function of a superoperator B is reduced to a direct sum of functions of lower dimensional matrices

$$f\left(\mathbf{B}\right)=\sum_{m=-3}^{3}\mathbf{e}_m f\left(\mathbf{B}^{(m)}\right)\mathbf{e}_m^T . \tag{2.63}$$

Further simplifications can be obtained if one considers the properties of the parity superoperator. Using the properties of the SIT's under inversion, the matrix elements of the parity superoperator, denoted **Π**, are simply given by: [9]

$$\langle\langle l,-m\,|\,\mathbf{\Pi}\,|\,lm\rangle\rangle=\left(-\right)^{l}. \tag{2.64}$$

If an operator B commutes with the pair **Π**, $\mathbf{J}_Z$ further simplifications in the matrix element's structure in (2.55) occur:

$$\left[\mathbf{\Pi},\mathbf{B}\right]=0\Rightarrow\mathbf{\Pi B\Pi}=\mathbf{B}\Rightarrow\langle\langle l,-m\,|\,\mathbf{B}\,|\,\lambda,-m\rangle\rangle=\left(-\right)^{l+\lambda}\langle\langle lm\,|\,\mathbf{B}\,|\,\lambda m\rangle\rangle . \tag{2.65}$$

While the reduction to lower dimensions is rigorously expressed by equations (2.61) and (2.63), the notations are inconvenient for algebraic manipulation. Therefore, a simpler notation namely,

$$\mathrm{e}_m\,\mathbf{B}^{(m)}\equiv\mathbf{e}_m\mathbf{B}^{(m)}\mathbf{e}_m^T . \tag{2.66}$$

is used in this thesis.

2.4. Static interactions

The general density matrix associated with a spin 3/2 particle can be expanded as a finite sum

$$|\,\rho\rangle\rangle=\sum_{l=1}^{3}\sum_{m=-l}^{l}\rho^{(lm)}\,|\,lm\rangle\rangle \tag{2.67}$$

The most general interaction that such a system could experience is given by a Hamiltonian with similar decomposition

$$|\,H\rangle\rangle=\sum_{l=1}^{3}\sum_{m=-l}^{l}H^{(lm)}\,|\,lm\rangle\rangle \tag{2.68}$$

The coefficients in the previous expansion characterize the external, applied fields. A simultaneous rotation of both the system and the environment should leave unchanged the total

energy of the system. In other words, the quantity $\langle\langle \rho \,|\, H \rangle\rangle$ is invariant (it transforms as a scalar under arbitrary rotations).

The interaction with a time independent, uniform, magnetic field is described by the coupling of two pseudo-vectors

$$-\gamma \vec{J}\vec{B}_0 \tag{2.69}$$

Choosing the quantization Z-axis along the direction of the magnetic field, the Hamiltonian becomes

$$H_0 = -\gamma B_0 J_z = -\gamma B_0 T_{10} \tag{2.70}$$

The eigenstates are given by the angular momentum basis (2.6) while the eigenvalues, exhibit the equidistant pattern

$$E_m^0 = -\left(\gamma B_0\right) m = -\omega_0 m \tag{2.71}$$

The evolution of a pure state is governed by the Schroedinger equation

$$i\frac{d}{dt}|\psi\rangle = \left(-\gamma B_0 J_z\right)|\psi\rangle \tag{2.72}$$

with the solution given by the rotation around the Oz axis, in the negative direction, with Larmor frequency $\omega_0=\gamma B_0$

$$|\psi(t)\rangle = \exp\left(i\left(\gamma B_0 t\right) J_z\right)|\psi(0)\rangle = \exp\left(i\omega_0 t\, J_z\right)|\psi(0)\rangle \tag{2.73}$$

It is the simple rotation nature of the solution that makes the transformation to rotating frame useful. The transformation to a frame rotating with an angular frequency ω in respect with the fixed frame of reference is the time dependent rotation

$$R(\omega t) = \exp\left(-i\omega t J_z\right) \tag{2.74}$$

such that, at any moment of time

$$|\psi^R(t)\rangle = R(\omega t)|\psi(t)\rangle = \exp\left(-i(\omega-\omega_0)t\,J_z\right)|\psi(0)\rangle \tag{2.75}$$

Obviously, whenever the rotation frequency matches the Larmor frequency, the evolution in rotating frame is trivial; the state is unmodified. In the class of applications analyzed here, there is no a priori knowledge about the exact value of the static magnetic field, but there is very accurate information about the frequency of the applied radio-frequency field. In the end, it is the RF field that governs the rotating frame frequency; therefore, an off-resonance parameter is naturally introduced by

$$\delta = \omega - \omega_0 . \tag{2.76}$$

In the rotating frame, the free precession is described by a slow rotation (the off-resonance parameter is of the order of magnitude of hundred of Hz, while the Larmor frequency is in the MHz range)

$$|\psi^R(t)\rangle = \exp\left(-i\delta t\,J_z\right)|\psi(0)\rangle \tag{2.77}$$

The Liouvillian associated with this interaction is obtained by simple substitution of operators with superoperators in (2.70)

$$\mathbf{L}_0 = -\gamma B_0 \mathbf{J}_z = -\omega_0 \mathbf{T}_{10} \tag{2.78}$$

The solution of the Liouville equation

$$\frac{d}{dt}|\rho\rangle\rangle = -i\mathbf{L}_0\,|\rho\rangle\rangle \tag{2.79}$$

is obtained as the matrix exponential

$$|\rho(t)\rangle\rangle = \exp\left(i\omega_0 t\,\mathbf{J}_z\right)|\rho(0)\rangle\rangle \tag{2.80}$$

The principal characteristic of sodium ions, the presence of a non-vanishing quadrupolar moment, made their dynamics sensitive to the external gradients of electric fields. Classically, the energy of quadrupolar interaction of a localized charge distribution, q, in the presence of

external electric field characterized by the potential Φ, is defined using the Taylor expansion of the external potential [10]

$$W_{\text{class}} \approx \Phi(0)\int d^3\vec{r}\,q(\vec{r}) + \sum_{i=1}^{3} E_i(0)\int d^3\vec{r}\; x_i q(\vec{r}) + \frac{1}{2!}\sum_{i,j=1}^{3}\left.\frac{\partial E_i}{\partial x_j}\right|_{\vec{r}=0}\int d^3\vec{r}\left(x_i x_j - \frac{\vec{r}^{\,2}}{3}\right)q(\vec{r}) \quad (2.81)$$

In the previous expression, the terms represent the electrostatic energy contributions associated with the total charge, electric dipole interaction and, the third term, quadrupolar electric interaction.

The quantum mechanical counter part is constructed by noticing that the quadrupolar contribution is a contraction of two spherical tensors, therefore the Hamiltonian has to be a contraction between the second order constructed in SIT basis and a tensor constructed in terms of second derivatives of the external potential. The expression of such tensor is well known, [11]

$$V_0 = \frac{1}{2}V_{zz} \quad V_{\pm 1} = \mp\frac{1}{\sqrt{6}}\left(V_{zx} \pm iV_{zy}\right) \quad V_{\pm 2} = \frac{1}{2}\frac{1}{\sqrt{6}}\left[\left(V_{xx} - V_{yy}\right) \pm 2iV_{xy}\right] \quad (2.82)$$

therefore, the contraction between the second order tensor takes the form

$$H_Q = 6C_Q\sum_{m=-2}^{2}(-)^m V_{-m}T_{2m} \quad (2.83)$$

When the expressions (2.82) are evaluated in the principal system of axes associated with the external field $V_{xy}=V_{yz}=V_{zx}=0$ and the expression of the quadrupolar Hamiltonian reduces to the text book form, [10]

$$\begin{aligned} H_Q &= 6C_Q\left\{V_{zz}T_{20} + \frac{1}{\sqrt{6}}\left(V_{xx} - V_{yy}\right)\left(T_{22} + T_{2-2}\right)\right\} = 6C_Q V_{zz}\left\{T_{20} + \eta\frac{1}{\sqrt{6}}\left(T_{22} + T_{2-2}\right)\right\} \\ &= C_Q V_{zz}\left\{\left(3J_z^2 - \vec{J}^2\right) + \eta\left(J_x^2 - J_y^2\right)\right\} \end{aligned}. \quad (2.84)$$

The asymmetry parameter, η, describes the deviation of the external field from cylindrical symmetry. Whenever the ion interacts with ordered structures (*e.g.* at interfaces) the asymmetry

may occur. When the ion is placed in a fluctuating, disordered environment, it may be assumed that the asymmetry is a random variable with mean zero. In this situation, the quadrupolar Hamiltonian takes the simpler form, [12]

$$H_Q = \omega_Q T_{20} . \tag{2.85}$$

We note that this is an expression in the system of principal axis associated with electric field gradients. In the ion's system of axis, in terms of the angle between the systems' Oz axis, Θ,

$$H_Q = \left(\frac{3\cos^2 \Theta - 1}{2} \right) \omega_Q T_{20} \tag{2.86}$$

This observation is the basis for multi-domain model of the biological systems, in which is assumed that each individual domain is characterized by a specific quadrupolar frequency given by (2.86). The measured quantities, sum over domains, are expressed as the averages over the director angles, [12].

2.5. Superoperator description of RF hard pulses

The differential equation governing the evolution of density matrix during the application of an RF field with frequency ω, duration T, amplitude $B_1(t)$, and phase φ, is given in the rotating frame by the differential equation

$$\frac{d}{dt} | \rho(t) \rangle\rangle = -i \left(-\omega_1(t) \mathbf{J}_\varphi - \delta \mathbf{J}_Z \right) | \rho(t) \rangle\rangle . \tag{2.87}$$

Here, $\omega_1=\gamma B_1(t)$, and the inhomogeneity parameter is defined by the differences between Larmor angular frequency and the applied RF angular frequency $\delta=\gamma B_0-\omega$.

For the class of hard pulses, the amplitude of the RF field is constant, $\omega_1(t)=\omega_1$; as a consequence, the density matrix at the end of the pulse $\rho(T)$ is expressed in terms of the density matrix before the pulse, $\rho(0)$, in terms of a matrix exponential

$$|\rho(T)\rangle\rangle = \exp\left\{i\left(\omega_1 T \mathbf{J}_\varphi - \delta T \mathbf{J}_Z\right)\right\} |\rho(0)\rangle\rangle . \tag{2.88}$$

Taking in consideration that a rotation with angle θ around a direction described by the unit vector $\vec{U}$ is described in superspace by the exponential $\exp\left(-i\theta\vec{U}\vec{\mathbf{J}}\right)$, the expression in Eq (2.88) represents a finite rotation with the angle $-\tilde{\theta}$, around an axis characterized by the latitude -η and the azimuth φ. Requiring the agreement between the Cartesian and spherical coordinates representations

$$\omega_1 T \mathbf{J}_\varphi - \delta T \mathbf{J}_Z = \tilde{\theta}\left(-\sin\eta \mathbf{J}_Z + \cos\eta\left(\mathbf{J}_X \cos\varphi + \mathbf{J}_Y \sin\varphi\right)\right), \tag{2.89}$$

the expression for the rotation parameters are given by the chain of equations

$$\theta = \omega_1 T, \quad \psi = \delta T, \quad \tilde{\theta} = \sqrt{\theta^2 + \psi^2}, \quad \tan\eta = \psi/\theta . \tag{2.90}$$

From the physical point of view, θ is the flip angle in the absence of inhomogeneity while ψ is the precession angle in the absence of RF.

In order to obtain the transformation of QM operators under a rotation, the representation in terms of Euler angles is required. The evaluation of the exponential in (2.88) is performed in terms of the Euler angles (α_L,β,α_R) by the identity

$$\exp\left\{i\tilde{\theta}\left(-\sin\eta \mathbf{J}_Z + \cos\eta\left(\mathbf{J}_X \cos\varphi + \mathbf{J}_Y \sin\varphi\right)\right)\right\} = \exp\left(-i\alpha_L \mathbf{J}_Z\right)\exp\left(-i\beta \mathbf{J}_Y\right)\exp\left(-i\alpha_R \mathbf{J}_Z\right). \tag{2.91}$$

Their expression is valid regardless of the specific representation used for the rotation group.
By using the 1/2 representation (when the operators become 2x2 matrices), the expression for Euler angles are obtained whenever $0\le\theta\le\pi$ and $-\pi/2\le\eta\le\pi/2$, by the parametric expressions,

$$\alpha_L = \alpha - \left(\varphi + \frac{\pi}{2}\right), \quad \alpha_R = \alpha + \left(\varphi + \frac{\pi}{2}\right) \quad \beta = 2\arcsin\left(\cos\eta \sin\frac{\theta}{2\cos\eta}\right), \tag{2.92}$$

with the common angle,

$$\alpha = \arctan\left(\sin\eta \tan\left(\frac{\theta}{2\cos\eta}\right)\right). \tag{2.93}$$

As a product of three exponentials, the off-resonance pulse **P**(θ,φ,δ) is expressed

$$\mathbf{P}(\theta,\varphi,\delta) = \exp\left(-i\alpha_L \mathbf{J}_Z\right)\exp\left(-i\beta\mathbf{J}_Y\right)\exp\left(-i\alpha_R\mathbf{J}_Z\right). \tag{2.94}$$

The usefulness of this representation becomes obvious in the SIT basis, where the matrix element has a particularly simple structure

$$\langle\langle lm \,|\, \mathbf{P}(\theta,\varphi,\delta) \,|\, \lambda\mu\rangle\rangle = \exp\left(i(\mu - m)\left(\varphi + \frac{\pi}{2}\right) - i\alpha(m+\mu)\right)\langle\langle lm \,|\, e^{-i\beta\mathbf{J}_Y} \,|\, \lambda\mu\rangle\rangle . \tag{2.95}$$

The last matrix elements are defining the Wigner functions, [13], when l=λ, and are zero when l≠λ,

$$\langle\langle lm \,|\, e^{-i\beta\mathbf{J}_Y} \,|\, \lambda\mu\rangle\rangle = \delta_{l\lambda} d_l^{m\mu}(\beta). \tag{2.96}$$

Similar considerations could be found in [14], where the equivalence between an off-resonance and an on-resonance pulse is explored. In the present thesis, an approximation of the previous formulation is sought. While the expression (2.95) solves the problem of constructing the matrix associated with the RF pulse superoperators, more insight in the question of the dephasing during the RF pulse could be gained by comparing off-resonance and on-resonance pulses. In superoperator form, the relationship between the off-resonance pulse and the on-resonance pulse characterized by the same B_1, is described by the transformation

$$\mathbf{P}(\theta,\varphi,\delta) = \exp\left(-i\delta T_{\theta,\delta}\mathbf{L}_Z\right)\mathbf{P}(\beta,\varphi)\exp\left(-i\delta T_{\theta,\delta}\mathbf{L}_Z\right), \tag{2.97}$$

where the effective length of the pulse is introduced

$$T_{\theta,\delta} = \frac{\cos\eta}{\theta \sin\eta} \arctan\left(\sin\eta \tan\left(\frac{\theta}{2\cos\eta} \right) \right). \tag{2.98}$$

The effect of the pulse could be described as the transfer from of the coherence (lμ) to coherences with the same principal number (lm). The amplitude of the transfer is the real function $d_l^{m\mu}(\beta)$, which could take positive as well as negative values. Apart of this amplitude, there is a relative phase gained by the resulting coherence. It originates from two mechanisms. First, the rotation itself is responsible for the factor exp(i(μ-m)(φ+π/2)), and second, the off-resonance evolution during a period $T_{\theta,\delta}$ is responsible for the factor exp(-iδ$T_{\theta,\delta}$ (m+μ)).

For flip angles around π/2 and small inhomogeneities, the following approximations could be used,cosη≈1, sinη≈tanη≈η=ψ/θ, from where

$$\begin{cases} \beta = 2\arcsin\left(\cos\eta \sin\dfrac{\theta}{2\cos\eta} \right) \cong \theta \\ T_{\theta,\delta} = \dfrac{T\cos\eta}{\theta\sin\eta} \arctan\left(\sin\eta \tan\left(\dfrac{\theta}{2\cos\eta} \right) \right) \cong \dfrac{T}{\theta} \tan\left(\dfrac{\theta}{2} \right) \equiv T_\theta \end{cases} \tag{2.99}$$

By numerically comparing with the exact expressions with their approximations, we conclude that the approximations are characterized by an error less than 1% whenever 60°≤θ≤120° and 20°≤ψ≤20° (named here the MRI imperfections domain). In Figure 2.1 the difference between the apparent and on-resonance flip angle is presented. The MRI imperfection region is completely contained in the 1% error domain.

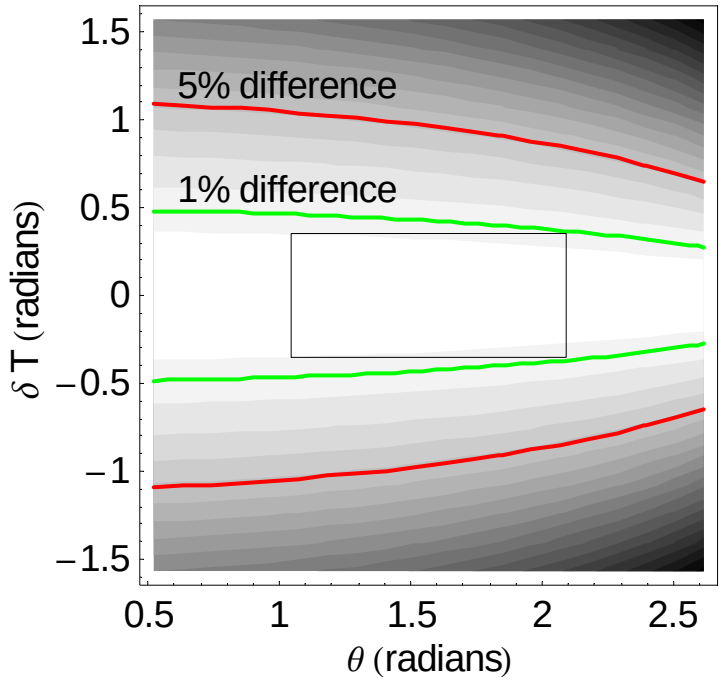

Figure 2.1 The contour plot of the difference between the flip angle (θ) and the apparent flip angle (β)

The same conclusion could be drawn from the inspection of Figure 2.2 where the relative difference between the exact factor $T_{\theta,\delta}$ and its off-resonance independent approximation, T_{θ} is presented. In this situation, the MRI imperfection region is contained in the 1% error domain, also.

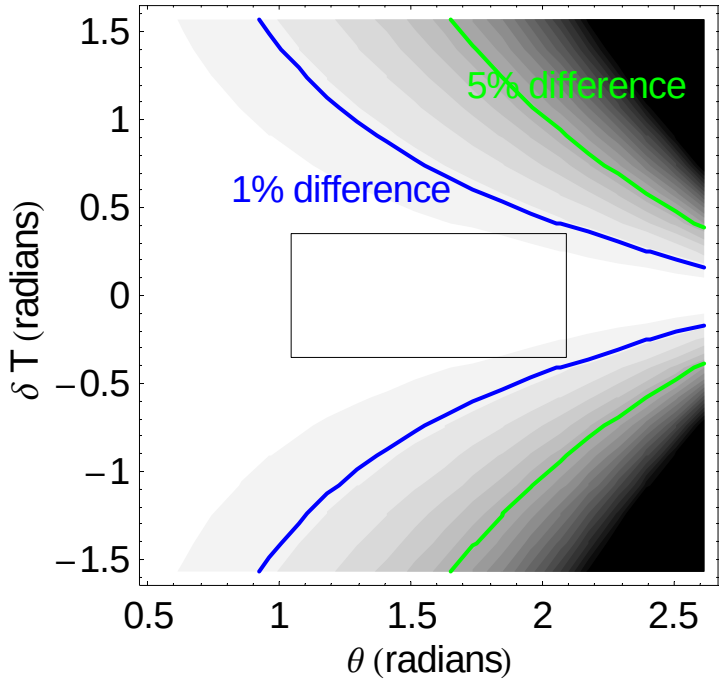

Figure 2.2 The contour plot of the difference between the exact expression $T_{0,\delta}$ and the approximate T_0

The conditions being easily satisfied for typical experiments, the off-resonance pulse superoperator is described in terms of the on-resonance pulse with the same flip angle, and an effective length T_θ depending on the flip angle, only. In superoperator form, the approximation becomes

$$\mathbf{P}(\theta,\varphi,\delta) = \exp(-i\delta T_\theta \mathbf{L}_Z)\,\mathbf{P}(\theta,\varphi)\exp(-i\delta T_\theta \mathbf{L}_Z). \qquad (2.100)$$

The last formula generates the non-vanishing matrix elements between elements of SIT basis

$$\langle\langle lm\,|\,\mathbf{P}(\theta,\varphi,\delta)\,|\,l\mu\rangle\rangle = \exp\left(-i\delta T_\theta (m+\mu)\right)\exp\left(i(\mu-m)\left(\varphi+\frac{\pi}{2}\right)\right)d_l^{m\mu}(\theta). \qquad (2.101)$$

In symbolic calculations, a more compact form is used

$$\langle\langle lm \,|\, \mathbf{P}(\theta,\varphi,\delta) \,|\, l\mu \rangle\rangle = \mathrm{e}^{i(\mu-m)\varphi}\, \mathrm{e}^{-i\delta T(m+\mu)}\, p_l^{m\mu}(\theta), \tag{2.102}$$

in which T is understood as the effective time, and the newly introduced p-functions are related to the Wigner functions by a phase

$$p_l^{m\mu}(\theta) = d_{m\mu}^{l}(\theta)\, \mathrm{e}^{i\frac{\pi}{2}(\mu-m)}. \tag{2.103}$$

The filtering schemes analyzed in this thesis contain 90° degree pulses, only (the B_1 inhomogeneity manifests in deviations from this ideal value), therefore a simpler approximation is used for the effective pulse length,

$$T_{\theta,\delta} \approx T\frac{2}{\pi}. \tag{2.104}$$

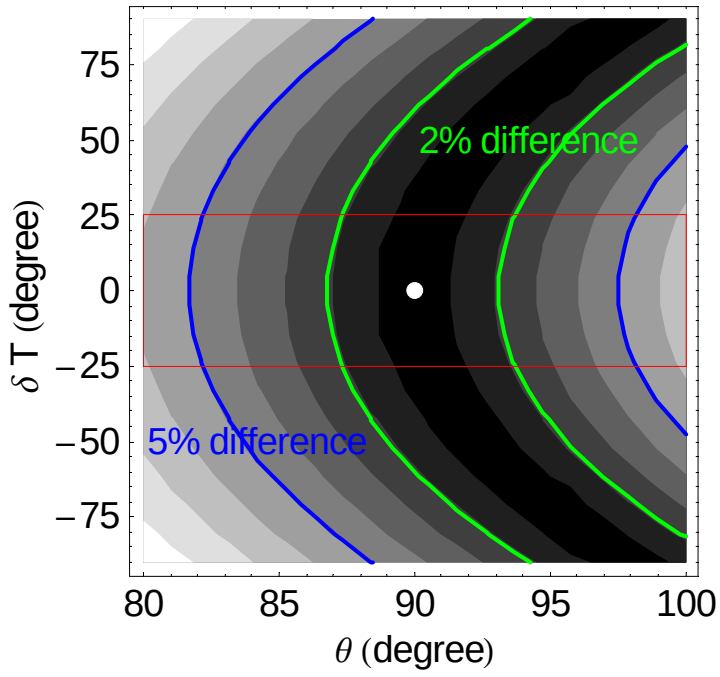

Figure 2.3 The difference between the effective length of a 90 degree pulse and a θ pulse, as a function of inhomogeneity and flip angle.

3. RELAXATION MATRIX THEORY

In Section 3.1, the formal theory of the relaxation is presented by using a quantum description of the bath. The systematical use of Liouville representation makes the both the calculations and the physical assumptions transparent. The relaxation matrix is constructed in terms of product of superoperators associated with the fluctuation. In Section 3.2, the relaxation of spin 3/2 particles experiencing quadrupolar fluctuations is constructed as a quadratic form in SIT superoperators. In Section 3.3, the algebraic calculation of the propagator describing the relaxation of spin 3/2 is offered.

The Hamiltonian model of a system interacting with a bath is constructed in the direct product of Hilbert spaces associated with the Hilbert space of the system H_S and Hilbert space of the bath H_b. In order to make the formulas more intuitive we reserve the Latin lowercase symbols for the quantities referring to the bath. The subscript notation $_F$ denotes quantities referring to the full system. The bath is considered described by the Boltzmann distribution, with a temperature $T = 1/(k_B\beta)$

$$b = e^{-\beta h} / z, \quad z = \mathrm{Tr}_b \left\{ e^{-\beta h} \right\} \tag{3.1}$$

The notation Tr_b represents the trace operation considered on the bath degrees of freedom, only.

For any two operators, a and c, acting on the Hilbert space of the bath, the time correlation function is defined as the trace over the bath's states of their product, [15]

$$\left\langle a(t)c(0) \right\rangle \equiv \mathrm{Tr}\left\{ ba(t)c(0) \right\}, \tag{3.2}$$

where the time dependent operator a(t) is understood in the bath's Heisenberg representation

$$a(t) = \exp(-iht)\, a \exp(iht). \tag{3.3}$$

By using the invariance of the trace under cyclic permutations and the form of bath density matrix at canonical equilibrium, (3.1) the following relations are obvious

$$\begin{aligned} \langle a(t)c(0)\rangle &= \mathrm{Tr}\left\{e^{-\beta h}e^{-ith}a(0)e^{ith}c(0)\right\} = \mathrm{Tr}\left\{e^{-\beta h}a(0)e^{ith}c(0)e^{-ith}\right\} = \langle a(0)c(-t)\rangle \\ \langle a(t)c(0)\rangle &= \mathrm{Tr}\left\{e^{-\beta h}e^{-ith}a(0)e^{ith}c(0)\right\} = \mathrm{Tr}\left\{e^{-\beta h}c(0)e^{-\beta h}e^{-ith}a(0)e^{ith}e^{\beta h}\right\} = \langle b(0)c(t+i\beta)\rangle \end{aligned} \tag{3.4}$$

Because the bath is stationary, the correlations functions are time shift invariant

$$\langle a(t+\tau)c(\tau)\rangle = \langle a(t)c(0)\rangle \tag{3.5}$$

The symmetrized and anti-symmetrized correlation functions are defined

$$\begin{aligned} \langle a(t)c(0)\rangle^{+} &= \frac{1}{2}\langle a(t)c(0) + a(0)c(t)\rangle \\ \langle a(t)c(0)\rangle^{-} &= \langle a(t)c(0) - a(0)c(t)\rangle \end{aligned} \tag{3.6}$$

The quantities of the interest are the Fourier transforms of the time-correlations functions, the spectral densities

$$\langle ac\rangle_{\omega} \equiv \frac{1}{2\pi}\int_{-\infty}^{\infty} dt\, e^{-i\omega t}\langle a(t)c(0)\rangle \tag{3.7}$$

Using the previous formula, (3.4), one could prove the frequency analogous of the detailed balance relation [15]

$$\langle ac\rangle_{-\omega} = e^{-\beta\omega}\langle ca\rangle_{\omega} \tag{3.8}$$

For the symmetrized and anti-symmetrized spectral densities similar relations can be written,

$$\langle ac\rangle_{\omega}^{+} = \langle ac\rangle_{\omega}\cosh(\beta\omega) \quad \langle ac\rangle_{\omega}^{-} = \langle ac\rangle_{\omega} 2e^{-\beta\omega/2}\sinh(\beta\omega/2), \tag{3.9}$$

from where,

$$\langle ac\rangle_{\omega}^{-} = \langle ac\rangle_{\omega}^{+} e^{-\beta\omega/2}\frac{1}{2}\tanh\left(\frac{\beta\omega}{2}\right). \tag{3.10}$$

One could see that in the high temperature limit, $\beta \to 0$, the anti-symmetric spectral densities are negligible, compared with the symmetric counterparts.

3.1. General expression of relaxation matrix

The density matrix of the composite system, ρ_F, at the initial moment in which the spin 3/2 is prepared, is the direct product of system's density matrix, $\rho(0)$ and bath's density matrix, b(0)

$$\rho_F(0) = \rho(0) \otimes b(0) \in \mathsf{H_S} \otimes \mathsf{H_b} \tag{3.11}$$

The full Hamiltonian considered here (covering all situation of interest) is given as a sum of three contributions

$$H_F = H \otimes 1_b + 1_S \otimes h + G = H \otimes 1_b + 1_S \otimes h + \sum V^k \otimes v^k \ . \tag{3.12}$$

The first contribution, $H \otimes 1_b$, represents the Hamiltonian for an isolated 3/2 system, the second, $1_S \otimes h$ represents the Hamiltonian of the isolated bath, while the third term describes the coupling between the system and the bath.

The evolution of the full density matrix, in Hamiltonian form is given by the Liouville von Neumann equation in the product space

$$i\frac{d}{dt}\rho_F = \left[H \otimes 1_b + 1_S \otimes h + G, \rho_F\right] \tag{3.13}$$

In order to offer the superspace formulation, the following four notations are introduced. The left, right, commutator, and anti-commutator superoperators associated with a given operator, A, are defined by their action on an arbitrary operator B in the expected way, as represented in the equation below

$$
\begin{aligned}
&\left[A\right]^{L} B \equiv AB \\
&\left[A\right]^{R} B \equiv BA \\
&\left[A\right]^{-} B \equiv AB - BA = \left(\left[A\right]^{L} - \left[A\right]^{R}\right) B \\
&\left[A\right]^{+} B \equiv \frac{1}{2}\left(AB + BA\right) = \frac{1}{2}\left(\left[A\right]^{L} + \left[A\right]^{R}\right) B
\end{aligned}
\tag{3.14}
$$

Because of its form, the Liouville equation requires the calculation of the commutator superoperator associated with direct products of operators.

Unless the case of left and right multiplication superoperators, where straightforward composition relations can be written in the form

$$
\left[A \otimes a\right]^{L} = \left[A\right]^{L} \otimes \left[a\right]^{L} \quad \left[A \otimes a\right]^{R} = \left[A\right]^{R} \otimes \left[a\right]^{R}, \tag{3.15}
$$

(justified from the property of the Kronecker product $\left(A \otimes a\right)\left(B \otimes b\right) = \left(AB\right) \otimes \left(ab\right)$), the commutator superoperators do not have the same property, by their definition

$$
\left[A \otimes a\right]^{-} \left(B \otimes b\right) \equiv \left(A \otimes a\right)\left(B \otimes b\right) - \left(B \otimes b\right)\left(A \otimes a\right) = AB \otimes ab - BA \otimes ba, \tag{3.16}
$$

therefore,

$$
\left[A \otimes a\right]^{-} \neq \left[A\right]^{-} \otimes \left[a\right]^{-}.
$$

Instead, the more cumbersome expression can be proved

$$
\left[A \otimes a\right]^{-} = \left[A\right]^{-} \otimes \left[a\right]^{+} + \left[A\right]^{+} \otimes \left[a\right]^{-} \tag{3.17}
$$

To prove the identity one could start with the definition of the anti-commutator superoperator; its action on an arbitrary direct product can be expressed, (3.16)

$$
\begin{aligned}
\left[A \otimes a\right]^{-} \left(B \otimes b\right) &= AB \otimes ab - BA \otimes ba \\
&= \left(AB - BA\right) \otimes ab + BA \otimes \left(ab - ba\right)
\end{aligned}
,
$$

which is just a sum of direct products of superoperators

$$\left[A\otimes a\right]^{-}=\left[A\right]^{-}\otimes\left[a\right]^{L}+\left[A\right]^{R}\otimes\left[a\right]^{-}.$$

A similar relation is obtained, by following the same type of manipulations, in which

$$\begin{aligned}\left[A\otimes a\right]^{-}\left(B\otimes b\right)&=AB\otimes ab-BA\otimes ba\\&=AB\otimes\left(ab-ba\right)+\left(AB-BA\right)\otimes ba\end{aligned},$$

which reduces to,

$$\left[A\otimes a\right]^{-}=\left[A\right]^{L}\otimes\left[a\right]^{-}+\left[A\right]^{-}\otimes\left[a\right]^{R}.$$

By taking the average of the two results, the equation in (3.17) is demonstrated. Now, we can apply the found representation, (3.17), for each of the terms occurring in the Liouville equation, which can be rewritten in terms of the superoperators

$$i\frac{d}{dt}\rho_{F}=\left[H\otimes 1_{b}+1_{S}\otimes h+G\right]^{-}\rho_{F}$$

The superoperators associated with the identity operator are trivial; the commutator vanishes, while the other are acting as the identity

$$\left[1\right]^{-}=0\quad\text{and}\quad\left[1\right]^{+}=\left[1\right]^{L}=\left[1\right]^{R},\tag{3.18}$$

As a notational convenience, the equalities $1=[1]^{L}=[1]^{R}=[1]^{+}$ are understood whenever the unit superoperator is encountered, for the remainder of this section.

The first two terms are easily expanded as direct products of superoperators

$$\left[H\otimes 1_{b}\right]^{-}=\left[H\right]^{-}\otimes 1_{b}\quad\left[1_{S}\otimes h\right]^{-}=1_{S}\otimes\left[h\right]^{-},\tag{3.19}$$

In order to transform the last term, the system-bath coupling, by making use of the (3.17),

$$\left[V^{k}\otimes v^{k}\right]^{-}=\left[V^{k}\right]^{-}\otimes\left[v^{k}\right]^{+}+\left[V^{k}\right]^{+}\otimes\left[v^{k}\right]^{-},\tag{3.20}$$

the Liouville equation becomes the linear equation in superspace,

$$i\frac{d}{dt}\rho_{F}=\left\{\left[H\right]^{-}\otimes 1_{b}+1_{S}\otimes\left[h\right]^{-}+\sum\left(\left[V^{k}\right]^{-}\otimes\left[v^{k}\right]^{+}+\left[V^{k}\right]^{+}\otimes\left[v^{k}\right]^{-}\right)\right\}\rho_{F}\tag{3.21}$$

Once the superoperator of a direct product is decomposed in direct product of superoperators, simple multiplication rules can be used in the Taylor expansion of the exponential function to prove

$$\begin{aligned} \exp\left(\alpha\left[H\right]^{-}\otimes 1_b\right) &= \exp\left(\alpha\left[H\right]^{-}\right)\otimes 1_b \\ \exp\left(\alpha 1_S\otimes\left[h\right]^{-}\right) &= 1_S\otimes\exp\left(\alpha\left[h\right]^{-}\right) \end{aligned} \tag{3.22}$$

As an immediate application of these rules of exponentiation, the transition to Heisenberg representation, in respect with both system and bath, is realized by the unitary transformation

$$U_{Sb}\left(t\right)=\exp\left(it\left(\left[H\right]^{-}\otimes 1_b+1_S\otimes\left[h\right]^{-}\right)\right)=\exp\left(it\left[H\right]^{-}\right)\otimes\exp\left(it\left[h\right]^{-}\right). \tag{3.23}$$

Practically, by the use of the substitution

$$\rho_F\left(t\right)=U_{Sb}\left(t\right)\left(\rho'_F\left(t\right)\right). \tag{3.24}$$

the evolution equation takes the simpler form in which the individual Liouvillian contribution have disappeared. The remaining term describes the system-bath coupling, in the introduced interaction representation

$$\begin{aligned} i\frac{d}{dt}\rho'_F\left(t\right) &= \left\{\sum\left(\left[V^k\left(t\right)\right]^{-}\otimes\left[v^k\left(t\right)\right]^{+}+\left[V^k\left(t\right)\right]^{+}\otimes\left[v^k\left(t\right)\right]^{-}\right)\right\}\rho'_F\left(t\right) \\ &\equiv G\left(t\right)\rho'_F\left(t\right) \end{aligned}. \tag{3.25}$$

Apart of the prime notation for density matrices, there is no need for extra labeling of the interaction representation quantities, their time dependence distinguish them from the original, Schroedinger representation, counterparts

$$\begin{aligned} \left[V^k\left(t\right)\right]^{-} &= \exp\left(-it\left[H\right]^{-}\right)\left[V^k\right]^{-}\exp\left(it\left[H\right]^{-}\right) \\ \left[v^k\left(t\right)\right]^{-} &= \exp\left(-it\left[h\right]^{-}\right)\left[v^k\right]^{-}\exp\left(it\left[h\right]^{-}\right) \end{aligned} \tag{3.26}$$

The same observation applies for the coupling superoperator, which is expressed by the superspace analog of the previous relation

$$G(t) = U_{Sb}^{-1}(t) G U_{Sb}(t). \tag{3.27}$$

The equation (3.25) as belonging to a well-known class of linear equations with initial conditions

$$\begin{cases} \dfrac{d}{dt}\rho'_F(t) = -iG(t)\rho'_F(t) \\ \rho'_F(t=0) = \rho'_F(0) \end{cases} \tag{3.28}$$

An integral equation can be written, which contains the same information as the preceding differential equation together with its initial condition

$$\rho'_F(t) = \rho'_F(0) - i\int_0^t dt_1 G(t_1)\rho'_F(t_1)$$

By substitution the previous integral representation for the integrand

$$\rho'_F(t) = \rho'_F(0) - i\int_0^t dt_1 G(t_1)\rho'_F(0) - \int_0^t\int_0^{t_1} dt_1 dt_2 G(t_1)G(t_2)\rho'_F(t_2) \tag{3.29}$$

Continuing this process, indefinitely, the time ordered, Dyson series is obtained

$$\rho'_F(t) = \left(\sum_{n=0}^{\infty}(-i)^n \int_0^t dt_1 \cdots \int_0^{t_{n-1}} dt_n G(t_1)\cdots G(t_n)\right)\rho'_F(0) \tag{3.30}$$

which is the definition of the propagator, as the time-ordered exponential

$$\begin{aligned} \rho'_F(t) &= \Gamma(t)\rho'_F(0) \\ \Gamma(t) &= \mathrm{T}\exp\left(-i\int_0^t dt' G(t')\right) \end{aligned} \tag{3.31}$$

This expression can be considered as the starting point of a systematic cummulants expansion [16] or it can be used to derive the standard Nakajima-Zwanzig memory function approach [17].

For NMR applications when the result aimed is the Redfield equation [18], a less sophisticated approach can be followed, starting with (3.29). The necessary ingredient, for obtaining a tractable form of the evolution equation, consists in performing the average over bath states, as the interest is not in the exact evolution of the system, but in its statistical averaged evolution. Recalling the fact that at the moment t=0 the system is prepared in a well defined state, uncorrelated with the bath state, the initial condition, in Heisenberg representation is written, also

$$\rho'_F(0) = \rho'(0) \otimes b'(0) = \rho(0) \otimes b(0). \tag{3.32}$$

The average evolution of the system is defined by the average over the bath states

$$\rho'_{\text{av}}(t) \equiv \text{Tr}_b \left\{ \rho'_F(t) \right\} \overset{notation}{=} \left\langle \rho'_F(t) \right\rangle_b. \tag{3.33}$$

Using the propagator of the composite system-bath, the reduced density matrix becomes

$$\rho'_{\text{av}}(t) = \text{Tr}_b \left\{ \Gamma(t) \rho'(0) \otimes b'(0) \right\}. \tag{3.34}$$

Time ordered cummulants expansion could be used at this level, to construct a hierarchy of evolution equations. When only the second order is seek, by using the double integral representation of the exact solution (3.29), and taking the bath average, the following, still exact representation is obtained

$$\rho'_{\text{av}}(t) = \rho'_{\text{av}}(0) - i \int_0^t dt_1 \left\langle G(t_1) \rho'(0) \otimes b'(0) \right\rangle_b - \int_0^t dt_1 \int_0^{t_1} dt_2 \left\langle G(t_1) G(t_2) \rho'_F(t_2) \right\rangle_b, \tag{3.35}$$

from where, an integral-differential equation is found by taking the time derivative

$$\frac{d}{dt} \rho'_{\text{av}}(t) = -i \left\langle G(t) \rho'(0) \otimes b'(0) \right\rangle_b - \int_0^t dt_1 \left\langle G(t) G(t_1) \rho'_F(t_1) \right\rangle_b. \tag{3.36}$$

Using the form of the interaction, (3.25), the first term evaluates to the sum over bath anti-commutators (because the terms involving the traces of commutators vanishes) which using the invariance under cyclic permutations of the trace can be written

$$\left\langle G(t)\rho'(0)\otimes b'(0)\right\rangle_b = \sum\left[V^k(t),\rho'(0)\right]\mathrm{Tr}\left\{v^k(t)b'(0)\right\}. \tag{3.37}$$

The last expression is zero, also. The traces are the averages of the bath fluctuations, which are zero (when not the case, the redefinition of the static interaction can be made). Finally, the equation (3.36) can be written, in Heisenberg representation,

$$\frac{d}{dt}\rho'_{\mathrm{av}}(t) = -\int_0^t dt_1 \left\langle G(t)G(t_1)\rho'_F(t_1)\right\rangle_b \tag{3.38}$$

The last equation is an exact equation of evolution, (under the specified assertions about the nature and dynamics of the bath) but unfortunately, it contains, under integral, the full density matrix. The natural simplifying assumption at this point is that the bath evolves independently of the system (weak system-bath coupling).

These assumptions translate in the decomposition of the full density matrix as the direct product

$$\rho'_F(t) = \rho'_S(t)\otimes b'(t) \tag{3.39}$$

with the evolution of bath's density matrix, as dictated by the Heisenberg evolution, reducing to a constant

$$b'(t) = \exp\left(-it\left[h\right]^-\right)b = \exp(-ith)\,b\exp(ith) = b. \tag{3.40}$$

The system's density matrix is found to be the aforementioned reduced density matrix, due to the identity

$$\mathrm{Tr}_b\left\{a\otimes b\right\} = a\,\mathrm{Tr}_b\left\{b\right\}.$$

Those considerations reduce the evolution equation to the form

$$\frac{d}{dt}\rho'_{\mathrm{av}}(t) = -\int_0^t dt_1 \left\langle G(t)G(t_1)\left(\rho'_{\mathrm{av}}(t_1)\otimes b\right)\right\rangle_b, \tag{3.41}$$

which, takes the equivalent form

$$\frac{d}{dt}\rho'_{\mathrm{av}}(t) = -\int_0^t dt_1 \left\langle G(t)G(t_1)\bullet b\right\rangle_b \rho'_{\mathrm{av}}(t_1) \tag{3.42}$$

The product can be expanded, taking advantage of the expansion in direct products of superoperators

$$\begin{aligned}\left\langle G(t)G(t')\bullet b\right\rangle_b = \sum_{m,k} \\ \Big(\left[V^k(t)\right]^- \left[V^m(t')\right]^- \left\langle \left[v^k(t)\right]^+ \left[v^m(t')\right]^+ b \right\rangle_b + \\ \left[V^k(t)\right]^- \left[V^m(t')\right]^+ \left\langle \left[v^k(t)\right]^+ \left[v^m(t')\right]^- b \right\rangle_b + \\ \left[V^k(t)\right]^+ \left[V^m(t')\right]^- \left\langle \left[v^k(t)\right]^- \left[v^m(t')\right]^+ b \right\rangle_b \\ \left[V^k(t)\right]^+ \left[V^m(t')\right]^+ \left\langle \left[v^k(t)\right]^- \left[v^m(t')\right]^- b \right\rangle_b \Big)\end{aligned} \tag{3.43}$$

By simple inspection, the last two terms can be discarded because the trace of a commutator is identical zero. The only two contributions remaining in (3.43) are evaluated by reducing them to correlation functions of fluctuations. First, due to the invariance of a trace under circular permutations, the obvious identities could be used

$$\begin{aligned}\left\langle \{a,\{b,c\}\}\right\rangle &= \frac{1}{4}\left\langle abc + acb + bca + cba\right\rangle = \left\langle \{a,b\}c\right\rangle \\ \left\langle \{a,[b,c]\}\right\rangle &= \frac{1}{4}\left\langle abc - acb + bca - cba\right\rangle = \left\langle [a,b]c\right\rangle\end{aligned} \tag{3.44}$$

obtaining, in terms of the symmetric and anti-symmetric correlation functions (3.6)

$$\begin{aligned}\left\langle \left[v^k(t)\right]^+ \left[v^m(t')\right]^+ b \right\rangle_b &= \mathrm{Tr}\left\{\left\{v^k(t), v^m(t')\right\} b\right\} = \left\langle v^k(t)v^m(t')\right\rangle^+ \\ \left\langle \left[v^k(t)\right]^+ \left[v^m(t')\right]^- b \right\rangle_b &= \mathrm{Tr}\left\{\left[v^k(t), v^m(t')\right] b\right\} = \left\langle v^k(t)v^m(t')\right\rangle^-\end{aligned} \tag{3.45}$$

$$\left\langle G(t)G(t')\bullet b\right\rangle_b = \sum_{m,k}\begin{pmatrix} \left[V^k(t)\right]^- \left[V^m(t')\right]^- \left\langle v^k(t)v^m(t')\right\rangle^+ + \\ \left[V^k(t)\right]^- \left[V^m(t')\right]^+ \left\langle v^k(t)v^m(t')\right\rangle^- \end{pmatrix} \tag{3.46}$$

The last reduction of the number of terms entering the evolution equation is based on the high temperature approximation. The relation between the anti-symmetric and symmetric spectral densities of fluctuations (3.10),

$$\left\langle ab-ba\right\rangle_{\omega}=\left\langle ab+ba\right\rangle_{\omega}e^{-\beta\omega/2}\tanh\left(\frac{\beta\omega}{2}\right),$$

shows that, in the high temperature limit, all the anti-symmetric contributions are one order higher in (βω), when compared with their symmetric counterparts. Finally, the only surviving terms in the bath average of the bath-system interaction product are

$$\left\langle G(t)G(t')\bullet b\right\rangle_{b}=\sum_{m,k}\left[V^{k}(t)\right]^{-}\left[V^{m}(t')\right]^{-}\left\langle v^{k}(t)v^{m}(t')\right\rangle^{+} \tag{3.47}$$

Neglecting the terms containing the anti-symmetric function has a physical consequence the loss of the ability of the model to describe the approach to equilibrium. [19]

The evolution of the reduced density matrix is given by an equation in which only the commutator superoperators appear

$$\frac{d}{dt}\rho'_{\mathrm{av}}(t)=-\int_{0}^{t}dt_{1}\sum_{m,k}\left[V^{k}(t)\right]^{-}\left[V^{m}(t_{1})\right]^{-}\left\langle v^{k}(t)v^{m}(t_{1})\right\rangle^{+}\rho'_{\mathrm{av}}(t_{1}). \tag{3.48}$$

Due to the fact that there is no longer the danger of confusion, we can return to the simpler notation for the commutator superoperator, as the bold-faced symbols. Also, from this moment the Hilbert space associated with the bath is no more necessary. The interaction with the environment is completely described by the symmetric correlation functions. (For NMR applications, the computation of correlation functions in a QM framework is a difficult task, most of the calculations are carried in a semi-classical formalism.) [19]

The last equation is recast, in these friendlier notations

$$\frac{d}{dt}|\rho'(t)\rangle\rangle = -\sum_{m,k}\int_0^t dt_1\, j_{km}(t-t_1)\mathbf{V}^k(t)\mathbf{V}^m(t_1)|\rho'(t_1)\rangle\rangle \tag{3.49}$$

The correlation function j_{mk} is characterized by a correlation time τ_{mk} assumed much shorter than the time scale defining the evolution of the density matrix (fast fluctuation assumption). Therefore, replacing in the previous equation, $\rho(t_1)$ with $\rho(t)$, a negligible error is introduced. As pointed in [20, 21], the extra accuracy one would hope to gain from keeping the "exact" form (3.49), is illusory, at this stage of calculations, terms describing the short time dynamics, of the same of order of magnitude have been already discarded.

$$\frac{d}{dt}|\rho'(t)\rangle\rangle = -\sum_{m,k}\left(\int_0^t dt_1\, j_{km}(t-t_1)\mathbf{V}^k(t)\mathbf{V}^m(t_1)\right)|\rho'(t)\rangle\rangle \tag{3.50}$$

The last expression defines time dependent relaxation superoperators

$$R'_{km}(t) = \int_0^t dt_1\, j_{km}(t-t_1)\mathbf{V}^k(t)\mathbf{V}^m(t_1) = \int_{-t}^0 d\tau\, j_{km}(\tau)\mathbf{V}^k(t)\mathbf{V}^m(t+\tau) \tag{3.51}$$

Again, keeping the time dependence in relaxation matrices gives an illusory sense of accuracy, finally, in the evolution of the density matrix is governed by the linear equation

$$\frac{d}{dt}|\rho'(t)\rangle\rangle = -R'|\rho'(t)\rangle\rangle \tag{3.52}$$

with the time independent relaxation superoperator

$$R' = \sum_{k,m}\int_0^\infty d\tau\, j_{km}(\tau)\mathbf{V}^k(\tau)\mathbf{V}^m(0) \tag{3.53}$$

In the case of interest in this thesis $\mathbf{V}^k = \mathbf{T}_{2k}$ $\quad j_{km}(\tau) = (-1)^m \delta_{k,-m} j_m(\tau)$ therefore

$$R' = \sum_m (-1)^m \int_0^\infty d\tau\, j_m(\tau)\mathbf{T}_{2,m}(\tau)\mathbf{T}_{2,-m}(0) \tag{3.54}$$

3.2. Calculation of relaxation matrix for sodium ions

Invoking the same symmetry argument as in Section 2.4, the most general expression for the quadrupolar fluctuations is found as the contraction between second order spherical tensors constructed from spin and bath variables

$$H_F(t) = \sum_{m=-2}^{2} T_{2m} \otimes u_{2m}^{\dagger}(t) = \sum_{m=-2}^{2} (-)^m T_{2m} \otimes u_{2,-m}(t) \tag{3.55}$$

The time dependence of the bath operators is given solely by their evolution under the bath Hamiltonian

$$u_{2m}(t) = e^{-iht} u_{2m}(0) e^{iht} \tag{3.56}$$

The assumption of a spherical symmetric environment, translates in the invariance of the bath Hamiltonian, f, under an arbitrary rotation. Denoting the action of a rotation on the bath Hilbert space by R (which is an unitary transform $R^{+}R=1$), the following identity can be written

$$\left\langle \left(R u_{2m} R^{\dagger} \right)(t) u_{2n}(0) \right\rangle = \mathrm{Tr}\left\{ e^{-\beta f} e^{-it f} R u_{2m}(0) R^{\dagger} e^{it f} u_{2n}(0) \right\} = \left\langle u_{2m}(t) \left(R^{\dagger} u_{2n}(0) R \right) \right\rangle . \tag{3.57}$$

By particularizing the nature of rotation, selection rules could be inferred for the correlation functions. Choosing the particular case of a rotation with angle φ around the Oz axis and using the SIT property $\exp(-i\varphi J_Z) u_{2m} \exp(i\varphi J_Z) = \exp(-im\varphi) u_{2m}$, the correlation functions have to satisfy

$$\left\langle u_{2m}(t) u_{2n}(0) \right\rangle = \delta_{n,-m} \left\langle u_{2m}(t) u_{2,-m}(0) \right\rangle , \tag{3.58}$$

which defines the correlation density j_m,

$$\left\langle u_{2m}(t) u_{2n}(0) \right\rangle = \delta_{n,-m} j_m(t) . \tag{3.59}$$

A more general analysis result is obtained in [22], based on Wigner-Eckart theorem and on properties of Clebsch Gordan coefficients.

Assuming the exponential decay of the correlation functions, with correlation times, τ_m, the intermediate result is obtained

$$\left\langle u_{2,m}(t)u_{2,-m}(0)\right\rangle = j_m(t) = \frac{\alpha_m}{\tau_m}\exp\left(-\frac{t}{\tau_m}\right) \tag{3.60}$$

For a biological media, at the room temperature, the environment can be considered as being not only axial symmetric, but also, isotropic. The interaction with the external static magnetic field is too weak to noticeably break the rotation symmetry. By using Wigner-Eckart theorem and simple Clebsch-Gordan manipulations, in the sphericall symmetric case [22]

$$\left\langle u_{2,m}(t)u_{2,-m}(0)\right\rangle = (-1)^m\frac{\sigma^2}{\tau}\exp\left(-\frac{t}{\tau}\right) \tag{3.61}$$

The approach to thermal equilibrium can only be obtained in a full quantum mechanical description of both the 3/2 spin system and the thermal bath, when the anti-symmetric correlation functions are kept in the calculation. The semiclassical theory, obtained by considering the fluctuations as classical stochastic variables, requires the ad hoc introduction of thermal equilibrium, extensively discussed in [19]. In the high temperature case and in the presence of a strong static magnetic field, the equilibrium density matrix takes the form of the Maxwell-Boltzmann distribution,

$$\sigma_{\mathrm{Eq}} = \frac{1}{Z}\exp\left(-\beta\omega_0 J_Z\right),\ \text{with } Z = \mathrm{Tr}\left\{\exp\left(-\beta\omega_0 J_Z\right)\right\}. \tag{3.62}$$

Separating the solution of the Liouville equation, Eq., into its deterministic (σ_D) and fluctuating (σ_F) components

$$|\,\sigma(t)\rangle\rangle = |\,\sigma_D(t)\rangle\rangle + |\,\sigma_F(t)\rangle\rangle, \tag{3.63}$$

the evolution towards thermal equilibrium imposes the limit condition

$$\lim_{t\to\infty}\sigma_D(t) = \sigma_{\mathrm{Eq}}. \tag{3.64}$$

Due to the strong static magnetic field assumption, the dynamical shift contributions are negligible, and the deterministic component of the density matrix satisfies the equation [19]

$$\frac{d}{dt}|\sigma_D(t)\rangle\rangle = -i\mathbf{L}_S^L\,|\sigma_D(t)\rangle\rangle - R\left(|\sigma_D(t)\rangle\rangle\right) \tag{3.65}$$

The relaxation function satisfies the relation $R(\sigma_{Eq})=0$, in accordance with the Boltzmann form of thermal equilibrium. Because of the "deterministic" nature of this last differential equation, the subscript indicating the deterministic component of the density matrix can be safely discarded. In the case of high temperatures, in pulse NMR experiments, the difference $\sigma(t)-\sigma_{Eq}$ can be assumed to be of first order in $\beta\omega_0$. By neglecting terms of second order in $\beta\omega_0$ (violating, in this order, the detailed balance relations) (3.65) is written: [19]

$$\frac{d}{dt}\left(|\sigma(t)\rangle\rangle - |\sigma_{Eq}\rangle\rangle\right) = -i\mathbf{L}_S^L\left(|\sigma(t)\rangle\rangle - |\sigma_{Eq}\rangle\rangle\right) - \mathbf{R}\left(|\sigma(t)\rangle\rangle - |\sigma_{Eq}\rangle\rangle\right). \tag{3.66}$$

The relaxation superoperator, **R**, is constructed in terms of the static Liouvillian as the average over fluctuations, which in interaction representation takes the form

$$R' = \sum_m (-1)^m \int_0^\infty d\tau\; j_{km}(\tau)\exp\left(-i\tau\mathbf{L}_S^L\right)\mathbf{T}_{2,m}\exp\left(i\tau\mathbf{L}_S^L\right)\mathbf{T}_{2,-m}\,. \tag{3.67}$$

For weak quadrupolar interactions the static Liouvillian is dominated by the B_0 contribution in the exponentials and we thus obtain

$$R' = \sum_m (-1)^m \int_0^\infty d\tau\; j_m(\tau)\exp\left(i\omega_0\tau\mathbf{J}_Z\right)\mathbf{T}_{2,m}\exp\left(-i\omega_0\tau\mathbf{J}_Z\right)\mathbf{T}_{2,-m}\,. \tag{3.68}$$

Due to the properties of SIT superoperators,

$$\exp\left(i\omega_0\tau\mathbf{J}_Z\right)\mathbf{T}_{2,m}\exp\left(-i\omega_0\tau\mathbf{J}_Z\right) = e^{-im\omega_0\tau}\mathbf{T}_{2,m} \tag{3.69}$$

This expression is evaluated in terms of spectral densities of (symmetrized) correlation function of fluctuations, $j_m(k\omega)$. Considering the fact that the products $T_{2,m}T_{2,-m}$ are invariant under a rotation around Oz, in the laboratory frame

$$\mathbf{R} = \sum_m (-1)^m j_m(m\omega_0)\mathbf{T}_{2,-m}\mathbf{T}_{2,m}. \tag{3.70}$$

With the convenient notations, $j_0=j_0(0)$, $j_1=(-1)j_1(\omega_0)$, $j_2=j_2(2\omega_0)$, the evolution in the absence of the RF field, is therefore described by a linear equation with time independent coefficients

$$\frac{d}{dt}\left(|\sigma_D(t)\rangle\rangle - |\sigma_{\mathrm{Eq}}\rangle\rangle\right) = -\left(i\omega_0\mathbf{J}_z + i\omega_Q\mathbf{T}_{20} + j_0\mathbf{R}_0 + j_1\mathbf{R}_1 + j_2\mathbf{R}_2\right)\left(|\sigma_D(t)\rangle\rangle - |\sigma_{\mathrm{Eq}}\rangle\rangle\right) \tag{3.71}$$

where the individual relaxation matrices are defined by products of SIT superoperators

$$\mathbf{R}_0 = \mathbf{T}_{2,0}\mathbf{T}_{2,0} \quad \mathbf{R}_1 = -\left(\mathbf{T}_{2,1}\mathbf{T}_{2,-1} + \mathbf{T}_{2,-1}\mathbf{T}_{2,1}\right) \quad \mathbf{R}_2 = \mathbf{T}_{2,2}\mathbf{T}_{2,-2} + \mathbf{T}_{2,-2}\mathbf{T}_{2,2}. \tag{3.72}$$

Each individual term in the relaxation superoperator commutes with the superoperator for the Z-component of the angular momentum,

$$\left[\mathbf{J}_Z, \mathbf{T}_{2m}\mathbf{T}_{2,-m}\right] = \left[\mathbf{J}_Z, \mathbf{T}_{2m}\right]\mathbf{T}_{2,-m} + \mathbf{T}_{2m}\left[\mathbf{J}_Z, \mathbf{T}_{2,-m}\right] = (m-m)\mathbf{T}_{2m}\mathbf{T}_{2,-m} = 0. \tag{3.73}$$

Therefore, the rotating frame analog of (3.71) has the form

$$\frac{d}{dt}\left(|\rho(t)\rangle\rangle - |\rho_{\mathrm{Eq}}\rangle\rangle\right) = -\left(i\delta\mathbf{J}_z + i\omega_Q\mathbf{T}_{20} + j_0\mathbf{R}_0 + j_1\mathbf{R}_1 + j_2\mathbf{R}_2\right)\left(|\rho(t)\rangle\rangle - |\rho_{\mathrm{Eq}}\rangle\rangle\right). \tag{3.74}$$

All terms in the Liouvillian and relaxation superoperator commute with $\mathbf{\Pi}$, therefore, the direct sum representation can be written (using the convenient notation introduced by (2.66))

$$\begin{aligned}
\mathbf{R}_0 &= (\mathrm{e}_1 + \mathrm{e}_{-1})\mathbf{R}_0^{(1)} + (\mathrm{e}_2 + \mathrm{e}_{-2})\mathbf{1}_2, \\
\mathbf{R}_1 &= \mathrm{e}_0\,\mathbf{R}_1^{(0)} + (\mathrm{e}_1 + \mathrm{e}_{-1})\mathbf{1}_3 + (\mathrm{e}_2 + \mathrm{e}_{-2})(\mathbf{1}_2 + \mathbf{J}_Z) + (\mathrm{e}_3 + \mathrm{e}_{-3}), \\
\mathbf{R}_2 &= \mathrm{e}_0\,\mathbf{R}_2^{(0)} + (\mathrm{e}_1 + \mathrm{e}_{-1})\mathbf{R}_2^{(1)} + (\mathrm{e}_2 + \mathrm{e}_{-2})\mathbf{1}_2 + (\mathrm{e}_3 + \mathrm{e}_{-3}), \\
\mathbf{L}_Q &= (-\mathrm{e}_1 + \mathrm{e}_{-1})\mathbf{L}_Q^{(1)} + (-\mathrm{e}_2 + \mathrm{e}_{-2})\mathbf{J}_X,
\end{aligned} \tag{3.75}$$

$$\mathbf{R}_1^{(0)} = \frac{2}{5}\begin{pmatrix} 1 & 0 & 2 \\ 0 & 1 & 0 \\ 2 & 0 & 4 \end{pmatrix}, \mathbf{R}_2^{(0)} = \frac{2}{5}\begin{pmatrix} 4 & 0 & -2 \\ 0 & 1 & 0 \\ -2 & 0 & 1 \end{pmatrix},$$
$$\mathbf{R}_0^{(1)} = \frac{1}{5}\begin{pmatrix} 3 & 0 & \sqrt{6} \\ 0 & 1 & 0 \\ \sqrt{6} & 0 & 2 \end{pmatrix}, \mathbf{R}_2^{(1)} = \frac{1}{5}\begin{pmatrix} 2 & 0 & -\sqrt{6} \\ 0 & 2 & 0 \\ -\sqrt{6} & 0 & 3 \end{pmatrix}, \mathbf{L}_Q^{(1)} = \frac{-1}{\sqrt{5}}\begin{pmatrix} 0 & \sqrt{3} & 0 \\ \sqrt{3} & 0 & \sqrt{2} \\ 0 & \sqrt{2} & 0 \end{pmatrix}. \tag{3.76}$$

The solution of (3.74) is constructed for any initial condition, by using the forward propagator, defined by the matrix equation

$$\frac{d}{dt}\mathbf{U}_\delta\left(\omega_Q, j_0, j_1, j_2, t\right) = -\left(i\delta\mathbf{J}_z + i\omega_Q\mathbf{T}_{20} + j_0\mathbf{R}_0 + j_1\mathbf{R}_1 + j_2\mathbf{R}_2\right)\mathbf{U}_\delta\left(\omega_Q, j_0, j_1, j_2, t\right) \tag{3.77}$$

The solution of this equation is obtained through the matrix exponential

$$\mathbf{U}_\delta\left(\omega_Q, j_0, j_1, j_2, t\right) = \exp\left(-\left(i\delta\mathbf{J}_z + i\omega_Q\mathbf{T}_{20} + j_0\mathbf{R}_0 + j_1\mathbf{R}_1 + j_2\mathbf{R}_2\right)t\right). \tag{3.78}$$

Once this quantity is computed, the evolution of the full density matrix takes an inhomogeneous linear form, symbolized here by the operation $\tilde{\mathbf{U}}(t)\bullet$ and defined by the following equation,

$$|\,\rho(t_2)\rangle\rangle = \tilde{\mathbf{U}}_\delta(t_2 - t_1)\bullet|\,\rho(t_1)\rangle\rangle = \mathbf{U}_\delta(t_2 - t_1)\left(|\,\rho(t_1)\rangle\rangle - |\,\rho_{\mathrm{Eq}}\rangle\rangle\right) + |\,\rho_{\mathrm{Eq}}\rangle\rangle. \tag{3.79}$$

The inhomogeneous term emerges only in the longitudinal component of the density matrix in the form of a time dependent function denoted $\rho_{rec}(t)$

$$|\,\rho_{\mathrm{rec}}(t)\rangle\rangle = \left(\mathbf{1} - \mathbf{U}_\delta(t)\right)|\,\rho_{\mathrm{Eq}}\rangle\rangle \tag{3.80}$$

and referred to as the "longitudinal magnetization recovery" function. Finally,

$$|\,\rho(t_2)\rangle\rangle = \mathbf{U}_\delta(t_2 - t_1)\,|\,\rho(t_1)\rangle\rangle + |\,\rho_{\mathrm{rec}}(t_2 - t_1)\rangle\rangle. \tag{3.81}$$

3.3. Calculation of the free propagator

The closed form of the propagator is the subject of this section. Its construction uses the axial symmetry (already explored in Section 2.3) and straightforward properties of projectors.

If A commutes with a projector P (an operator satisfying P^2=P), then, for any analytic function f, in terms of the projector and its complement Q=1-P we can write,

$$f\left(\mathbf{A}\right)=\mathbf{P}f\left(\mathbf{PA}\right)+\mathbf{Q}f\left(\mathbf{QA}\right) \tag{3.82}$$

Specific cases are the decomposition itself,

$$\mathbf{A}=\mathbf{PA}+\mathbf{QA} \tag{3.83}$$

the exponentiation of such operators

$$\exp\left(\alpha\mathbf{A}\right)=\mathbf{P}\exp\left(\alpha\mathbf{PA}\right)+\mathbf{Q}\exp\left(\alpha\mathbf{QA}\right) \tag{3.84}$$

and the exponentiation of a projector

$$\exp\left(\alpha\mathbf{P}\right)=\mathbf{P}\,\mathrm{e}^{\alpha}+\mathbf{Q}=\mathbf{1}+\mathbf{P}\left(\mathrm{e}^{\alpha}-1\right). \tag{3.85}$$

The first factorization, relating the general propagator U_δ with the on-resonance (δ=0) propagator, denoted simply U, is obtained using the commutation of the Liouvillian with $\mathbf{J}_Z$

$$\mathbf{U}_{\delta}\left(\omega_Q,j_0,j_1,j_2,t\right)=\exp\left(-i\delta t\mathbf{J}_Z\right)\mathbf{U}\left(\omega_Q,j_0,j_1,j_2,t\right) \tag{3.86}$$

The $\mathbf{R}_0$ matrix is a projector, this fact can be verified either from the general commutation relations, (2.49), or from its explicit form, (3.75). In terms of the orthogonal complement, $\mathbf{P}_0$=**1**-$\mathbf{R}_0$, according to (3.84), the commutation of the Liouvillian with $\mathbf{R}_0$ implies

$$\exp\left(-t\mathbf{L}\right)=\mathbf{R}_0\exp\left(-t\mathbf{R}_0\mathbf{L}\right)+\mathbf{P}_0\exp\left(-t\mathbf{P}_0\mathbf{L}\right). \tag{3.87}$$

The $\mathbf{P}_0$ component of the propagator is computed using mutual orthogonal projectors $\mathbf{P}_{0i}$, $\mathbf{P}_{0i}\mathbf{P}_{0j}=\delta_{ij}\mathbf{P}_{0i}$,

$$\begin{aligned}
\mathbf{P}_{01} &= \mathbf{P}_0\left(\mathbf{R}_1-\mathbf{R}_2\right)\left(\mathbf{R}_1-\mathbf{R}_2+\mathbf{2}\right)/8,\\
\mathbf{P}_{02} &= \mathbf{P}_0\left(\mathbf{R}_1-\mathbf{R}_2\right)\left(\mathbf{R}_1-\mathbf{R}_2-\mathbf{2}\right)/8,\\
\mathbf{P}_{03} &= \mathbf{P}_0\left(\mathbf{R}_1+\mathbf{R}_2-\mathbf{2}\right)/8,\\
\mathbf{P}_{04} &= \mathbf{P}_0-\left(\mathbf{P}_{01}+\mathbf{P}_{02}+\mathbf{P}_{03}\right),
\end{aligned} \tag{3.88}$$

in terms of which the $\mathbf{P}_0$ component of the Liouvillian can be written

$$\mathbf{P}_0\mathbf{L} = 2j_1\mathbf{P}_{01}+2j_2\mathbf{P}_{02}+2\left(j_1+j_2\right)\mathbf{P}_{03}+\left(j_1+j_2\right)\mathbf{P}_{04}. \tag{3.89}$$

The exponentiation is obtained from (3.84)

$$\mathbf{P}_0\,\mathrm{e}^{-t\mathbf{P}_0\mathbf{L}} = \mathbf{P}_{01}\,\mathrm{e}^{-2j_1t}+\mathbf{P}_{02}\,\mathrm{e}^{-2j_2t}+\mathbf{P}_{03}\,\mathrm{e}^{-2(j_1+j_2)t}+\mathbf{P}_{04}\,\mathrm{e}^{-(j_1+j_2)t}. \tag{3.90}$$

For the $\mathbf{R}_0$ component, the following operators commuting with $\mathbf{R}_0$ are defined, with α=1,2

$$\mathbf{K}_{\alpha 3} = \mathbf{R}_0\left(\mathbf{R}_\alpha-\mathbf{1}\right)/2,\quad \mathbf{K}_{\alpha 1} = 2\mathbf{K}_{\alpha 3}\mathbf{T}_{20}\mathbf{K}_{\alpha 3},\quad \mathbf{K}_{\alpha 2} = -2i\mathbf{K}_{\alpha 3}\mathbf{K}_{\alpha 1} \tag{3.91}$$

They satisfy the commutation relations of two independent s=1/2 spins

$$\left[\mathbf{K}_{1i},\mathbf{K}_{2j}\right]=0,\left(i,j=1,2,3\right)\quad \left[\mathbf{K}_{\beta 1},\mathbf{K}_{\beta 2}\right]=i\mathbf{K}_{\beta 3},\ \text{and circular permutations} \tag{3.92}$$

Using those spin-like operators, the $\mathbf{R}_0$ component of the Liouvillian can be written

$$\mathbf{R}_0\mathbf{L} = \left(j_0+j_1+j_2\right)\mathbf{R}_0+2\sum_{\alpha=1,2}\left(j_\alpha\mathbf{K}_{\alpha 3}-\omega_Q\mathbf{K}_{\alpha 1}\right), \tag{3.93}$$

and its exponentiation reads

$$\mathbf{R}_0\,\mathrm{e}^{-t\mathbf{R}_0\mathbf{L}} = e^{-(j_0+j_1+j_2)t}\mathbf{R}_0\sum_{\alpha=1,2}\mathbf{M}_\alpha\quad\text{with}\quad \mathbf{M}_\alpha=\exp\left[-2t\left(j_\alpha\mathbf{K}_{\alpha 3}-\omega_Q\mathbf{K}_{\alpha 1}\right)\right]. \tag{3.94}$$

The final exponentials are well known from Pauli matrix algebra, with $\Delta_\alpha=\sqrt{j_\alpha^2-\omega_Q^2}$,

$$\mathbf{M}_\alpha = \mathbf{M}_\alpha\left(\omega_Q,j_\alpha,t\right)=\frac{\mathrm{sh}\left(t\Delta_\alpha\right)}{\Delta_\alpha}\left(j_\alpha\left(1-\mathbf{R}_\alpha\right)-i\omega_Q\mathbf{T}_{20}\left(1-\mathbf{R}_\alpha\right)^2\right)+\mathrm{ch}\left(t\Delta_\alpha\right)\left(1-\mathbf{R}_\alpha\right)^2. \tag{3.95}$$

The final formula for longitudinal and transversal components, in a basis free formulation, reads

$$\begin{aligned}\mathbf{U}^{L}\left(j_1,j_2,t\right)&=\mathbf{P}_{01}\,\mathrm{e}^{-2j_1t}+\mathbf{P}_{02}\,\mathrm{e}^{-2j_2t}+\mathbf{P}_{03}\,\mathrm{e}^{-2(j_1+j_2)t}\\ \mathbf{U}^{T}\left(j_{0,}j_1,j_2,\omega_Q,t\right)&=\mathrm{e}^{-(j_1+j_2)t}\,\mathbf{P}_{04}+\mathrm{e}^{-(j_0+j_1+j_2)t}\,\mathbf{R}_0\sum_{\alpha=1,2}\mathbf{M}_{\alpha}\left(\omega_Q,j_{\alpha},t\right)\end{aligned}. \tag{3.96}$$

The 'basis free' syntagm used here has the meaning that, regardless of the basis choice in the Liouville space, once the set of SIT superoperators $\mathbf{T}_{lm}$ is constructed, the free propagator can be obtained by mechanically following the succession of transformations described by Eq(3.72), Eq(3.88), Eq(3.91), and Eq(3.96).

One of the frequently encountered cases is the relaxation in isotropic environments, where $\omega_Q\to 0$ simultaneously with $j_1\to j_2$. In this situation, $\Delta_{\alpha}\to j_{\alpha}$, and, with the auxiliary notations $f\left(t\right)=\mathrm{e}^{-t(j_0+j_2)}, s\left(t\right)=\mathrm{e}^{-2tj_2}$, the propagator takes the form

$$\mathbf{U}\left(j_{0,}j_2,j_2,0,t\right)=s\mathbf{P}_0-s\left(1-s\right)\mathbf{P}_{03}+2f\left(\left(1+s\right)\left(\mathbf{K}_{13}^2+\mathbf{K}_{23}^2\right)-\frac{1}{2}\left(1-s\right)\left(\mathbf{K}_{13}+\mathbf{K}_{23}\right)\right) \tag{3.97}$$

Using the axial symmetry and parity considerations the structure of the propagator is expressed in terms of fourteen functions $u_{l\lambda}^{m}, 0\le m\le\lambda\le l\le 3$

$$\begin{aligned}\mathbf{U}=&\begin{pmatrix}u_{11}^0&0&u_{31}^0\\0&u_{22}^0&0\\u_{31}^0&0&u_{33}^0\end{pmatrix}\mathbf{e}_0+\begin{pmatrix}u_{11}^1&u_{21}^1&u_{31}^1\\u_{21}^1&u_{22}^1&u_{32}^1\\u_{31}^1&u_{32}^1&u_{33}^1\end{pmatrix}\mathbf{e}_1+\begin{pmatrix}u_{11}^1&-u_{21}^1&u_{31}^1\\-u_{21}^1&u_{22}^1&-u_{32}^1\\u_{31}^1&-u_{32}^1&u_{33}^1\end{pmatrix}\mathbf{e}_{-1}+\\&\begin{pmatrix}u_{22}^2&u_{32}^2\\u_{32}^2&u_{33}^2\end{pmatrix}\mathbf{e}_2+\begin{pmatrix}u_{22}^2&-u_{32}^2\\-u_{32}^2&u_{33}^2\end{pmatrix}\mathbf{e}_{-2}+u_{33}^3\left(\mathbf{e}_3+\mathbf{e}_{-3}\right)\end{aligned} \tag{3.98}$$

In the case of zero quadrupolar splitting, the structure simplifies, requiring only ten functions

$$\begin{aligned}\mathbf{U}=&\begin{pmatrix}u_{11}^0&0&u_{31}^0\\0&u_{22}^0&0\\u_{31}^0&0&u_{33}^0\end{pmatrix}\mathbf{e}_0+\begin{pmatrix}u_{11}^1&0&u_{31}^1\\0&u_{22}^1&0\\u_{31}^1&0&u_{33}^1\end{pmatrix}\mathbf{e}_1+\begin{pmatrix}u_{11}^1&0&u_{31}^1\\0&u_{22}^1&0\\u_{31}^1&0&u_{33}^1\end{pmatrix}\mathbf{e}_{-1}+\\&\begin{pmatrix}u_{22}^2&0\\0&u_{33}^2\end{pmatrix}\mathbf{e}_2+\begin{pmatrix}u_{22}^2&0\\0&u_{33}^2\end{pmatrix}\mathbf{e}_{-2}+u_{33}^3\left(\mathbf{e}_3+\mathbf{e}_{-3}\right).\end{aligned} \tag{3.99}$$

Comparing this expression with (3.96) and the explicit expression of the auxiliary projectors (3.100) - (3.104) the individual matrix elements are easily found, and they are presented below. Using the short form introduced in Eq.(2.66), the auxiliary projectors are given by

$$\mathbf{P}_{01}=\frac{1}{5}\begin{pmatrix}1&0&2\\0&0&0\\2&0&4\end{pmatrix}\mathbf{e}_0,\ \mathbf{P}_{02}=\frac{1}{5}\begin{pmatrix}4&0&-2\\0&0&0\\-2&0&1\end{pmatrix}\mathbf{e}_0,\ \mathbf{P}_{03}=\begin{pmatrix}0&0&0\\0&1&0\\0&0&0\end{pmatrix}\mathbf{e}_0, \tag{3.100}$$

$$\mathbf{P}_{04}=\left(\mathbf{e}_1+\mathbf{e}_{-1}\right)\frac{1}{5}\begin{pmatrix}2&0&-\sqrt{6}\\0&0&0\\-\sqrt{6}&0&3\end{pmatrix}+\left(\mathbf{e}_3+\mathbf{e}_{-3}\right), \tag{3.101}$$

$$\mathbf{K}_{11}=\left(\mathbf{e}_{-2}-\mathbf{e}_2\right)\frac{1}{2}\begin{pmatrix}0&1\\1&0\end{pmatrix},\ \mathbf{K}_{12}=\left(\mathbf{e}_{-2}-\mathbf{e}_2\right)\frac{1}{2}\begin{pmatrix}0&-i\\i&0\end{pmatrix},\ \mathbf{K}_{13}=\left(\mathbf{e}_2+\mathbf{e}_{-2}\right)\frac{1}{2}\begin{pmatrix}1&0\\0&-1\end{pmatrix}, \tag{3.102}$$

$$\mathbf{K}_{21}=\frac{\sqrt{5}}{10}\begin{pmatrix}0&\sqrt{3}&0\\\sqrt{3}&0&\sqrt{2}\\0&\sqrt{2}&0\end{pmatrix}\left(\mathbf{e}_{-1}-\mathbf{e}_1\right),\ \mathbf{K}_{22}=\frac{i\sqrt{5}}{10}\begin{pmatrix}0&\sqrt{3}&0\\-\sqrt{3}&0&-\sqrt{2}\\0&\sqrt{2}&0\end{pmatrix}\left(\mathbf{e}_1-\mathbf{e}_{-1}\right), \tag{3.103}$$

$$\mathbf{K}_{23}=\frac{-1}{10}\begin{pmatrix}3&0&\sqrt{6}\\0&-5&0\\\sqrt{6}&0&2\end{pmatrix}\left(\mathbf{e}_1+\mathbf{e}_{-1}\right). \tag{3.104}$$

With the notations

$$\begin{cases}C_\alpha=\mathrm{e}^{-j_\alpha t}\cosh\left(t\Delta_\alpha\right)\\S_\alpha=\mathrm{e}^{-j_\alpha t}\dfrac{\sinh\left(t\Delta_\alpha\right)}{\Delta_\alpha}\end{cases},\quad \Delta_\alpha=\sqrt{j_\alpha^2-\omega_{\mathrm{Q}}^2},\ s\left(t\right)=\mathrm{e}^{-2j_2t},\ f\left(t\right)=\mathrm{e}^{-\left(j_0+j_2\right)t}, \tag{3.105}$$

the matrix elements of the free propagator are displayed here, together with their values in the limit case $j_1\rightarrow j_2$ and $\omega_{\mathrm{Q}}\rightarrow 0$

$$
\begin{aligned}
u_{11}^{0} &= \frac{1}{5}e^{-2j_1 t}+\frac{4}{5}e^{-2j_2 t} \rightarrow s(t) & u_{22}^{2} &= e^{-(j_0+j_2)t}\left(C_1 - j_1 S_1\right) \rightarrow f(t)s(t)\\
u_{22}^{0} &= e^{-2(j_1+j_2)t} \rightarrow s^2(t) & u_{32}^{2} &= -i\omega_Q e^{-(j_0+j_2)t} S_1 \rightarrow 0\\
u_{33}^{0} &= \frac{4}{5}e^{-2j_1 t}+\frac{1}{5}e^{-2j_2 t} \rightarrow s(t) & u_{33}^{2} &= e^{-(j_0+j_2)t}\left(C_1 + j_1 S_1\right) \rightarrow f(t)\\
u_{31}^{0} &= \frac{2}{5}\left(e^{-2j_1 t}-e^{-2j_2 t}\right) \rightarrow 0 & u_{33}^{3} &= e^{-(j_1+j_2)t} \rightarrow s(t)
\end{aligned}
\tag{3.106}
$$

$$
\begin{aligned}
u_{11}^{1} &= \frac{2}{5}e^{-(j_1+j_2)t}+\frac{3}{5}e^{-(j_0+j_1)t}\left(C_2 + j_2 S_2\right) \rightarrow \frac{2}{5}s(t)+\frac{3}{5}f(t)\\
u_{21}^{1} &= -i\sqrt{\frac{3}{5}}e^{-(j_0+j_1)t}\,\omega_Q S_2 \rightarrow 0\\
u_{31}^{1} &= -\frac{\sqrt{6}}{5}e^{-(j_1+j_2)t}+\frac{\sqrt{6}}{5}e^{-(j_0+j_1)t}\left(C_2 + j_2 S_2\right) \rightarrow \frac{\sqrt{6}}{5}\left(f(t)-s(t)\right)\\
u_{22}^{1} &= e^{-(j_0+j_1)t}\left(C_2 - j_2 S_2\right) \rightarrow f(t)s(t)\\
u_{32}^{1} &= -i\sqrt{\frac{2}{5}}e^{-(j_0+j_1)t}\,\omega_Q S_2 \rightarrow 0\\
u_{33}^{1} &= \frac{3}{5}e^{-(j_1+j_2)t}+\frac{2}{5}e^{-(j_0+j_1)t}\left(C_2 + j_2 S_2\right) \rightarrow \frac{3}{5}s(t)+\frac{2}{5}f(t)
\end{aligned}
\tag{3.107}
$$

Similar results are obtained in [23] for single and double quantum coherence evolution. From the point of view of our approach, we can describe the calculation in [23] as performed from the very beginning in subspaces with given m (1 and 2). We consider that the operator approach is more illuminating, offering an overall image about the dynamics of the system.

4. ALGEBRAIC DESCRIPTION OF NMR EXPERIMENTS

In Section 4.1, the decomposition of the NMR signal in terms of coherence pathways is offered, based on the superspace description. The off-resonance effects are considered for both of the relevant regimes, namely, free relaxation and RF pulse application. In Section 4.2, the multiple quantum filtered (MQF) experiments are defined. Several concepts are introduced and precisely defined: T_2 filtered experiments (in which the contributions from the recovery of the longitudinal magnetization disappear), maximally filtered experiments (in which the contribution from exactly one coherence pathway survives). In Section 4.3, the classical one-, two-, and three-pulse experiments are theoretically analyzed and the predictions are verified on both phantom and in-vitro experiments (presented in Section 4.4). In Section 4.5, the TQ based determination of T_2 relaxation times, is presented.

4.1. Coherence pathway decomposition of NMR signal

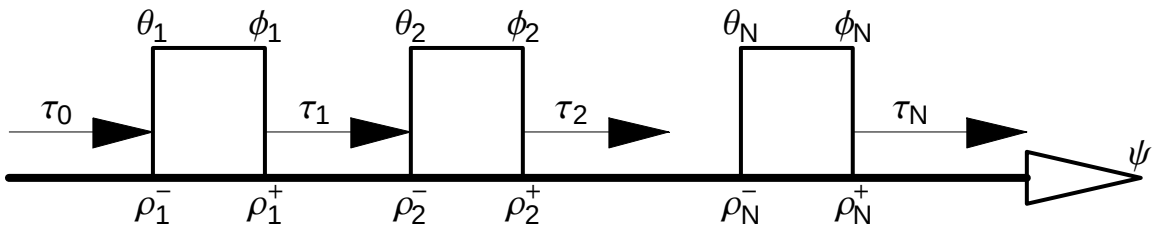

Figure 4.1 The generic, N-pulse sequence.

A general NMR experiment is realized as the repetition of the excitation–acquisition cycle schematically depicted in Figure 4.1. The excitation consists of a sequence of hard pulses, $P_1,\ldots,P_N$, characterized by the flip angles θ_k, the phases φ_k and followed by the delays τ_k. The initial delay, τ_0, is considered to be measured from the last excitation of the previous sequence. Measurements are performed at times $t=\tau_N$; whenever the quantity "t" is mentioned, the equality $t=\tau_N$ is understood.

The formation of the NMR signal can be described step by step, as a succession of hard pulses and free propagators. Denoting the density matrix before the k^{th} pulse as ρ^-_k and the density matrix after the k^{th} pulse as ρ^+_k, the evolution of the density matrix during the experiment is uniquely defined by the set of 2N supervectors ρ^-_1, $\rho^+_1,\ldots,$ ρ^-_N, ρ^+_N and it is schematically depicted below:

$$\rho_1^- \xrightarrow[\text{pulse}]{P(0)} \rho_1^+ \xrightarrow[\text{relax}]{U(1)} \rho_2^- \cdots \xrightarrow[\text{relax}]{U(N-1)} \rho_N^- \xrightarrow[\text{pulse}]{P(N)} \rho_N^+ \xrightarrow[\text{relax}]{U(N)} \rho(t).$$

Mathematically, according to the superspace formalism introduced in the previous sections, the signal is given by the chain of equations,

$$\begin{aligned} |\rho_k^+\rangle\rangle &= \mathbf{P}_k\,|\rho_k^-\rangle\rangle \\ |\rho_{k+1}^-\rangle\rangle &= \tilde{\mathbf{U}}_\delta(\tau_k)\bullet|\rho_k^+\rangle\rangle = \mathbf{U}_\delta(\tau_k)\,|\rho_k^+\rangle\rangle + |\rho_{rec}(\tau_k)\rangle\rangle \end{aligned}, \tag{4.1}$$

where, P_k is the superoperator associated with the k^{th} RF pulse

$$\mathbf{P}_k = \mathbf{P}(\theta_k, \varphi_k, \delta), \tag{4.2}$$

$U_\delta(\tau_k)$ is the superoperator associated with the free propagation during the time period τ_k, and $\rho_{rec}(\tau)$ describes the recovery of the longitudinal magnetization during the same period of time,

$$|\rho_{\text{rec}}(\tau_k)\rangle\rangle = \left(\mathbf{1} - \mathbf{U}_\delta(\tau_k)\right)|\rho_{\text{Eq}}\rangle\rangle\,. \tag{4.3}$$

At one end of the chain, by considering the inter sequence separation (*i.e.*,τ_0) long compared with both the longitudinal and transversal relaxation times, the starting point of the previous recurrence can be considered given by the equilibrium density matrix

$$|\rho_1^-\rangle\rangle \approx |\rho_{\text{rec}}(\tau_0)\rangle\rangle \approx |\rho_{\text{Eq}}\rangle\rangle \approx |10\rangle\rangle\,. \tag{4.4}$$

At the other end of the recurrence, the measured signal is the average of the transverse magnetization. For perfect quadrature detection when both X and Y projections are being measured, the signal can be considered as being the component m^+ of the magnetization. Due to its proportionality with the angular momentum, the quantity J^+ is measured, which is the l=1, m=1 component of the density matrix. Therefore, assuming a receiver phase ψ, the measured signal is given by

$$e^{i\psi}\tilde{S}_\delta(\vec{\theta}, \vec{\phi}, \vec{\tau}) = e^{i\psi}\langle\langle 11|\,\rho(\tau_N)\rangle\rangle\,. \tag{4.5}$$

In conclusion, the NMR signal is represented by the superspace expression,

$$\tilde{S}_\delta(\vec{\theta}, \vec{\phi}, \vec{\tau}) = \langle\langle 11|\,\tilde{\mathbf{U}}_\delta(\tau_N)\bullet\mathbf{P}_N\tilde{\mathbf{U}}_\delta\bullet(\tau_{N-1})\mathbf{P}_{N-1}\ldots\tilde{\mathbf{U}}_\delta(\tau_1)\bullet\mathbf{P}_1\,|\,\rho_{\text{rec}}(\tau_0)\rangle\rangle\,, \tag{4.6}$$

where the "~" notation denotes the fact that the recovery of longitudinal magnetization is taken into account, while the "δ" subscript emphasizes the off-resonance character of the calculation.

At this moment a numerical calculations can begin and such pathway have been followed in [24]. While possible, and, with the recent progresses in computer technology, not less practical, we consider the numerical approach not illuminating. In the approach we develop in this chapter, we are able to obtain information about the result of a certain experiment before any calculation takes place. Simply put, we want to be able to specify what really needs to be computed before to start computing.

Taking in to consideration (4.1), the last expression transforms in a sum of N terms, comprising a main (K=0) and N-1 residual signals (K≠0),

$$\mathrm{e}^{i\psi}\,\tilde{S}_{\delta}\left(\vec{\theta},\vec{\phi},\vec{\tau}\right)=\sum_{K=0}^{N-1}e^{i\psi}S_{\delta}^{(K)}\left(\vec{\theta},\vec{\phi},\vec{\tau}\right) \tag{4.7}$$

where each of the sub-signals is expressed as true matrix elements of products of linear operators

$$S_{\delta}^{(K)}\left(\vec{\theta},\vec{\phi},\vec{\tau}\right)=\langle\langle 11\,|\,\mathbf{U}_{\delta}\left(\tau_{N}\right)\mathbf{P}_{N}\left(\theta_{N},\phi_{N}\right)\ldots\mathbf{U}_{\delta}\left(\tau_{K+1}\right)\mathbf{P}_{K+1}\left(\theta_{K+1},\phi_{K+1}\right)|\,\rho_{\mathrm{rec}}\left(\tau_{K}\right)\rangle\rangle\,. \tag{4.8}$$

The source of the K^{th} contribution is the recovered longitudinal magnetization during the inter-pulse time period τ_K, therefore it is independent of the previous part of the sequence. The property of the K^{th} residual to have no dependence of the first K pulses makes it possible to design a filtering scheme in which all residual contributions are canceled. This class of filtered experiments named 'T_2 experiments' is described in this thesis and it will be explicitly characterized at in the next section. At this moment, the existence of such filtering scheme is just assumed. For T_2 experiments, after the filtering, the non-vanishing contribution comes from the main signal, only, and the relation, denoted by '$\underset{AF}{=}$', has the meaning that the equality holds after a proper filtering

$$S_{\delta}\left(\vec{\theta},\vec{\phi},\vec{\tau}\right)\underset{\mathrm{AF}}{=}S_{\delta}^{(0)}\left(\vec{\theta},\vec{\phi},\vec{\tau}\right)=\langle\langle 11\,|\,\mathbf{U}_{\delta}\left(\tau_{N}\right)\mathbf{P}_{N}\left(\theta_{N},\phi_{N}\right)\ldots\mathbf{U}_{\delta}\left(\tau_{1}\right)\mathbf{P}_{1}\left(\theta_{1},\phi_{1}\right)|\,10\rangle\rangle \tag{4.9}$$

The manifestations of the off-resonance RF irradiation have a double origin, in the hard pulse superoperator and in the propagators. First the RF pulses contains a dependence of δ described as

$$\mathbf{P}(\theta,\varphi,\delta)=\exp(-i\delta T_\theta \mathbf{L}_Z)\,\mathbf{P}(\theta,\varphi)\exp(-i\delta T_\theta \mathbf{L}_Z) \tag{4.10}$$

Second, the off-resonance propagators are described in terms of the on-resonance quantities

$$\mathbf{U}_\delta(\tau)=\exp(-i\delta\tau \mathbf{J}_Z)\,\mathbf{U}(\tau) \tag{4.11}$$

The effect of the off-resonance irradiation can be absorbed into the RF pulse phases. By using the properties

$$\begin{aligned}
&\mathrm{e}^{-i\delta\tau\mathbf{J}_Z}\,\mathbf{P}(\theta,\phi)=\mathrm{e}^{-i\delta\tau\mathbf{J}_Z}\,\mathrm{e}^{-i\phi\mathbf{J}_Z}\,\mathbf{P}(\theta,0)\mathrm{e}^{i\phi\mathbf{J}_Z}=\mathbf{P}(\theta,\varphi+\delta\tau)\mathrm{e}^{-i\delta\tau\mathbf{J}_Z}\\
&\mathrm{e}^{-i\delta\tau\mathbf{J}_Z}\,\mathbf{P}(\theta,\phi,\delta)=\mathrm{e}^{-i\delta\tau\mathbf{J}_Z}\,\mathrm{e}^{-i\delta T\mathbf{J}_Z}\,\mathrm{e}^{-i\phi\mathbf{J}_Z}\,\mathbf{P}(\theta,0)\mathrm{e}^{i\phi\mathbf{J}_Z}\,\mathrm{e}^{-i\delta T\mathbf{J}_Z}=\mathbf{P}\big(\theta,\varphi+\delta(\tau+T)\big)\mathrm{e}^{-i\delta\tau\mathbf{J}_Z}\,\mathrm{e}^{-i2\delta T\mathbf{J}_Z}
\end{aligned}, \tag{4.12}$$

in which T is the effective pulse length, any of the matrix elements in (4.8) is brought in the equivalent form

$$\begin{aligned}
&\langle\langle 11\,|\,\mathbf{U}_\delta(\tau_N)\mathbf{P}_N(\theta_N,\phi_N)\ldots\mathbf{U}_\delta(\tau_k)\mathbf{P}_k(\theta_k,\phi_k)\,|\,\rho_{\mathrm{rec}}(\tau_{K-1})\rangle\rangle=\\
&\langle\langle 11\,|\,\mathbf{U}(\tau_N)\mathbf{P}_N(\theta_N,\phi_N^\delta)\ldots\mathbf{U}(\tau_k)\mathbf{P}_k(\theta_k,\phi_k^\delta)\exp\big(-i\delta(\tau_N+2T_N\ldots+\tau_k+2T_k)\mathbf{J}_Z\big)\,|\,\rho_{\mathrm{rec}}(\tau_{K-1})\rangle\rangle
\end{aligned} \tag{4.13}$$

with the distorted phases defined by

$$\phi_m^\delta=\phi_m+\delta\left(\tau_N+T_N+\tau_{N-1}+2T_{N-1}+\ldots+\tau_{m+1}+2T_{m+1}+\tau_m+T_m\right). \tag{4.14}$$

The density matrix at the right hand side of (4.13) is longitudinal, therefore, the last exponential acts as the identity

$$\mathrm{e}^{-i\alpha\mathbf{J}_Z}\,|\,\rho_{\mathrm{rec}}(\tau)\rangle\rangle=|\,\rho_{\mathrm{rec}}(\tau)\rangle\rangle. \tag{4.15}$$

The result of this part of the discussion could be formulated: the off resonance signal is equivalent with the on resonance signal with distorted phases taking place of the original ones

$$e^{i\psi} S_\delta\left(\vec{\theta},\vec{\phi},\vec{\tau}\right) = e^{i\psi} S\left(\vec{\theta},\vec{\phi}^{\,\delta},\vec{\tau}\right). \tag{4.16}$$

The reverse is also true, once the on resonance signal as a function of the phases is known, the off resonance signal is obtained redefining the RF phases according to (4.14).

The explicit dependence of the matrix element $S\left(\vec{\theta},\vec{\phi},\vec{\tau}\right)$ on the RF phases is a prerequisite for phase cycling design. In order to obtain this information, the projectors over subspaces with given quantum magnetic numbers m, $\mathbf{M}_m = \sum_{l=|m|}^{3} |lm\rangle\rangle\langle\langle lm|$ are used. By expanding the propagators and hard pulses in terms of the m-projectors,

$$\begin{aligned} \mathbf{U}(t) &= \sum_m \mathbf{U}(t)\mathbf{M}_m \\ \mathbf{P}(\theta,\phi) &= \sum_{m,\mu} \mathrm{e}^{i\phi(\mu-m)}\, \mathbf{M}_m \mathbf{P}(\theta)\mathbf{M}_\mu \end{aligned} \tag{4.17}$$

Using this decomposition, the signal is given by the sum over intermediate magnetic numbers

$$\mathrm{e}^{i\psi}\, S_\delta\left(\vec{\theta},\vec{\phi},\vec{\tau}\right) = \sum\nolimits_{\vec{m}} \mathrm{e}^{i\psi}\, \mathrm{e}^{-i\vec{\xi}\vec{\phi}}\, \mathrm{e}^{-i\delta\vec{m}\vec{\tau}}\, \mathrm{e}^{-i\delta\vec{m}\vec{\eta}}\, A_{\vec{m}}\left(\vec{\theta},\vec{\tau}\right) \tag{4.18}$$

where the auxiliary quantities, the "coherence-transfer pathway" vector $\vec{\xi}$, [25], and the "pathway vector" $\vec{m}$ [26] are given by

$$\begin{aligned} \vec{\xi} &= \left(m_1, m_2 - m_1, \cdots, m_{N-1} - m_{N-2}, 1 - m_{N-1}\right) \\ \vec{m} &= \begin{pmatrix} m_1 & m_2 & \cdots & m_{N-1} & m_N \end{pmatrix} \end{aligned} \tag{4.19}$$

Also, we introduce the vector of effective delay times, which takes in consideration the finite width of the pulses by

$$\begin{aligned} \eta_k &= T_k^{eff} + T_{k+1}^{eff}, \quad k = 1,\cdots,N-1 \\ \eta_N &= T_N^{eff} \end{aligned}. \tag{4.20}$$

In the previous expression, we denote the effective pulse width, in the approximation introduced before:

$$T_k^{eff} = \begin{cases} T_k \dfrac{2}{\pi} & \text{if } \theta_k \sim \dfrac{\pi}{2} \\ 0 & \text{if } \theta_k \sim \pi \end{cases}.$$

The summation in (4.18) is restricted at both ends, m_1=-1, 0, 1 and m_N=1therefore there are $3\times7^{N-2}$ distinct terms in summation for N≥2, and a single term for N=1. For T_2 experiments, due to the restrictions m_1= -1,1 and $m_i\neq0$, only $2x6^{N-2}$ terms survive

$$\mathrm{e}^{i\psi}\, S_\delta\left(\vec{\theta},\vec{\phi},\vec{\tau}\right) \underset{\mathrm{AF}}{=} \sum_{m_1=-1}^{1} \sum_{m_2,\ldots m_{N-1}=-3}^{3} \mathrm{e}^{i\psi}\, \mathrm{e}^{-i\vec{\xi}\vec{\phi}}\, \mathrm{e}^{-i\delta\vec{m}\vec{\tau}}\, \mathrm{e}^{-i\delta\vec{m}\vec{\eta}}\, A_{\vec{m}}\left(\vec{\theta},\vec{\tau}\right)\Big|_{m_N=1, m_i\neq0} . \tag{4.21}$$

The complex amplitudes

$$A_{\vec{m}} = \langle\langle 11 \,|\, \mathbf{M}_{m_N} \mathbf{U}\left(\tau_N\right) \mathbf{M}_{m_N} \mathbf{P}\left(\theta_N\right) \ldots \mathbf{M}_{m_1} \mathbf{U}\left(\tau_1\right) \mathbf{M}_{m_1} \mathbf{P}\left(\theta_1\right) \,|\, 10\rangle\rangle \tag{4.22}$$

can be further expressed in terms of propagator and hard pulse matrix elements

$$A_{\vec{m}} = \sum_{l_{N-1}=|m_{N-1}|}^{3} \cdots \sum_{l_2=|m_2|}^{3} u_{l_N l_{N-1}}^{m_N}\left(\tau_N\right) p_{l_{N-1}}^{m_N m_{N-1}}\left(\theta_N\right) \ldots u_{l_2 l_1}^{m_2}\left(\tau_2\right) p_{l_1}^{m_2 m_1}\left(\theta_2\right) u_{l_1 l_0}^{m_1}\left(\tau_1\right) p_{l_0}^{m_1 m_0}\left(\theta_1\right) \tag{4.23}$$

with the constraints l_N=1, m_N=1, m_0=0. In a compact notation

$$\mathrm{e}^{i\psi}\, S_\delta\left(\vec{\theta},\vec{\phi},\vec{\tau}\right) \underset{\mathrm{AF}}{=} \sum_{\vec{m}} \mathrm{e}^{i\psi}\, \mathrm{e}^{-i\vec{\xi}\vec{\phi}}\, \mathrm{e}^{-i\delta\vec{m}\vec{\tau}}\, \mathrm{e}^{-i\delta\vec{m}\vec{\eta}} \sum_{\vec{l}>\vec{m}} U_{\vec{l},1}^{\vec{m}}\left(\vec{\tau}\right) P_{\vec{l},1}^{\vec{m},0}\left(\vec{\theta}\right) \tag{4.24}$$

where the following products of matrix elements are defined

$$\begin{aligned} U_{\vec{l},\lambda}^{\vec{m}}\left(\vec{\tau}\right) &= \prod_{\alpha=1}^{N} u_{l_\alpha l_{\alpha-1}}^{m_\alpha}\left(\tau_\alpha\right), \quad l_0 = \lambda \\ P_{\vec{l},\lambda}^{\vec{m},\mu}\left(\vec{\theta}\right) &= \prod_{\alpha=1}^{N} p_{l_{\alpha-1}}^{m_\alpha m_{\alpha-1}}\left(\theta_\alpha\right), \quad l_0 = \lambda, \mathrm{m}_0 = \mu \end{aligned} \tag{4.25}$$

and the inequality $\vec{l} \geq \vec{m}$ is understood as $l_i \geq m_i$, for each i=1,…,N. When there is no possibility of confusion, the short forms are used

$$\begin{aligned} U_{l_1 \cdots l_{N-1}}^{m_1 \cdots m_{N-1}} &\equiv U_{\vec{l},1}^{\vec{m}}\left(\vec{\tau}\right) \equiv U_{\vec{l}}^{\vec{m}} \\ P_{l_1 \cdots l_{N-1}}^{m_1 \cdots m_{N-1}} &\equiv P_{\vec{l},1}^{\vec{m},0}\left(\vec{\theta}\right) \equiv P_{\vec{l}}^{\vec{m}} \end{aligned} \tag{4.26}$$

The advantage of this formalism resides in the fact that it automatically generates the coherence pathways in a form suitable for symbolic calculation. The study of various filtering schemes can be realized without explicit calculation of the amplitudes. The analytic form of the signal, (4.24), offers a clear description of the maximum amount of information that could be extracted from pulsed NMR experiments.

4.2. Multiple quantum filtered NMR

The phase cycling filtering of the signal is performed by averaging the signal N_F times, over pulses phases, ϕ, and receiver phases, ψ. The filtered signal (denoted with superscript F) is the sum

$$S^F = \frac{1}{N_F} \sum_{\vec{\phi},\psi} \left\{ \mathrm{e}^{i\psi} \, S_\delta \left(\vec{\theta}, \vec{\phi}, \vec{\tau} \right) \right\} \tag{4.27}$$

By applying the summation on the coherence pathways representation, and by performing the sum over phases first, the signal takes a form similar to the original (4.18)

$$S^F = \sum_{\vec{m}} A_{\vec{m}} \left(\vec{\theta}, \vec{\tau} \right) \, f_{\vec{m}} \, \mathrm{e}^{-i\delta \vec{m} (\vec{\tau} + \vec{\eta})} \tag{4.28}$$

where, now, the filtering-scheme-dependent coefficients, f_m, appear

$$f_{\vec{m}} \equiv \frac{1}{N_F} \sum_{\vec{\phi},\psi} \mathrm{e}^{i\left(\psi - \vec{\xi}\vec{\phi}\right)} \, . \tag{4.29}$$

The contribution of a given pathway $\vec{m}$ is canceled by the filtering provided that $f_{\vec{m}} = 0$, and this is the basic property of MQF experiments [25].

Using the results above, the class of T_2 experiments can be properly defined. A T_2 experiment is a filtered experiment in which $f_{\vec{m}}$ vanishes whenever an intermediate magnetic quantum number, m_i, is zero.

The connection with the NMR experiments requires, as a supplementary step, spatial averaging over a distribution of both offset values and flip angles. For simplicity, it is assumed that the distribution of flip angles is independent of the off resonance distribution. The averages denoted $\langle\ \rangle_\theta$ and $\langle\ \rangle_\delta$ can then be performed separately, bringing the measured signal to the form

$$\left\langle S^F(t)\right\rangle = \sum_{\vec{m}} f_{\vec{m}} \left\langle \mathrm{e}^{-i\delta\vec{m}(\vec{\tau}+\vec{\eta})}\right\rangle_\delta \left\langle A_{\vec{m}}\left(\vec{\theta},\vec{\tau}\right)\right\rangle_\theta = \sum_{\vec{m}} f_{\vec{m}} \left\langle \mathrm{e}^{-i\delta\vec{m}\vec{\tau}}\right\rangle_\delta \sum_{\vec{l}\geq\vec{m}} \left\langle P_{\vec{l}}^{\vec{m}}\left(\vec{\theta}\right)\right\rangle_\theta U_{\vec{l}}^{\vec{m}}\left(\vec{\tau}\right). \quad (4.30)$$

Note that, because the distribution of inhomogeneities is unknown, the averages $\left\langle P_{\vec{l}}^{\vec{m}}\left(\vec{\theta}\right)\right\rangle_\theta$ as well as $\left\langle \mathrm{e}^{-i\delta\vec{m}(\vec{\tau}+\vec{\eta})}\right\rangle_\delta$ are also unknown, which renders the direct fit of (4.30) unreliable for the purpose of determining physical properties of the system. Further implications of this observation are discussed below.

A component, $\vec{m}$, and its associated pathway, is called "echo-like" if the quantity

$$t_0 = -\vec{m}\left(\vec{\tau}+\vec{\eta}\right) \geq 0 \quad (4.31)$$

For echo-like components, the off-resonance dependent factor becomes exactly one at the time $\tau_N=t_0$ during the measurement period. Provided that a filtering scheme can be designed to select such a component, $\vec{m}$, the direct, non-B_0 biased, determination of the quantity

$$\left\langle A_{\vec{m}}\left(\vec{\theta},\vec{\tau}\right)\right\rangle_\theta = \sum_{\vec{l}>\vec{m}} \left\langle P_{\vec{l}}^{\vec{m}}\left(\vec{\theta}\right)\right\rangle_\theta U_{\vec{l}}^{\vec{m}}\left(\vec{\tau}\right) \quad (4.32)$$

is attainable, by performing a multidimensional experiment. By contrast, for the non-echo components, any measurement is biased by the effect of the B_0 inhomogeneities.

Due to B_1 inhomogeneities, the averages $\left\langle P_{\vec{l}}^{\vec{m}}\left(\vec{\theta}\right)\right\rangle_\theta$ are unknown, independent quantities rendering the direct fit of (4.32) unreliable, unless a factorization of the flip angle dependent terms is possible.

Two strategies are possible for experimentally measuring the products of matrix elements $U_{\vec{l}}^{\vec{m}}\left(\vec{\tau}\right)$, namely, the "variable echo" and "fixed echo" time strategies.

In the "variable echo" time strategy, only one, echo-like, coherence pathway is selected. By simultaneously varying the pulse delays, the quantity $U_{\vec{l}}^{\vec{m}}\left(\vec{\tau}\right)$ is measured for $\vec{m}\left(\vec{\tau}+\vec{\eta}\right)=0$, up to a multiplicative constant. In general this approach is undermined by the occurrence of multiple terms with different principal quantum numbers $\vec{l}$ in the summation (4.32). The only cases in which the selection of a single coherence pathway is possible is given by maximally quantum filtered signals, when only the coherences with extreme values of magnetic numbers survive

$$\left|m_1\right|=1,\ \left|m_2\right|=,\ldots,=\left|m_{N-1}\right|=3,\ m_N=1. \tag{4.33}$$

The other possible approach, the "fixed echo" time strategy, requiring also the maximal filtering, is possible when the position of the echo is kept constant

$$\tau_E\equiv\vec{m}\left(\vec{\tau}+\vec{\eta}\right)=\text{const.} \tag{4.34}$$

The signal acquired is proportional with the expression

$$S^F\left(t\right)\approx u_{10}^{m_1}\left(\tau_1\right)\ldots u_{l_{N-1}l_{N-2}}^{m_{N-1}}\left(\tau_{N-1}\right)u_{l_Nl_{N-1}}^{m_N}\left(t\right)\left\langle e^{i\delta\left(t-\tau_E\right)}\right\rangle_\delta \tag{4.35}$$

from where, by integrating over the acquisition time, the following non-biased expression is obtained

$$\int_{t_1}^{t_2}w\left(t\right)S^F\left(t\right)dt\approx u_{10}^{m_1}\left(\tau_1\right)\ldots u_{l_{N-1}l_{N-2}}^{m_{N-1}}\left(\tau_{N-1}\right). \tag{4.36}$$

While the specific choice of the windowing function, w(t), is not important from the point of view of the information provided by the experiment, it may affect the SNR of the experiment.

In imaging, a different class of MQF experiments is constructed, which has as a purpose the detection of the sodium ions in non-trivial environments. In this class of experiments, the quantity of interest is the total signal. From the SNR point of view, it is more convenient to acquire many components (echo and non-echo) together. The manifestation of B_0 inhomogeneity in the sum given by (4.30) is the possible destructive interference between various components. In some special cases, as long as the cancellation is not severe, and the B_0 distribution can be estimated (by performing different experiments) this effect can be corrected at the data processing stage. In the cases of severe cancellation, this direct approach fails, therefore different methods have to be designed that avoids he cancellation at the data acquisition stage.

4.3. Theoretical description of NMR experiments

In this subsection, the classical 1-, 2- and 3-pulse NMR experiments are analyzed using the coherence decomposition formalism. The pulse lengths are ignored; they can be always introduced at the end of the analysis, by using simple substitution rules. Apart of the illustration of the formalism, the main result of this section is represented by the offered prescription for TQ filtering schemes selecting various combinations of coherence pathways.

4.3.1. One Pulse Experiment

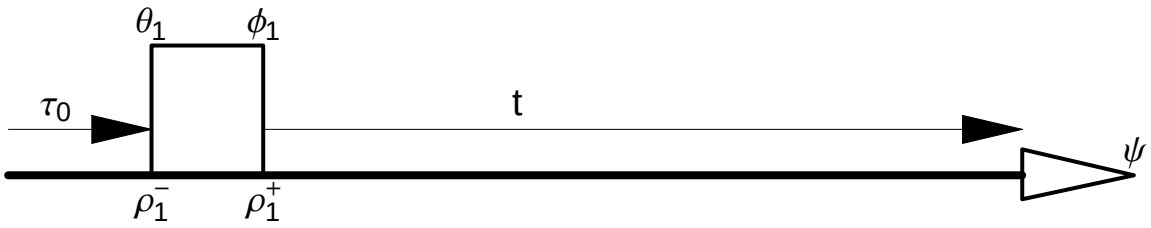

Figure 4.2 The schematic representation of the one-pulse experiment

The one pulse experiment, presented schematically in Figure 4.2, is often used in NMR for calibrating the 90° pulse. The signal measured is given, in the infinite repetition time limit, by

$$S_\delta\left(\theta_1,\phi_1,\psi,t\right)=e^{i\psi}\langle\langle 11\,|\,\mathbf{U}_\delta\left(t\right)\mathbf{P}\left(\theta_1,\phi_1\right)|\,10\rangle\rangle=e^{i(\psi-\phi_1-\delta t)}u_{11}^{1}\left(t\right)p_1^{10}\left(\theta\right) \tag{4.37}$$

The filtering scheme, based on addition-subtraction with $\phi_1=k\pi,\psi=k\pi,k=0,1$ (used in order to avoid DC baselines in the collected FID) produces the signal

$$S_\delta^F\left(\theta,t\right)=e^{-i\delta t}u_{11}^{1}\left(t\right)p_1^{10}\left(\theta\right)=\frac{i}{\sqrt{2}}e^{-i\delta t}u_{11}^{1}\left(t\right)\sin\theta\,. \tag{4.38}$$

After the average over B_0 and B_1 fields is taken

$$S_{macro}\left(t\right)=\left\langle e^{-i\delta t}u_{11}^{1}\left(t\right)p_1^{10}\left(\theta\right)\right\rangle_{\delta,\theta}\approx\left\langle e^{-i\delta t}\right\rangle_\delta u_{11}^{1}\left(t\right)\left\langle\sin\theta\right\rangle_\theta \tag{4.39}$$

The general form of the matrix element $u_{11}^{1}\left(t\right)$ is given in

The presence of the time dependent term $\left\langle \mathrm{e}^{-i\delta t}\right\rangle_\delta$ makes the direct fit of the FID in (4.39) unreliable for the estimation of the actual relaxation rates, unless special precautions are taken in preparing the sample. Nevertheless, variations of the one pulse experiment can be used to experimentally estimate the (in) homogeneity of the B_1 field.

4.3.2. Two-pulse Experiment

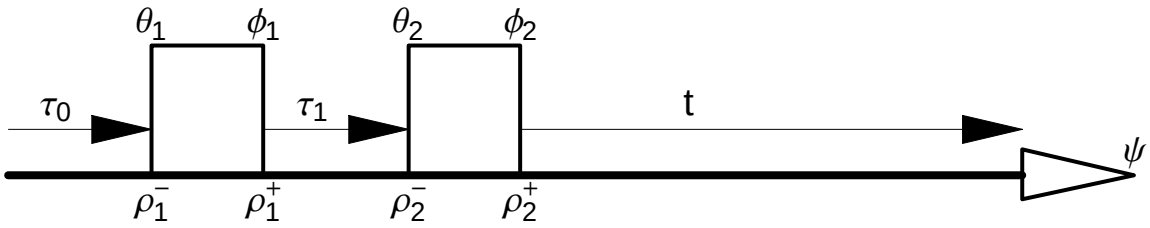

Figure 4.3 the schematic representation of the two-pulses experiment

The schematic representation of a two-pulse NMR experiment is presented in Figure 4.3. One of the most useful and non-trivial, applications of this generic pulse-acquire structure is the description of a spin echo experiment. For a given separation τ_1 between the pulses, the measured signal at time $t=\tau_2$ is given by,

$$e^{i\psi} S_\delta(\theta_1,\theta_2,\phi_1,\phi_2,\tau_1,t) = e^{i\psi}\langle\langle 11 | \mathbf{U}_\delta(t)\mathbf{P}(\theta_2,\phi_2)\mathbf{U}_\delta(\tau_1)\mathbf{P}(\theta_1,\phi_1)|10\rangle\rangle \tag{4.40}$$

In general, there are three distinct components: echo, residual, and non-echo (m_1=-1, 0, 1, respectively)

$$e^{i\psi} S_\delta = e^{i\psi - i\delta t}\left(e^{-i(2\phi_2-\phi_1)+i\delta\tau_1} A_{-1} + e^{-i\phi_2} A_0 + e^{-i\phi_1 - i\delta\tau_1} A_1\right), \tag{4.41}$$

where,

$$A_m(\theta_1,\theta_2,\tau_1,t) = \sum_{l=1}^{3} u_{l1}^1(t) u_{l1}^m(\tau_1) p_l^{1m}(\theta_2) p_1^{0m}(\theta_1). \tag{4.42}$$

To cancel the residual components (*i.e.* to obtain a T_2 experiment) using phase-cycling, the following condition has to be fulfilled

$$\sum_{\phi_2,\psi} e^{i(\psi-\phi_2)} = 0. \tag{4.43}$$

The pure echo component can thus be selected with a four phase scheme, satisfying the condition above, namely,

$$\phi_1 = -k\pi/2 \quad \phi_2 = 0 \quad \psi = k\pi/2, \quad k = 0,1,2,3. \tag{4.44}$$

After averaging over flip angles (to account for spatial inhomogeneities in the B_1 field) and B_0 inhomogeneities the macroscopic signal becomes,

$$S_{macro}^{F,-1}(\theta_1,\theta_2,\tau_1,t) = \left\langle e^{-i\delta(t-\tau_1)} \right\rangle_\delta \left\langle A_{-1}(\theta_1,\theta_2,\tau_1,t) \right\rangle_\theta . \tag{4.45}$$

Making use of the propagator property $U(t+\tau_1)=U(t)U(\tau_1)$, together with the symmetry relation $u_{lk}^{-m} = (-)^{l+k} u_{lk}^{m}$ the sum-of-times matrix element

$$u_{11}^{1}(t+\tau_1) = u_{11}^{1}(t)u_{11}^{-1}(\tau_1) - u_{21}^{1}(t)u_{21}^{-1}(\tau_1) + u_{31}^{1}(t)u_{31}^{-1}(\tau_1) \tag{4.46}$$

can be formed, and the amplitude of the echo component takes the form

$$i\sqrt{2}A_{-1} = \sin\theta_1 \left(\sin^2\frac{\theta_2}{2} u_{11}^{1}(t+\tau_1) - \sin^2\theta_2 u_{21}^{1}(t)u_{21}^{1}(\tau_1) - \frac{5}{8}\sin^2\theta_2(1-3\cos\theta_2)u_{31}^{1}(t)u_{31}^{1}(\tau_1) \right). \tag{4.47}$$

In particular, when the B_1 field is homogeneous the flip angle can be ideally calibrated, the condition $\theta_1=\pi/2$, $\theta_2=\pi$ is then easily realized leading to the following expression for the measured signal,

$$S_{macro}^{F,-1}\left(\frac{\pi}{2},\pi,\tau_1,t\right) = \left\langle e^{-i\delta(t-\tau_1)} \right\rangle_\delta u_{11}^{1}(t+\tau_1). \tag{4.48}$$

In this ideal case, it is possible to extract the function $u_{11}^{1}(2t)$ by a 2D experiment in which the delay between pulses, τ_1, is varied and the measurement takes place at the time $t=\tau_1$. In the general case, when the B_1 is not uniform across the sample volume, the quantity determined by the 2D experiment is the more complex $\left\langle A_{-1}(\theta_1,\theta_2,t,t) \right\rangle_\theta$

$$\left\langle A_{-1}\left(\theta_1,\theta_2,t,t\right)\right\rangle_\theta = \left\langle \sin\theta_1 \sin^2\frac{\theta_2}{2}\right\rangle_\theta u_{11}^1\left(2t\right) - \left\langle \sin\theta_1 \sin^2\theta_2\right\rangle_\theta u_{21}^1\left(t\right)u_{21}^1\left(t\right) - \frac{5}{8}\left\langle \sin\theta_1 \sin^2\theta_2\left(1-3\cos\theta_2\right)\right\rangle_\theta u_{31}^1\left(t\right)u_{31}^1\left(t\right) \tag{4.49}$$

For liquids, the identities $u_{21}^1 = u_{31}^1 = 0$ ensure the determination of $u_{11}^1\left(2t\right)$ even under non-ideal conditions

$$S_{macro,liquids}^{F,-1}\left(\theta_1,\theta_2,t,t\right) \approx \left\langle \sin\theta_1 \sin^2\frac{\theta_2}{2}\right\rangle_\theta u_{11}^1\left(2t\right). \tag{4.50}$$

In the general case, the flip angle dependent contributions from u_{21}^1 and u_{31}^1 terms make the direct extraction of u_{11}^1 in the presence of B_1 inhomogeneities impossible. Under such conditions, the extraction of physical parameters (relaxation rates) becomes unreliable. A similar conclusion has already been reached by Brown *et al*. [27]. In Brown's report, however, the unstable nature of a non-linear fit to a sum of three exponentials was described as the leading reason for the unsuitability of a two-pulse experiment as a mean to measure relaxation rates. Our analysis here indicates that, even for accurate fit, the biased nature of the 90°-180° experiment in the presence of B_1 inhomogeneities makes the estimation of relaxation rates unreliable.

As a further example, we consider the case in which the static quadrupolar interaction is absent. Under such conditions, the Hahn echo experiment produces a signal, which, at measurement time t is proportional to

$$A_{-1}^H = \left\langle \sin\theta_1 \sin^2\frac{\theta_2}{2}\right\rangle_\theta \left(\frac{3}{5}f^2 + \frac{2}{5}s^2\right) - \frac{5}{8}\left\langle \sin\theta_1 \sin^2\theta_2\left(1-3\cos 2\theta_2\right)\right\rangle_\theta \left(\frac{\sqrt{6}}{5}f - \frac{\sqrt{6}}{5}s\right)^2. \tag{4.51}$$

For this signal, the five parameter function,

$$a\frac{1}{5}\left(3\mathrm{e}^{-2t/T_f} + 2\mathrm{e}^{-2t/T_s}\right) - b\frac{6}{25}\left(\mathrm{e}^{-t/T_s} - \mathrm{e}^{-t/T_f}\right)^2 + c \tag{4.52}$$

is the natural choice for the extraction of the relaxation parameters with the amplitudes given by

$$a = \left\langle \sin\theta_1 \sin^2 \frac{\theta_2}{2} \right\rangle_\theta$$
$$b = \frac{5}{8}\left\langle \sin\theta_1 \sin^2 \theta_2 \left(1 - 3\cos 2\theta_2\right) \right\rangle_\theta \tag{4.53}$$

In the ideal situation of both perfect calibration and B_1 homogeneous field b=0. Note, however, that in the presence of B_1 inhomogeneities the calibration of the 180° pulse only guarantees that $\langle \sin\theta_2 \rangle_\theta = 0$ and the quantity $\frac{5}{8}\left\langle \sin\theta_1 \sin^2 \theta_2 \left(1 - 3\cos 2\theta_2\right) \right\rangle_\theta$ could be still non-zero. A fit to the first term of (4.52) (the standard bi-exponential form used in the literature) will still be biased leading to a poor determination of the underlying relaxation rates. The bias, reflected by the presence of the b-term, depends on the B_1 distribution in the sample, which depends in turn on the shape of the sample and coil-sample geometry. As a result of the strong correlation between the parameters obtained by nonlinear fit, the relaxation times are themselves biased.

4.3.3. Three-pulse experiment

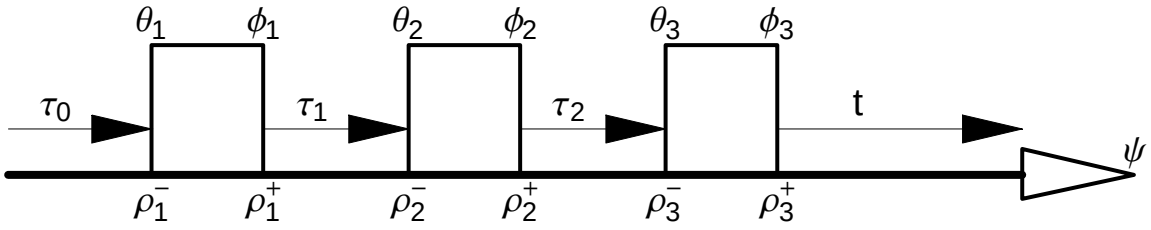

Figure 4.4 the schematic representation of the three pulse experiment.

Using the diagram in Figure 4.4, we have that the relevant matrix element giving the signal at time t=τ_3, for the three-pulse experiments, reads

$$e^{i\psi} S_\delta\left(\vec{\theta},\vec{\phi},\vec{\tau}\right) = e^{i\psi}\langle\langle 11 \,|\, \mathbf{U}\left(\tau_3\right)\mathbf{P}_3\mathbf{U}\left(\tau_2\right)\mathbf{P}_2\mathbf{U}\left(\tau_1\right)\mathbf{P}_1 \,|\, 10\rangle\rangle \tag{4.54}$$

from where the decomposition in terms of coherences reads

$$\mathrm{e}^{i\psi}\, S_\delta\left(\vec{\theta},\vec{\phi},\vec{\tau}\right) = \sum_{m_1=-1}^{1}\sum_{m_2=-3}^{3} \mathrm{e}^{i\psi}\, \mathrm{e}^{-i\left(m_1\phi_1+m_2(\phi_2-\phi_1)+(\phi_3-\phi_2)\right)}\, \mathrm{e}^{-i\delta\left(m_1\tau_1+m_2\tau_2+\tau_3\right)}\, A_{m_1m_2}\left(\vec{\theta},\vec{\tau}\right), \tag{4.55}$$

with the individual amplitudes having the explicit form (4.23),

$$A_{m_1m_2} = \sum_{l_\alpha=|m_\alpha|}^{3} u^{1}_{1l_2}\left(\tau_3\right) u^{m_2}_{l_2l_1}\left(\tau_2\right) u^{m_1}_{l_11}\left(\tau_1\right) p^{1m_2}_{l_2}\left(\theta_3\right) p^{m_2m_1}_{l_1}\left(\theta_2\right) p^{m_1 0}_{1}\left(\theta_1\right) = \sum_{l_\alpha=|m_\alpha|}^{3} U^{m_1m_2}_{l_1l_2} P^{m_1m_2}_{l_1l_2} \tag{4.56}$$

According to our previous discussion regarding the off-resonance RF pulses, whenever the RF pulses are considered of non-zero width, in the terms multiplying the inhomogeneity parameter, δ, it is understood that the delays are modified by the substitutions

$$\begin{aligned} \tau_1 &\to \tau_1 + 2T_{\mathrm{eff}} \\ \tau_2 &\to \tau_1 + 2T_{\mathrm{eff}} \\ \tau_3 &\to \tau_3 + T_{\mathrm{eff}} \end{aligned}, \tag{4.57}$$

where the effective pulse length is defined in terms of the RF pulse duration, T, by

$$T_{\text{eff}} = T\frac{1}{\theta}\tan\frac{\theta}{2} \approx T\frac{2}{\pi}. \tag{4.58}$$

The nature of most manipulation, make it safe for us to perform the substitutions at the very end of the calculation, as the "true" propagation times are always arguments of the propagator matrix elements, while the apparent delays are occurring only in the exponentials, multiplying the inhomogeneity, δ.

The classification for the terms occurring in (4.55) is straightforward. For a T_2 experiment, there are twelve terms, from which, as a general rule, six are echo like. There are exceptional situations when $\tau_2 \approx k\tau_1/2$, k=0,…,6. When the condition $\tau_2 < \tau_1/3$ is fulfilled, the six echoes are located at

$$\tau_3^{\text{e}}\left(m_2\right) = \tau_1 - m_2\tau_2, m_2 = -3,\ldots 3, m_2 \neq 0 \tag{4.59}$$

Even though the effect of the last two successive RF pulses is equivalent to that of a single RF pulse, the additional freedom to manipulate the relative phase between them allows the selection of a given m_2 order, therefore, reducing the number of matrix element products $u_{l1}^{1}u_{l1}^{m}$ entering in the summation in (4.56).

By selecting only the coherence pathways with $m_2=\pm 3$ (named here "total TQ filtering"), the corresponding amplitudes are completely factored

$$A_{m_1=\pm 1, m_2=\pm 3}\left(\vec{\theta},\vec{\tau}\right) = P_{33}^{m_1 m_2}\left(\vec{\theta}\right)U_{33}^{13}\left(\vec{\tau}\right) = P_{33}^{m_1 m_2}\left(\vec{\theta}\right)u_{31}^{1}\left(\tau_1\right)u_{33}^{3}\left(\tau_2\right)u_{31}^{1}\left(\tau_3\right). \tag{4.60}$$

The relevant, flip angle dependent, coefficients, organized in a matrix form for clarity, are given by

$$\begin{pmatrix} P_{33}^{-1,-3} \\ P_{33}^{-1,3} \\ P_{33}^{1,-3} \\ P_{33}^{1,3} \end{pmatrix} = \frac{15i}{16\sqrt{2}}\sin\theta_1\sin^2\theta_2\sin^2\theta_3 \begin{pmatrix} -c_2 s_3 \\ -s_2 c_3 \\ c_2 c_3 \\ s_2 s_3 \end{pmatrix}, \quad \text{with} \quad \begin{aligned} c_\alpha &= \cos^2\frac{\theta_\alpha}{2} \\ s_\alpha &= \sin^2\frac{\theta_\alpha}{2} \end{aligned} \tag{4.61}$$

In the case of identical pulses, with common flip angle $\theta_1 = \theta_1 = \theta_1 = \theta$,

$$\begin{pmatrix} P_{33}^{-1,-3} \\ P_{33}^{-1,3} \\ P_{33}^{1,-3} \\ P_{33}^{1,3} \end{pmatrix} = \sin^5\theta \begin{pmatrix} -\cos^2(\theta/2)\sin^2(\theta/2) \\ -\cos^2(\theta/2)\sin^2(\theta/2) \\ \cos^4(\theta/2) \\ \sin^4(\theta/2) \end{pmatrix} \tag{4.62}$$

When $\tau_2<\tau_1/3$, only the components (-1,±3) give echoes, located at $\tau_3=\tau_1\pm3\tau_2$. For $\tau_2>\tau_1/3$the echoes are given by the components (-1,-3) and (1, -3). In the most selective experiments, the individual components are isolated. This can be realized using cycling schemes with ten phases

$$\phi_1 = \alpha_1 k\pi/5 \quad \phi_2 = \alpha_2 k\pi/5 \quad \phi_3 = \alpha_3 k\pi/5 \quad \psi = k\pi \quad k = 0,\ldots,9 \tag{4.63}$$

with the coefficients for each component given in the following table

	TQ^{-+}	TQ^{--}	TQ^{+-}	TQ^{++}
(m_1, m_2)	$(-1,+3)$	$(-1,-3)$	$(+1,-3)$	$(+1,+3)$
α_1	1	1	1	1
α_2	2	0	0	4
α_3	1	–2	1	7

(4.64)

The selection of both echo components is realized with the eighteen-phase scheme, TQ^-

$$\phi_1 = \frac{\pi}{9}k \quad \phi_2 = \frac{2\pi}{9}k \quad \phi_3 = -\frac{\pi}{9}k \quad \psi = k\pi \quad k = 0,\ldots,17\,. \tag{4.65}$$

Finally, the simultaneous acquisition of all four TQ components is realized with the following composite twelve phases cycle (TQ)

$$\begin{cases} \phi_1 = \frac{\pi}{3}k + \frac{\pi}{6} \quad \phi_2 = \frac{\pi}{3}k - \frac{\pi}{3} \quad \phi_3 = 0 \quad \psi = k\pi \quad k = 0,\ldots,5 \\ \phi_1 = \frac{\pi}{3}k + \frac{5\pi}{6} \quad \phi_2 = \frac{\pi}{3}k - \frac{\pi}{3} \quad \phi_3 = 0 \quad \psi = k\pi + \pi \quad k = 6,\ldots,11 \end{cases} \tag{4.66}$$

The additional six phases, compared with are introduced to obtain a T_2 experiment.

The introduced experiments give the filtered signals

$$S_{\delta}^{-1,3} = \frac{15\,\mathrm{e}^{-i\delta(\tau_3-\tau_1-3\tau_2)}}{16\sqrt{2}i} U_{33}^{13}(\vec{\tau}) \sin\theta_1 \sin^2\theta_2 \sin^2\theta_3 \sin^2\frac{\theta_2}{2}\cos^2\frac{\theta_3}{2} \tag{4.67}$$

$$S_{\delta}^{-1,-3} = \frac{15\,\mathrm{e}^{-i\delta(\tau_3-\tau_1+3\tau_2)}}{16\sqrt{2}i} U_{33}^{13}(\vec{\tau}) \sin\theta_1 \sin^2\theta_2 \sin^2\theta_3 \cos^2\frac{\theta_2}{2}\sin^2\frac{\theta_3}{2} \tag{4.68}$$

$$S_{\delta}^{-1,\pm 3} = \frac{15\,\mathrm{e}^{-i\delta(\tau_3-\tau_1)}}{16\sqrt{2}i} U_{33}^{13}(\vec{\tau}) \sin\theta_1 \sin^2\theta_2 \sin^2\theta_3 \left(\mathrm{e}^{3i\delta\tau_2} \cos^2\frac{\theta_2}{2}\sin^2\frac{\theta_3}{2} + \mathrm{e}^{-3i\delta\tau_2} \sin^2\frac{\theta_2}{2}\cos^2\frac{\theta_3}{2} \right) \tag{4.69}$$

$$\begin{aligned} S_{\delta}^{\pm 1,\pm 3} = \frac{15\,\mathrm{e}^{-i\delta\tau_3}}{16\sqrt{2}} U_{33}^{13}(\vec{\tau}) \sin\theta_1 \sin^2\theta_2 \sin^2\theta_3 \Bigg\{ & \mathrm{e}^{+i\delta\tau_1} \left[\mathrm{e}^{-3i\delta\tau_2} \sin^2\frac{\theta_2}{2}\cos^2\frac{\theta_3}{2} + \mathrm{e}^{3i\delta\tau_2} \cos^2\frac{\theta_2}{2}\sin^2\frac{\theta_3}{2} \right] \\ & + \mathrm{e}^{-i\delta\tau_1} \left[\mathrm{e}^{-3i\delta\tau_2} \cos^2\frac{\theta_2}{2}\cos^2\frac{\theta_3}{2} + \mathrm{e}^{3i\delta\tau_2} \sin^2\frac{\theta_2}{2}\sin^2\frac{\theta_3}{2} \right] \Bigg\}. \end{aligned} \tag{4.70}$$

In the case in which all pulses are identical, $\theta_1 = \theta_2 = \theta_3 = \theta$, the signal simplifies to

$$S_{\delta}^{-1} = \frac{15\,\mathrm{e}^{-i\delta(\tau_3-\tau_1)}}{32\sqrt{2}i} U_{33}^{13}(\vec{\tau}) \sin^7\theta \cos(3i\delta\tau_2) \tag{4.71}$$

$$\begin{aligned} S_{\delta}^{TQ} = & \frac{15\,\mathrm{e}^{-i\delta\tau_3}}{16\sqrt{2}} U_{33}^{13}(\vec{\tau}) \sin^5\theta \times \\ & \left\{ \cos\delta\tau_1 \cos 3\delta\tau_2 - \cos\theta \sin\delta\tau_1 \sin 3\delta\tau_2 - i\cos\theta\left(\cos\delta\tau_1 \sin 3\delta\tau_2 + \cos\theta \sin\delta\tau_1 \cos 3\delta\tau_2\right) \right\}. \end{aligned} \tag{4.72}$$

4.4. Experimental verification of algebraic description

Phantom experiments are performed to illustrate the used of the proposed approach for the theoretical description of NMR experiments. These experiments were designed to illustrate the bias in the relaxation parameters that could result from variations in the B_0 and B_1 field across the sample and how the proposed approach can help isolate these effects during the analysis of the signal.

All experiments presented in this section were performed on a vertical bore, 7 Tesla, Bruker DMX300 spectrometer (Bruker AG, Germany). The phantoms consisted of agar gels, as

such gels are known to exhibit bi-exponential relaxation behavior due to the isotropic slow motion experienced by the sodium ions in the agar environment. [12]

In order to obtain a strong deuterium lock signal, the gel was prepared using D_2O instead of distilled water. All chemicals used (10 cc D_20, 0.2 g NaCl, 2 g agar powder) were acquired from Sigma-Aldrich, St. Louis, MO. The samples were prepared by bringing the mixture close to the boiling point while continuously mixing the NaCl and agar using a magnetic stirring plate and an uncovered Erlenmeyer flask. After mixing-in and dissolving the chemicals, the mixture was allowed to cool before being placed in 10 mm NMR tubes. The resulting samples (2) were cylindrical in shape (10 mm diameters) and of different lengths. The smallest sample, which had a height of 1cm, was used to illustrate the effects of B_0 inhomogeneities. The other sample had a height of 4 cm and was used to illustrate the effects of B_1 inhomogeneities. While the sample were identical prepared, due to their different sizes, they are affected in different ways by the evaporation process.

The one-pulse experiment data were acquired on both samples, using the same pulse sequence program. Eight FID's were added in each one-pulse experiment, using a phase cycling scheme with $\phi_1=k\pi,\psi=k\pi$, k=0,1.

The optimum value for shim gradients (shimming) were found using a two stage procedure. First, the lock signal level was maximized by modifying the shim gradients. Second, a modification of the *paropt* utility shipped with the XWIN-NMR software suite was used to maximize the amplitude of the spectral peak, by varying the shim gradients, followed by acquisition and Fourier transformation of the signal. The sensitivity of this approach is better than the one based on the lock signal. below presents a comparison between the measured data

and the non-linear fit (solid line) for the small (bullets) and large (stars) agar phantoms. The function used in fitting has the biexponential form.

$$a\left(3\exp\left(-t/T_{FAST}\right)+2\exp\left(-t/T_{SLOW}\right)\right)+b$$

The found b/a ratio found is less than 0.2 percents in both situations. Responsible for the absence of the baseline is on the one side the accurate on-resonance frequency determination (realized by using a linear fit of the FID's phase) and, on the other hand, the way data is handled. Instead of using the magnitude of the signal, a zero order phase correction is performed, such that the signal appears only on the real channel, while the data on the imaginary channel consist of remaining noise.

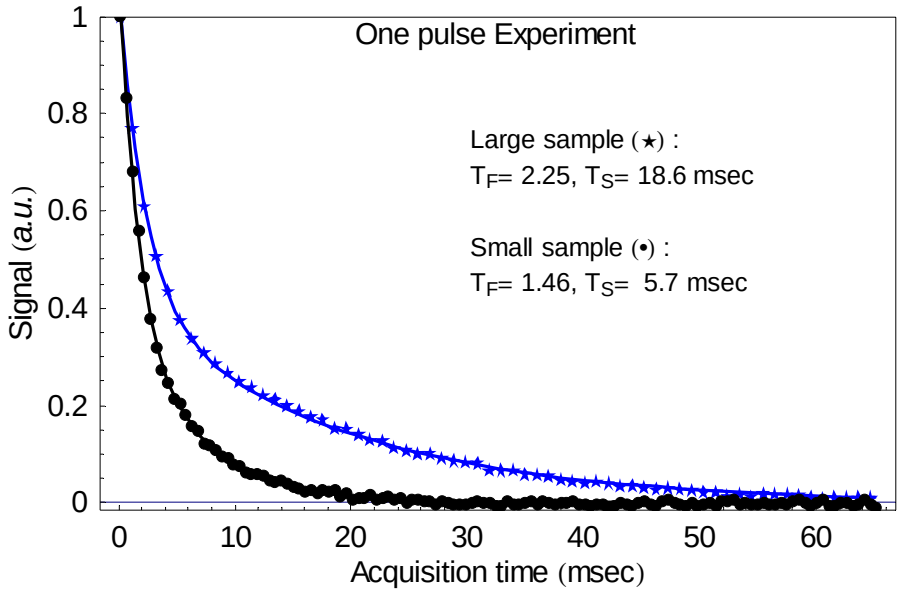

Figure 4.5 FID and non-linear fit using the biexponential, from a one pulse experiment on the small agar phantom (bullets) and the large agar phantom (stars). (TR=191ms, 8 averages).

To illustrate the effects of B_1 inhomogeneities across the sample, the one-pulse experiment was performed in a 2D fashion with the extra dimension being given by the pulse

length. Figure 4.6, below, present the integral of the measured data as a function of the pulse length (128 values between 10 and 518 microseconds).

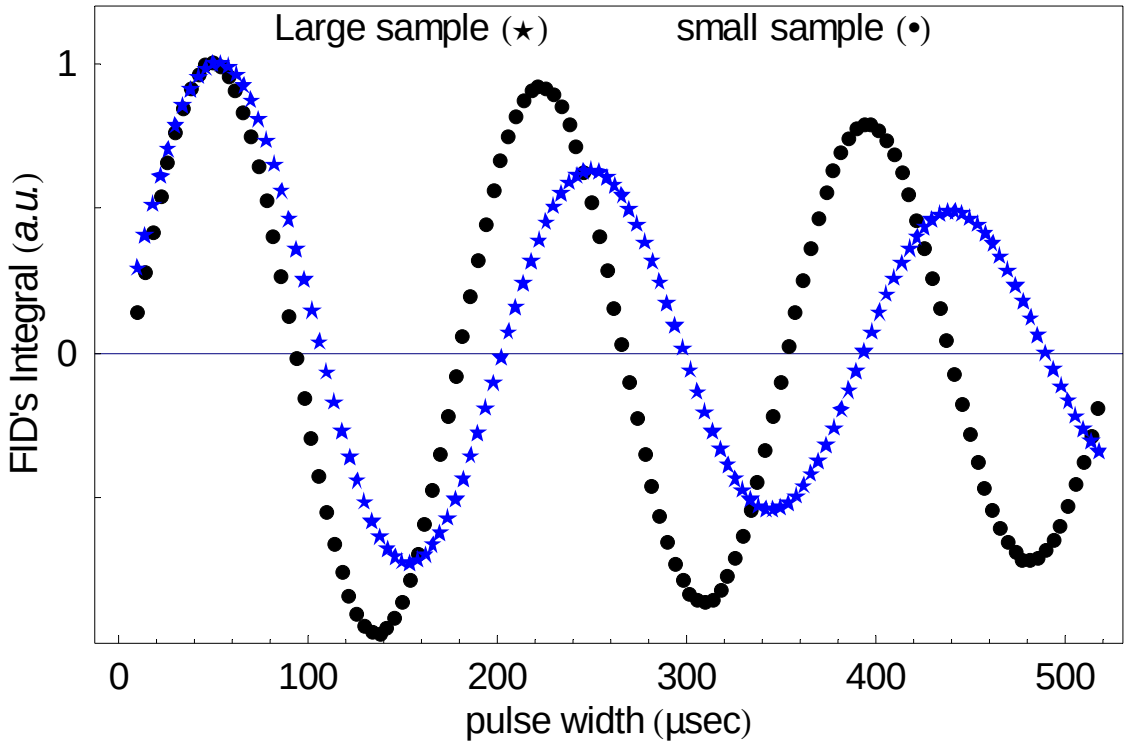

Figure 4.6 Dependence of the NMR signal on the RF pulse length for the small (bullets) and the large (stars) samples. Each data point corresponds to the integral of the FID (TR=191ms, 16 averages) following the RF pulse with corresponding pulse width.

The results of the two experiments indicate that the small sample is characterized by larger B_0 inhomogeneities leading to an "artificial" shortening of the relaxation times. This fact is to be expected, as the inhomogeneities are related with the discontinuities in susceptibility at the air-agar surface. Clearly, the larger B_1 inhomogeneities in the large agar sample lead to a higher degree of signal loss as the flip angle increases (increase in pulse length). This behavior is expected, also, as the longer sample has regions close to the ends of the coil, where the B_1 inhomogeneity is increased.

To illustrate the theoretical findings from the two-pulse theoretical model another set of measurements was performed. In these two-pulse experiments, the time delay between the pulses was increased from 0.3 to 38.4 milliseconds (128 equal steps). Each individual FID was recorded with a time resolution of four microseconds and twenty-four points in the FID averaged to obtain an estimate of the FID intensity at the echo. This estimated peak FID value was graphed as a function of the inter-pulse delay for the small and large agar samples.

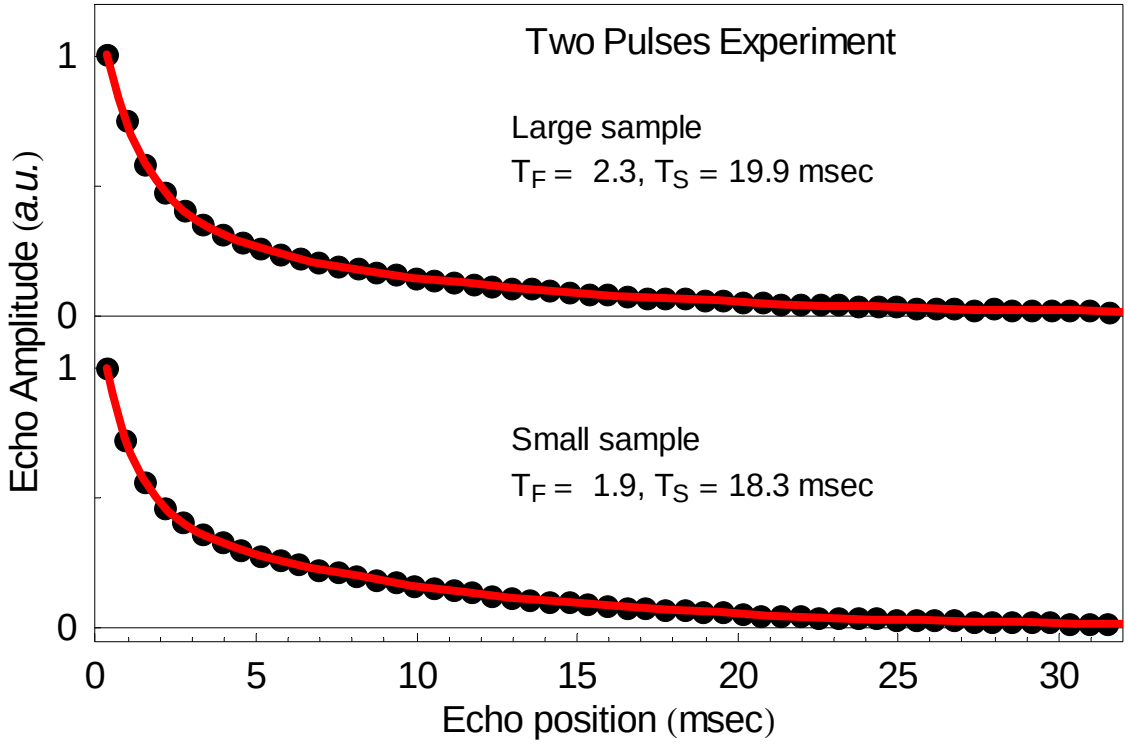

Figure 4.7 Dependence of the NMR signal from a two pulse experiment on the inter-pulse separation for the small agar phantom (lower part) and large phantom (upper part). Each data point corresponds to the peak amplitude of the corresponding FID (TR=209-285ms, 8 averages). The solid line indicates the fit to the signal envelope using the three terms function of the inter-pulse separation t.

The fit is performed using the function

$$5a\left(3\exp\left(-2t/T_{FAST}\right)+2\exp\left(-2t/T_{SLOW}\right)\right)-b\left(\exp\left(-t/T_{FAST}\right)-\exp\left(-t/T_{SLOW}\right)\right)^2+c$$

As expected, for the small sample the effect of B_0 inhomogeneities is largely removed. For the large sample, the quality of the data is not significantly enhanced. Note that from equation 112 above, one measure for the size of the B_1 inhomogeneities within the sample can be given by the ratio b/a, which can be obtained from the best fit to the function. For the small sample (homogeneous B_1) this ratio yields b/a=0.11 while for the large sample (inhomogeneous B_1) b/a=0.34.

The variable echo three-pulse experiment is demonstrated next using the ten phase cycle from equation(4.64). The results of this experimental procedure are presented in lower and upper parts of Figure 4.8, for the small and large agar samples, respectively. Selecting only the (-1,-3) component, an echo is formed and a 2D experiment is possible. The preparation delay is varied between 0.2 and 51.2 milliseconds, in 256 equidistant steps (the FID's are acquired with a time resolution of eight microseconds and eighty points are used in the estimation of the peak).

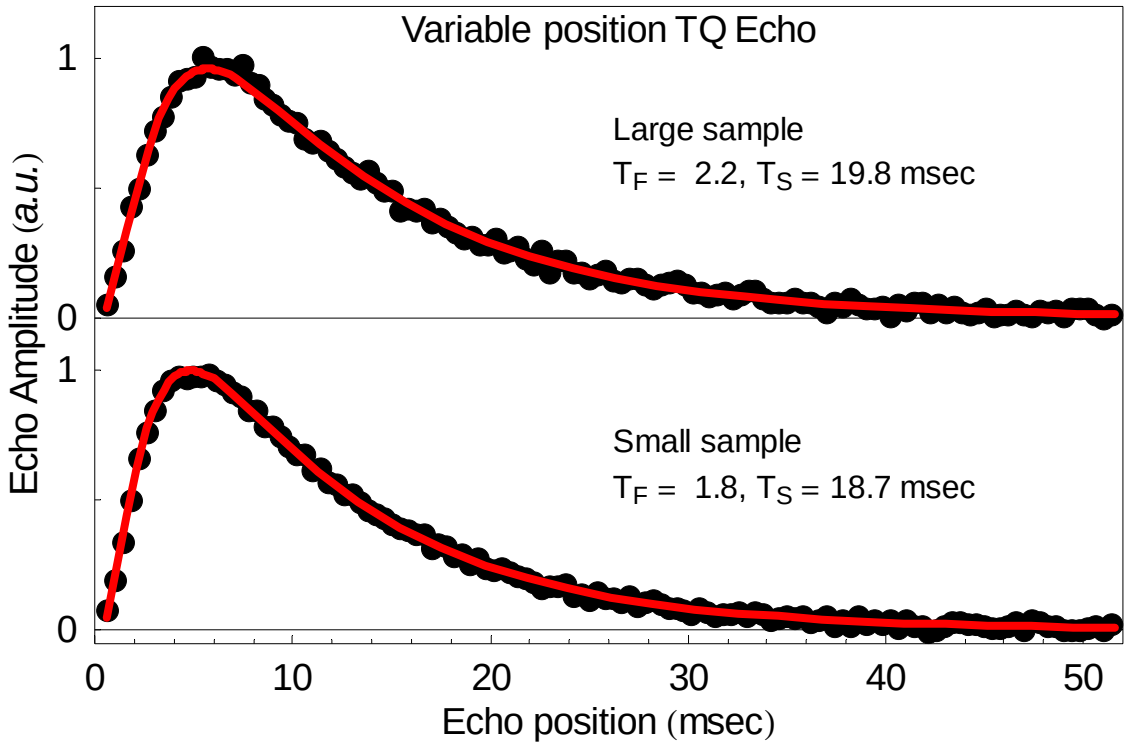

Figure 4.8 Dependence of the NMR signal from a three pulse experiment on position of the echo (a function of the inter-pulse delay) for the small (lower part of the plot) and large (upper part of the plot) agar phantom. Each data point corresponds to the amplitude of the echo (TR=157-259ms, 20 averages). The solid line indicates the fit to the signal envelope, as described in text.

In fitting the data, the effect of the finite pulse is accounted. The (-1,-3) echo forms at a position τ_1+x, with $x=3\tau_2+7T$, and where T is the effective length of the pulse, the right functional form to be used in the fit is given by

$$a\left(\exp\left(-t/T_S\right)-\exp\left(-t/T_F\right)\right)\left(\exp\left(-(t-x)/T_S\right)-\exp\left(-(t-x)/T_F\right)\right)+b$$

Finally, the fixed echo experiment was performed using a ten-phase cycle, selecting this time the (-1, 3) echo. The evolution delay was varied between 0.032 and 16.352 milliseconds in 256 equidistant steps. The preparation delay was incremented in steps three times larger than the ones used for incrementing the evolution time, ensuring the fixed echo location condition

discussed above. The time-integral of the FID's (estimated after discarding the first ten points) are shown versus the preparation time, for the small (lower) and large (upper) agar samples, together with their best fit (solid lines) in Figure 4.9.

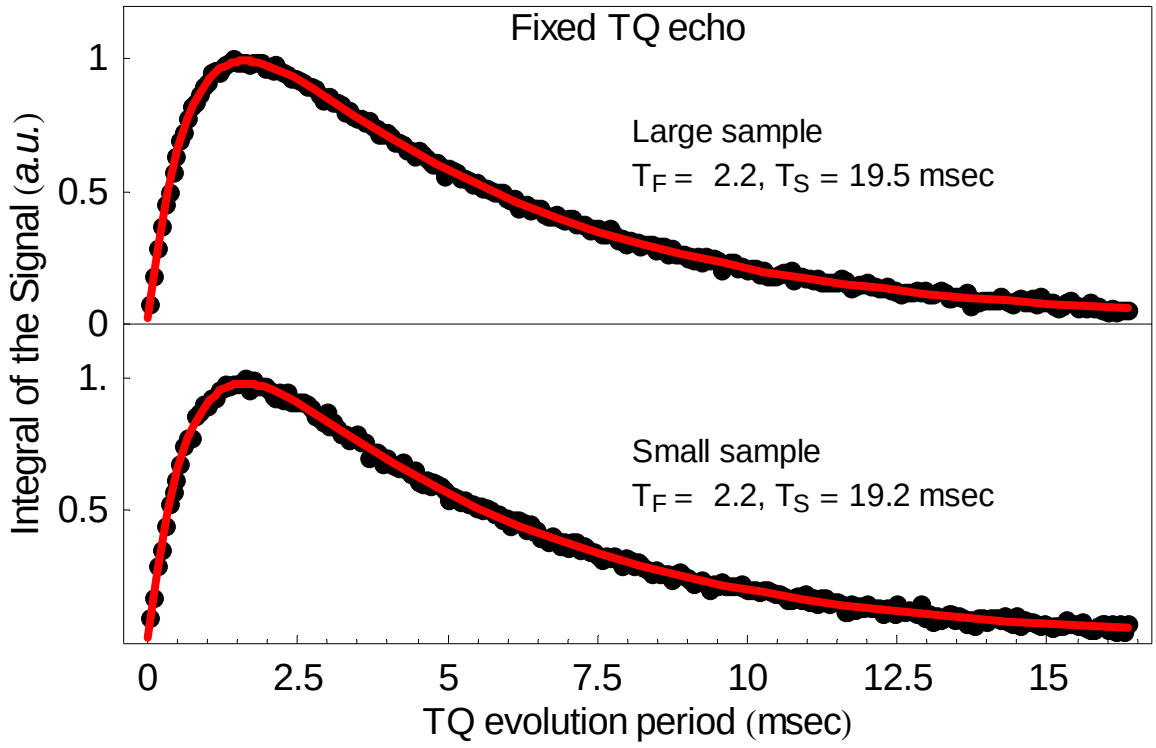

Figure 4.9 Dependence of the integral of NMR signal from a three pulse experiment on the TQ evolution time, for the small agar phantom (lower part) and large agar phantom (upper part). Each data point corresponds to the time integral of the corresponding FID (TR=217-282ms, 10 averages). The solid line indicates the fit to the signal envelope.

The fitting function used, in terms of the evolution time, t:

$$a\left(\exp\left(-3t/T_S\right)-\exp\left(-3t/T_F\right)\right)\exp\left(-3t/T_S\right)+b\,.$$

4.5. Accurate determination of T_2 *in vivo*

Whenever the macroscopic signal is measured, the sum over all spins in a certain volume is practically performed. In other words, the macroscopic signal is equivalent to the spatial average of the previous formulae, describing the TQ filtered signal, with f_{mn} depending on the filtering scheme

$$e^{i\psi} S\left(\theta,\vec{\phi},\vec{\tau}\right) = e^{i\psi} \sum_{\substack{m_1=-1,1 \\ m_2=-3,3}} f_{m_1 m_2} e^{-i\left(m_1\phi_1+m_2(\phi_2-\phi_1)+(\phi_3-\phi_2)\right)} \underbrace{\left\langle e^{-i\delta(m_1\tau_1+m_2\tau_2+\tau_3)}\right\rangle_{\delta}}_{g(m_1\tau_1+m_2\tau_2+\tau_3)} A_{m_1 m_2}\left(\theta,\vec{\tau}\right). \quad (4.73)$$

The propagator matrix elements are considered here as corresponding to a biexponential system, therefore, up to a common normalization constant,

$$u_{31}^{1}\left(t\right) = e^{-t/T_S} - e^{-t/T_F} \quad u_{33}^{3}\left(t\right) = e^{-t/T_S} \quad (4.74)$$

To illustrate the discussion in this section, for theoretical considerations, we choose, as an example, a biexponential system with the long and short relaxation times, T_L=20 milliseconds, and respectively, T_S=1.9 milliseconds. The function describing the effect of averaging over B_0 inhomogeneity is chosen here, as an example, the Gaussian with σ=8 milliseconds

$$g\left(t\right) = \exp\left(-t^2/\left(2\sigma^2\right)\right) \quad (4.75)$$

The TQ imaging relies on the accurate measurement of NMR properties of the system to be imaged. The accurate determination of the point in which the TQ has its maximum amplitude is particularly important. On one side, because the recorded TQ intensity has the form

$$s_{TQ} \sim u_{31}^{1}\left(\tau_1\right) \sim \left(e^{-\tau_1/T_L} - e^{-\tau_1/T_S}\right),$$

the maximum intensity is obtained when the preparation time attains its optimum value

$$T_{opt} = \frac{\log\left(T_L/T_S\right)}{1/T_S - 1/T_L} \quad (4.76)$$

In absence of inhomogeneities, the time dependence is the same for all four components, as exemplified in the Figure 4.10. In absence of inhomogeneities, the effect of varying the delays τ_1 and τ_2 manifests in scaling the signal, through the factor

$$u_{31}^{1}(\tau_1)u_{33}^{3}(\tau_2)u_{31}^{1}(t) \sim \left(e^{-\tau_1/T_L} - e^{-\tau_1/T_S}\right)e^{-\tau_2/T_L}\left(e^{-t/T_L} - e^{-t/T_S}\right) \tag{4.77}$$

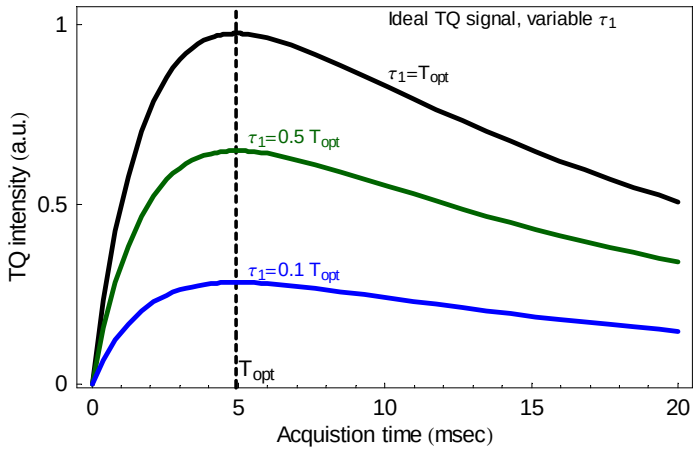

Figure 4.10 Behavior of ideal TQ with the variation of the preparation time.

The presence of inhomogeneities introduce another source of time dependence in which of the contributions, depending on the location of the associated echo (the point in time in which all spin packets have the same phase)

$$g\left(m_1\tau_1 + m_2\tau_2 + t\right) = \left\langle \mathrm{e}^{-i\delta\left(m_1\tau_1 + m_2\tau_2 + t\right)} \right\rangle_{\delta} = \begin{cases} g\left(t - \tau_1 - 3\tau_2\right) & \left(m_1, m_2\right) = \left(-1, -3\right) \\ g\left(t + \tau_1 - 3\tau_2\right) & \left(m_1, m_2\right) = \left(1, -3\right) \\ g\left(t - \tau_1 + 3\tau_2\right) & \left(m_1, m_2\right) = \left(-1, 3\right) \\ g\left(t + \tau_1 + 3\tau_2\right) & \left(m_1, m_2\right) = \left(1, 3\right) \end{cases} \tag{4.78}$$

In the presence of the inhomogeneities (here introduced by the function g(t)) the following typical behavior occurs

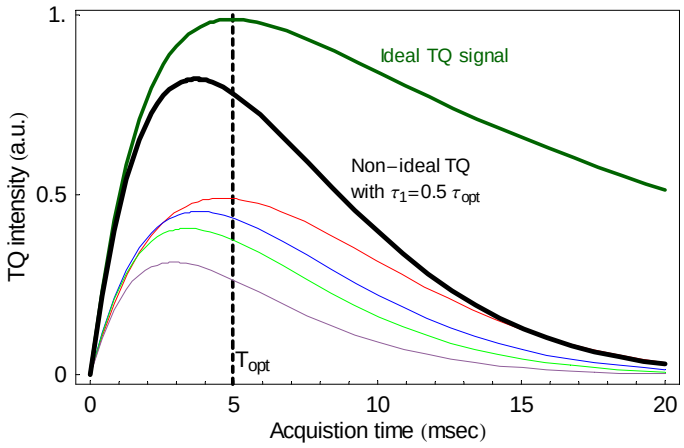

Figure 4.11 Behavior of non-ideal TQ with the variation of the preparation time. Thin lines represent the four components, while the thick dark line is their sum (scaled to half of its value, for display purposes)

Each of the components is distorted, in a way that is described by multiplication with a time translation of the inhomogeneity function. As a consequence, their sum is distorted.

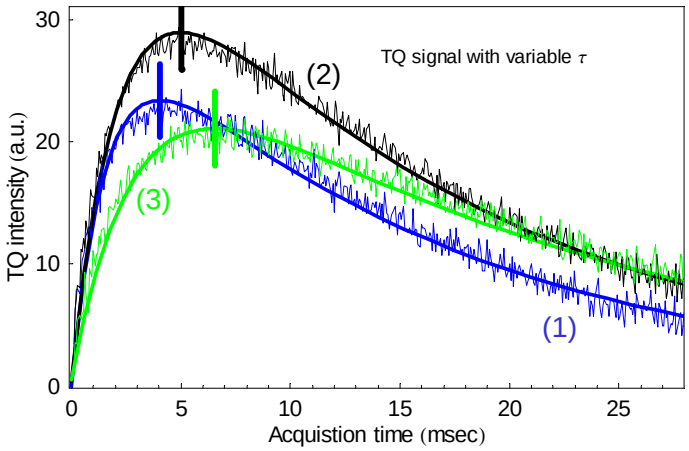

Figure 4.12 TQ FID's acquired on a small agar sample, using the Signa GE scanner and a solenoid coil. The FID's correspond to preparation times of 3, 5 and 8 milliseconds. As expected, the position of the maximum TQ signal depends on the preparation time, a clear sign of B_0 inhomogeneities across the sample. The solid lines represent biexponential fit of each data.

The manifestation of this effect is visible in the example data presented in Figure 4.12, where three TQ signals have been acquired with three preparation times. For each of them, the solid

lines represent the fit with biexponential function. There is no significant difference in the quality of the fit for any of them. Obviously, they predict different optimal preparation times, indicated on the plot by the vertical segments, also the fits return different set of long and short relaxation times: (15, 2), (16, 3) and (26, 3) milliseconds, for first, second and third data, respectively.

The conclusion of both the simple theoretical simulation and the sample data is that not only the measurements based on individual FID's are biased in the presence of B_0 inhomogeneities, but also, the approximate extraction of quantities of practical interest is impossible.

The first example is obtained on a sample consisting of an intact rat brain. The FID following a single pulse is presented in Figure 4.13

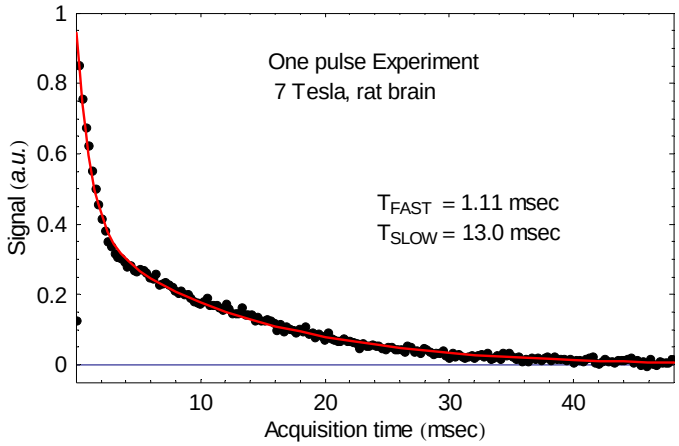

Figure 4.13 Single pulse experiment on a sample consisting of whole rat brain.

The next figure presents the TQ signal, acquired with a 6 millisecond preparation time

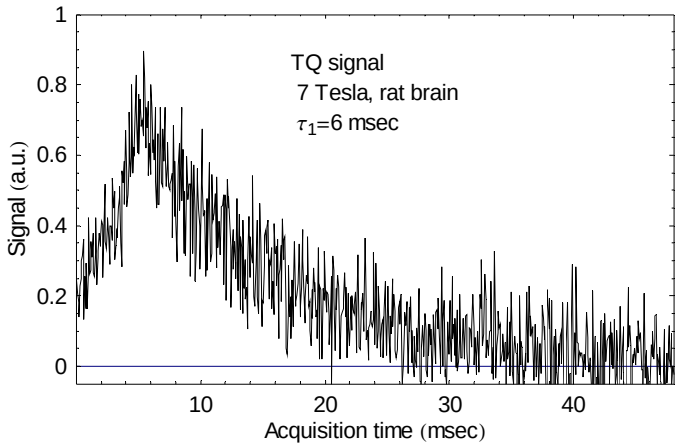

Figure 4.14 TQ signal acquired on an intact rat brain, preparation time τ_1=6 millisecond. The signal can not be fitted with a biexponential.

The quality of data is low, as the brain was kept intact. Its irregular geometry combined with the susceptibility discontinuity at the air-tissue interface (we did not use a solvent, in order to not alter the sodium concentration of the tissue) has as an effect strong B_0 inhomogeneity. The variable echo data is presented in Figure 4.15, the B_0 inhomogeneity is largely removed.

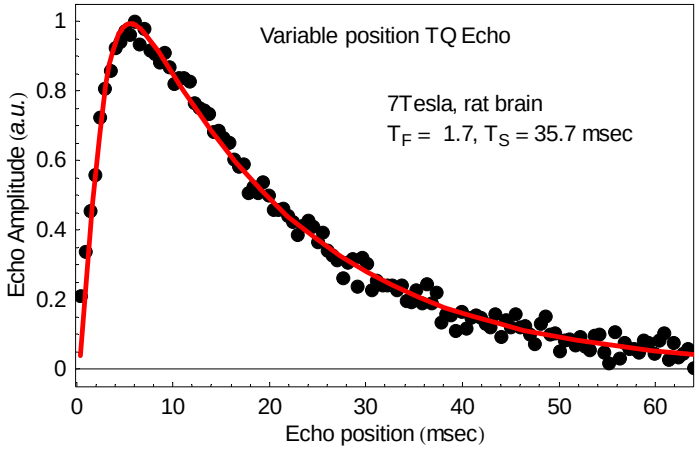

Figure 4.15 Variable echo method applied for a sample consisting of a whole, intact, rat brain. In spite of the low quality of the single FID data, the 2D acquisition is able to retrieve correct physical quantities.

The next experiment is meant to exemplify the fact that by performing one FID experiments only there is no possibility to estimate the errors, and misleading results are obtained. The sample consist of five mice brains, in saline and D_2O solution. A standard 10 mm (larger than the brain's diameters) NMR tube has been used. Due to the fact that now the probe has a more homogeneous magnetic susceptibility, the quality of data is enhanced.

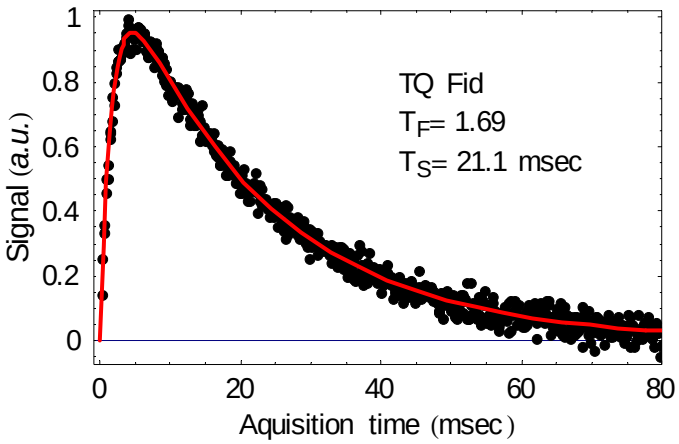

Figure 4.16 TQ FID obtained on a sample consisting of five intact mice brains. Due to the fact that the sample is placed in saline solution, the B_0 homogeneity is improved. Still, the values obtained by fitting are biased.

The variable echo experiment gives the results presented in the next figure. As expected, the long relaxation times are underestimated. More, as opposed to the plot in Figure 4.14, the quality of the single FID does not warn about such discrepancies.

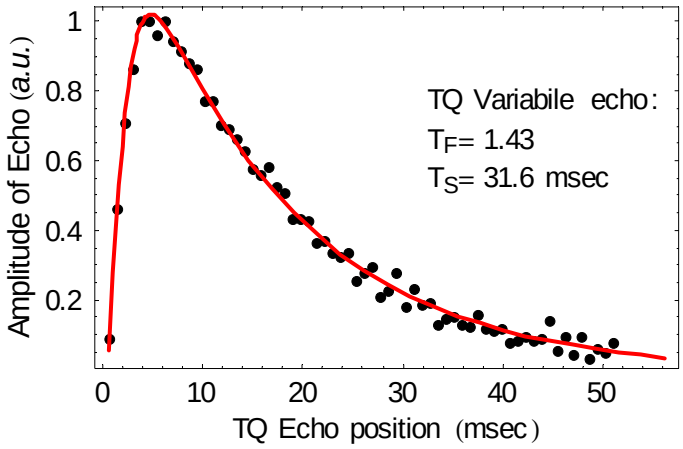

Figure 4.17 Variable echo method. Even tough the quality of the single TQ FID is high; the long relaxation times are underestimated.

5. IMAGING

In Section 5.1, is offered a simple mathematical procedure for the modeling of the MRI experiment steps: signal generation, data acquisition, data regridding, and Fourier Transform image reconstruction, in MRI. The suitability of the model is demonstrated by analyzing a specific problem, signal to noise ratio (SNR) maximization in respect with the readout time.

5.1. K-space description of MRI experiments

In the following discussion, the R-space denotes the domain of the object to be imaged and K-space denoted the spatial frequency domain. The object is described, in generic terms, by the amplitude of the imaged density, $\rho(\vec{r})$, with the restriction $\rho(\vec{r}) = 0$ whenever $|\vec{r}| \geq a$. The time decay in each point is described by a function $f(\vec{r}, t)$. The form of this function could be as simple as a mono-exponential decay or more complex as in the case of multiple quantum filter experiments.

In order to take in account the possibility of multiple excitations, the K-space trajectory is described by N branches (one for each RF excitation), with the position, at the moment t, on a branch n given by the equation $\vec{p}_n(t)$.

By assuming the time shift invariance of the experiment, (neither the pulses nor the object characteristics change from one sub experiment to another) the preparation times between the sub experiments can be ignored. The n-th experiment can be considered as starting at moment of time $t_n^- = (n-1)T_{\text{Read}}$ and ending at moment $t_n^+ = nT_{\text{Read}} = t_{n+1}^-$.

Considering the sensitivity of the receiving coil constant, the measured signal is the sum of the "true" signal and the "noise"

$$S_{meas}^{(n)}(t) = S^{(n)}(t) + \eta^{(n)}(t) = \int_V d\vec{r}\, \rho(\vec{r})\, f(\vec{r},t) \exp\left(2\pi i\, \vec{p}_n(t)\vec{r}\right) + \eta^{(n)}(t) \tag{5.1}$$

Under the hypothesis of identical relaxation properties of the system, the decay function has no dependence on the coordinates, $f(\vec{r},t) = f(t)$, and the theoretical signal takes the simpler form as the Fourier transform of the imaged density

$$S^{(n)}(t) = f(t) \int_V d\vec{r}\, \rho(\vec{r}) \exp\left(2\pi i\, \vec{p}_n(t)\vec{r}\right) = f(t)\, \hat{\rho}\left(\vec{p}_n(t)\right) \tag{5.2}$$

The complex quantity η(t), the additive noise, is described as a stationary Gaussian random process, with zero correlation time:

$$\left\langle \eta(t) \right\rangle = 0 \quad \left\langle \eta(t_1)\eta^*(t_2) \right\rangle = \sigma^2 \delta(t_1 - t_2). \tag{5.3}$$

For theoretical considerations, the definition of the signal in a discrete set of points, only, it is not convenient. By using standard regridding procedures one is able to define the intensity of the signal as a function of K-space position, $\vec{\kappa}$, using the convolution formula

$$\bar{R}(\vec{\kappa}) = \sum_{n=1}^{N} \sum_{m=1}^{M} W\left(\vec{\kappa}, \vec{p}_n(t_m)\right) S_{meas}^{(n)}(t_m) \tag{5.4}$$

This could be interpreted as the discrete approximation of the an integral expression

$$\hat{R}(\vec{\kappa}) = \int_T dt\, \hat{w}\left(\vec{\kappa}, \vec{p}(t)\right) S(t) \tag{5.5}$$

where the short notation is introduced for the sum of individual integrals

$$\int_T dt\, F\left(t, \vec{p}(t), \ldots\right) \equiv \sum_{n=1}^{N} \int_0^{T_{\text{Read}}^n} dt_n\, F\left(t_n, \vec{p}_n(t_n), \ldots\right) \tag{5.6}$$

For practical purposes, the convolution formula (5.4) is used to generate the data onto a new, Cartesian grid (regridding). The reconstruction from this point is accomplished using the Fast Fourier Transform.

In the case in which the signal is considering as originating from an imaging experiment, $S(t) = f(t)\hat{\rho}(\vec{p}(t))$ the K-space reconstructed signal is given by

$$\begin{aligned} \hat{R}(\vec{\kappa}) &= \int_V d^3\vec{r}\,\hat{\psi}(\vec{\kappa},\vec{r})\,\rho(\vec{r}) \\ \hat{\psi}(\vec{\kappa},\vec{r}) &= \int_T dt\; f(t)\,\hat{w}(\vec{\kappa},\vec{p}(t))\mathrm{e}^{2\pi i\vec{p}(t)\vec{r}} \end{aligned} \tag{5.7}$$

Regardless of the form chosen for the gridding kernel, the reconstructed signal in a point in R-space is defined by the K-space integral

$$R(\vec{r}) = \int_\Omega \mathrm{e}^{-2\pi i\vec{\kappa}\vec{r}}\;\hat{R}(\vec{\kappa})\,d^3\vec{\kappa} \tag{5.8}$$

where Ω is the domain in which data are acquired in K-space.

In terms of the signal acquired in time domain, the same value can be expressed as a time integral

$$\begin{aligned} R(\vec{r}) &= \int_T dt\, w(\vec{r},\vec{p}(t))S(t) \\ w(\vec{r},\vec{p}(t)) &= \int_\Omega d\vec{\kappa}\,\mathrm{e}^{-2\pi i\vec{\kappa}\vec{r}}\;\hat{w}(\vec{\kappa},\vec{p}(t)) \end{aligned}. \tag{5.9}$$

The kernel $w(\vec{r},\vec{p}(t))$, such defined, describes the way in which the value, measured at the moment t, is spread over the image, in the reconstruction process.

If the signal originates an imaging experiment,

$$\begin{aligned} R(\vec{r}) &= \int_V d^3\vec{r}'\,\psi(\vec{r},\vec{r}')\,\rho(\vec{r}') \\ \psi(\vec{r},\vec{r}') &= \int_T dt\; f(t)\,w(\vec{r},\vec{p}(t))\mathrm{e}^{2\pi i\vec{p}(t)\vec{r}'} \end{aligned} \tag{5.10}$$

Ideally, the original, regriding kernel should be chosen such that in the end the reconstructed image to be proportional with the density to be imaged

$$\psi(\vec{r},\vec{r}') = c(\vec{r})\delta(\vec{r}-\vec{r}') \tag{5.11}$$

Whether this is the case or not, is not the question in this analysis. The assumption made here is that the MRI experiment is described by the sequence of transformations

$$S(t) \xrightarrow{\hat{w}} \hat{R}(\vec{\kappa}) \xrightarrow{FT} R(\vec{r}) \xrightarrow{c^{-1}(\vec{r})} I_S(\vec{r}) = c^{-1}(\vec{r})R(\vec{r}) \tag{5.12}$$

5.2. SNR considerations

The statistics of the noise in the image is obtained by considering the measured signal, S(t), as given only by noise. It is easy to check that it has zero average and its variance is completely defined by the kernel $w(\vec{r},\vec{p}(t))$

$$\begin{aligned} \langle I_\eta(\vec{r})\rangle &= 0 \\ \sigma^2(\vec{r}) = \langle I_\eta(\vec{r}) I_\eta^*(\vec{r})\rangle &= \sigma^2 c(\vec{r})^{-2}\int_T dt \left| w(\vec{r},\vec{p}(t))\right|^2 \end{aligned} \tag{5.13}$$

Considering the ideal situation in which the density is localized in a given point

$$\rho(\vec{r}) = \delta(\vec{r}-\vec{r}_0) \tag{5.14}$$

the reconstructed signal is obtained from (5.10) and (5.12) in terms of the ψ kernel

$$I(\vec{r}_0) = c(\vec{r}_0)^{-1}\psi(\vec{r}_0,\vec{r}_0) \tag{5.15}$$

The SNR, denoted here by ν, is therefore calculated

$$\nu(\vec{r}_0) = \frac{\psi(\vec{r}_0,\vec{r}_0)}{\sigma\sqrt{\int_T \left| w(\vec{r}_0,\vec{p}(t))\right|^2}} \tag{5.16}$$

Considering the distribution localized in the center of FOV, the SNR expression simplifies further

$$\nu(0)=\frac{\psi(0,0)}{\sigma\sqrt{\int_T\left|w\left(0,\vec{p}(t)\right)\right|^2}}=\frac{\int_T dt\ f(t)\,w\left(0,\vec{p}(t)\right)}{\sigma\sqrt{\int_T\left|w\left(0,\vec{p}(t)\right)\right|^2}} \tag{5.17}$$

From the integral representation of the kernel, one could see that, neglecting the edge effects

$$w\left(0,\vec{p}(t)\right)=\int_\Omega d^3\vec{\kappa}\,\hat{w}\left(\vec{\kappa},\vec{p}(t)\right)\approx 1 \tag{5.18}$$

In the end, the signal-to-noise ration estimated in the center of FOV is given by a simple formula

$$\nu(0)=\frac{\left|\int_T dt\ f(t)\right|}{\sigma\sqrt{T_{\text{Acqu}}}} \tag{5.19}$$

Using this result, the question of dependence of SNR of the time of acquisition can be addressed. The optimum acquisition duration, T_{Acqu}, can be found with the same formula for a variety of trajectories, as long as we are interested in the SNR in the center of FOV by optimizing (5.19).

In the situation in which the K-space kernel could be chosen translation invariant

$$\hat{w}\left(\vec{\kappa},\vec{p}\right)=\hat{w}\left(\vec{\kappa}-\vec{p}\right) \tag{5.20}$$

the previous formulas simplify considerably

$$w\left(\vec{r},\vec{p}\right)=\mathrm{e}^{-2\pi i\vec{p}\vec{r}}\int_\Omega d\vec{\kappa}\,\mathrm{e}^{-2\pi i\left(\vec{\kappa}-\vec{p}\right)\vec{r}}\,\hat{w}\left(\vec{\kappa}-\vec{p}\right)\approx\mathrm{e}^{-2\pi i\vec{p}\vec{r}}\,w\left(\vec{r}\right) \tag{5.21}$$

$$\psi\left(\vec{r},\vec{r}'\right)=w\left(\vec{r}\right)\Phi_f\left(\vec{r}-\vec{r}'\right)=w\left(\vec{r}\right)\int_T dt\ f(t)\,\mathrm{e}^{2\pi i\vec{p}(t)\left(\vec{r}'-\vec{r}\right)} \tag{5.22}$$

$$R\left(\vec{r}\right)=w\left(\vec{r}\right)\int_T dt\,\mathrm{e}^{-2\pi i\vec{p}(t)\vec{r}}\,S(t) \tag{5.23}$$

$$R\left(\vec{r}\right)=w\left(\vec{r}\right)\int_V d^3\vec{r}'\,\Phi_f\left(\vec{r}-\vec{r}'\right)\rho\left(\vec{r}'\right) \tag{5.24}$$

5.2.1. Delta Function Object

The simplest estimation of the acquisition time is obtained in the case of a 1D object described as a delta function in the center of FOV. Then S(t)=f(0,t)=f(t) and

$$\nu(0) = \frac{\sum \int_0^{T_{\text{Read}}^n} dt\, f(t)}{\sigma\sqrt{\sum T_{\text{Read}}^n}} \tag{5.25}$$

For the case in which the time decay function is decreasing monotonically in time, *i.e.* whenever $t_1 \geq t_2$, $f(t)_1 \geq f(t)_2$, the maximization of the SNR with the constraint

$$\sum_{n=1}^{N} T_{\text{Read}}^n = T_{\text{Acqu}} \tag{5.26}$$

implies the equality of individual readout times $T_{\text{Read}}=T_{\text{Acqu}}/N$ and the SNR becomes

$$\nu = \frac{\sqrt{N}}{\sigma} \frac{\int_0^{T_{\text{Read}}} dt\, f(t)}{\sqrt{T_{\text{Read}}}} \tag{5.27}$$

By imposing the maximum condition in respect with the individual readout time, the following equation is obtained

$$\int_0^{T_{\text{Read}}} dt\, f(t) = 2T_{\text{Read}}\, f(T_{\text{Read}}) \tag{5.28}$$

For the pure exponential decay $f(t)=\exp(-t/T_2)$, with substitution $T_{\text{Read}}=T_2(w+1/2)$, the equation takes the form

$$we^w = -1/\left(2\sqrt{e}\right) \tag{5.29}$$

The solutions is given in terms of the well known Lambert W function,

$$T_{\text{Read}} = -T_2\left(\frac{1}{2} + W_{-1}\left(-\frac{1}{2\sqrt{e}}\right)\right) \cong 1.256T_2 \tag{5.30}$$

The conclusions of those simple considerations are in agreement with the results obtained previously in the context of pure NMR calculations [28].

5.2.2. Finite width object

In this section, the 1D imaging of a homogenous object with finite width is analyzed. Specifically, the density is given by a uniform distribution on the interval [-a,a]

$$\rho(x) = \frac{1}{2a}\begin{cases} 1, \text{ for } |x| \le a \\ 0, \text{ for } |x| > a \end{cases} \tag{5.31}$$

The field of view is chosen here as FOV=2a, V>a. In order to obtain, in R-space, the same spatial resolution, the same domain in K-space, denoted here $-b \le \kappa \le b$, is covered during the acquisition. The time sampling resolution (dwell time) is constant, regardless of the value of the gradient applied.

In the one shot acquisition scheme, the [-b,b] interval is covered with a constant gradient G starting from the lowest value of κ. The two shot acquisition covers the [-b,b] interval with a two branches starting from the center of K-space to the maximum value, b and minimum value, -b, respectively.

In terms of dimensionless quantities

$$y = \frac{\kappa}{b}, \text{ and } \beta = \frac{T_{\text{Acqu}}}{2T_2} \tag{5.32}$$

the one shot trajectory is parameterized

$$\kappa(y) = by \quad t(y) = T_2\beta(1+y) \quad y \in [-1,1] \tag{5.33}$$

while the two shot trajectory is given by

$$\kappa(y) = by \quad t(y) = T_2\beta|y| \quad y \in [-1,1] \tag{5.34}$$

Another dimensionless quantity is introduced by the geometry of the object

$$\varphi = 2\pi ab = \frac{\pi}{2} N_S \left(\frac{a}{V} \right) = \pi \frac{a}{R_{\text{res}}} = \pi N_{\text{voxels}} \tag{5.35}$$

For usual acquisitions, the parameter takes values in a range $\varphi \approx \pi\left(1 \div 16\right)$. Previously discussed case of a delta distribution could be recovered in the limit φ→0.

In absence of relaxation, the signal recorded from this geometry is given by the sinc function

$$g\left(\kappa\right) = \frac{\sin\left(2\pi ka\right)}{2\pi ka} = \operatorname{sinc}\left(\varphi y\right) \tag{5.36}$$

When the relaxation is taken into account, in terms of the dimensionless parameter y

$$\begin{aligned} S_1\left(y\right) &= e^{-\beta(1+y)} \operatorname{sinc}\left(\varphi y\right), \text{ for one shot scheme} \\ S_2\left(y\right) &= e^{-\beta|y|} \operatorname{sinc}\left(\varphi y\right), \text{ for two shot scheme} \end{aligned} \tag{5.37}$$

Then, up to a constant factor the SNR reads as

$$\begin{aligned} \nu_2\left(\beta\right) &= \sqrt{\beta} \int_{-1}^{1} dy\, e^{-\beta|y|} \operatorname{sinc}\left(\varphi y\right) \\ \nu_1\left(\beta\right) &= e^{-\beta} \sqrt{\beta} \int_{-1}^{1} dy\, e^{-\beta y} \operatorname{sinc}\left(\varphi y\right) = \mathrm{e}^{-\beta} \left(\nu_2\left(\beta\right) + \nu_2\left(-\beta\right) \right) / 2 \end{aligned} \tag{5.38}$$

In order to optimize the readout we have to find the maximum of this quantity in respect with the parameter β. Using the properly chosen analytic continuation of the second kind exponential integral , $\widetilde{\mathrm{Ei}}\left(z\right)$, the explicit formula is obtained

$$\begin{aligned} \nu_2\left(\beta\right) &= \sqrt{\beta}\, \frac{i}{\varphi} \left\{ \widetilde{\mathrm{Ei}}\left(-\beta - i\varphi\right) - \widetilde{\mathrm{Ei}}\left(-\beta + i\varphi\right) \right\} \\ \widetilde{\mathrm{Ei}}\left(z\right) &= \mathrm{Ei}\left(z\right) - \log\left(z\right) = -\mathrm{P} \int_{-z}^{\infty} \frac{e^{-x}}{x} dx - \log z \end{aligned} \tag{5.39}$$

As a useful check, the delta function case analyzed above is recovered in the limit φ→0 (the limit holds only when the right analytic continuation is chosen for the Ei(z) function).

$$\lim_{\varphi \to 0} \nu_1\left(\beta\right) = \sqrt{\beta} \left(1 - e^{-2\beta}\right) \tag{5.40}$$

In order to prove that those considerations are right the 1D acquisition is simulated for a FOV of 20 cm, with the final image containing 64 points. The T_2 has the value 16 milliseconds. The sampling rate is kept constant at a value dt of 8 microseconds. The object is chosen to fill half of FOV, therefore$\varphi=8\pi$. The gradients are varied between .1 and 1 Gauss per centimeter.

The simulated data points, in K-space, are generated for a maximum κ 1.575 cm^{-1}. The number of data points exceeds the desired number of points. In order to resample data on a 64 points grid the usual regridding prescriptions with a Kaiser-Bessel kernel having the window width of two.

The intensity values in the center of FOV are generated, for each value of the gradient. By choosing as signal a random Gaussian noise, following the same reconstruction procedure, the "image of a pure noise" is generated. The standard deviation is estimated from the pixels in the center of image, half of the object width, in order to avoid the edge effects. For a window width of Kaiser Bessel function equal with two, those effects are insignificant. Repeating the same calculations with larger window widths (up to six), no noticeable differences have been found.

The signal to noise ratio (scaled to its maximum value) is compared with the theoretical curve. The agreement is found to be excellent. This simple situation allows for an easy identification of the artifacts associated with the gridding procedure, by comparing the gridding reconstruction to the direct Fourier reconstruction (a luxury unavailable in the case of non-Cartesian sampling). In the direct reconstruction, all data points are used, generating in R-space a domain larger than the FOV. Only the pixels inside FOV are kept.

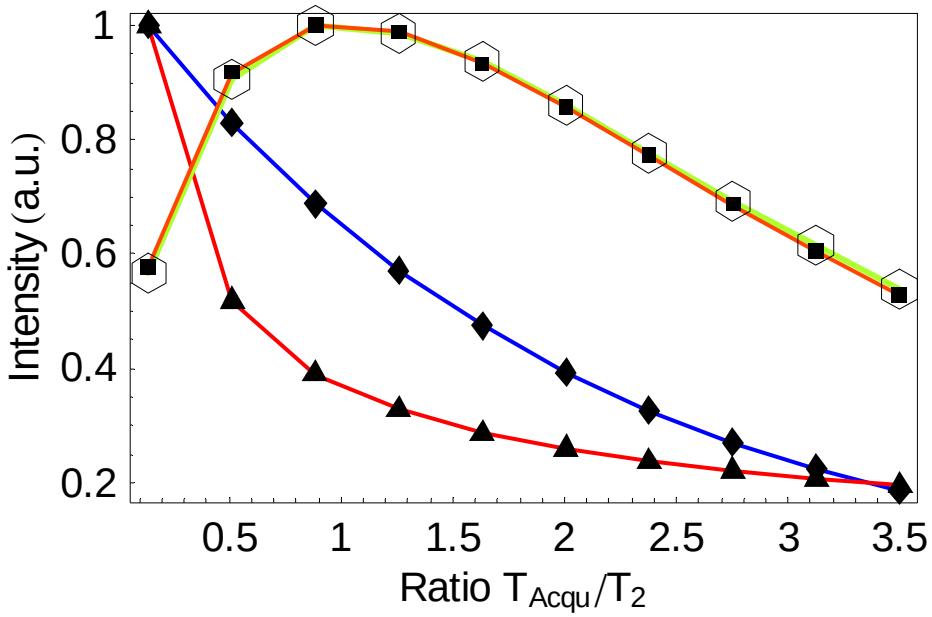

Figure 5.1 Direct, Fourier reconstruction, simulated signal (diamonds), simulated noise (triangles), simulated "experimental" SNR (hollow hexagons). The theoretical formula (boxes) compares excellent with the simulation

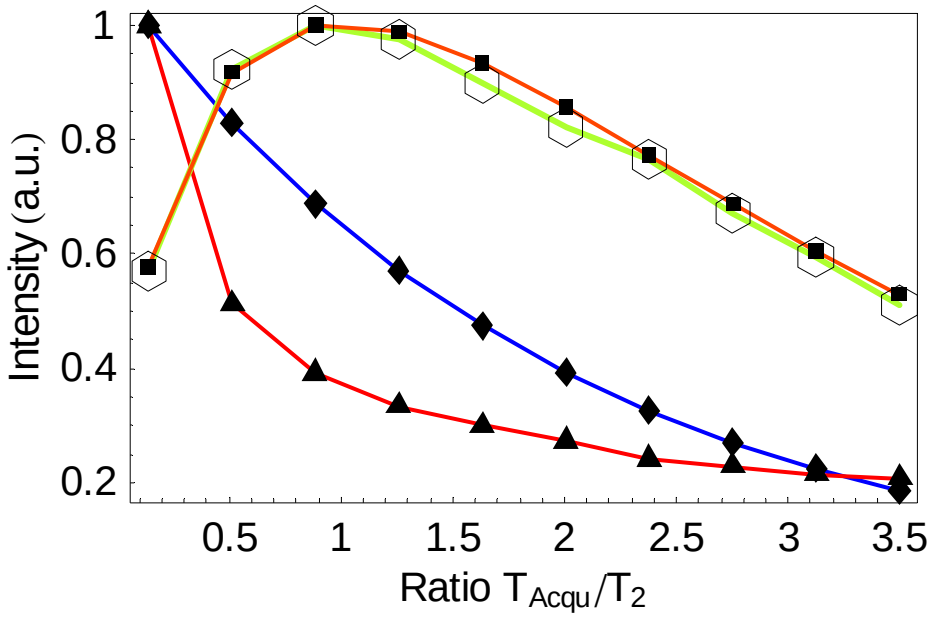

Figure 5.2 Gridding reconstruction, simulated signal (diamonds), simulated noise (triangles), simulated "experimental" SNR (hollow hexagons). The theoretical formula (boxes) compares well with the simulation

6. TQ sodium imaging in presence of both B_0 and B_1 inhomogeneities

In Section 6.1, a new scheme for TQ filtering is theoretically predicted and validated by NMR experiments. In Section 6.2, the design and applications of the TQ imaging protocol are presented, using an agar phantom (as the sodium relaxation in this system is biexponential). In Section 6.3, the application for TQ imaging of sodium in humans is offered

Multiple Quantum Filtered (MQF) techniques have been used extensively in NMR in order to separate the NMR signal from different environments. [29]. In the case of sodium, a very important ion in cell physiology, these techniques have been further explored for the separation of the NMR signal between the intra- and extracellular compartments in the context of animal models of disease. Triple quantum sodium NMR techniques, in particular, have been used for the observation of sodium ion shifts during ischemia [30] and for the identification of neoplastic changes in human and/or animal tissues. While well known in the NMR literature, the conventional implementation of TQ sodium NMR relies on the use of a four RF pulse coherence transfer filter. In this four pulse structure, the first pulse creates coherences that evolve freely and are refocused by the second RF pulse before being converted into triple quantum coherences and observable magnetization by third and four pulses, respectively. As shown by Hancu et al, [31], the four pulse structure, while being well suited for NMR experiments over small samples, introduces a strong dependence on the RF field leading to strong, and difficult to compensate, signal modulation across the field of view when imaging applications are considered. By eliminating the second RF pulse from this structure, the signal dependence on the RF field becomes less severe and moreover this dependence factors out from that of all other

experimental parameters. This feature of the three-pulse coherence transfer filter makes it better suited for imaging experiments because the aforementioned factorization allows for compensation of the signal modulation using an estimate of the B_1 field across the field of view [32].

The three-pulse implementation of TQ sodium MRI has been demonstrated on human subjects and has also been used for the observation of neoplastic changes in the human brain [33]. This implementation, because of the lack of a refocusing pulse during the preparation period, introduces a signal dependence on the main magnetic field inhomogeneities. This dependence on the field inhomogeneities can sometimes lead to unwanted signal loss and, therefore, constitutes an issue that needs to be addressed in the context of the quantification of the signal. In this thesis, we demonstrate that this signal loss is associated with differences in phase evolution for the different coherence pathways that contribute to the triple quantum signal. When the TQ signal is acquired as a simple summation over coherence pathways, destructive interference between the individual coherences might ensue leading to signal loss in the images. We further demonstrate that by using a modified phase cycling scheme, the individual coherences can be obtained separately and then re-combined with the aid of a B_0 map in order to avoid the aforementioned signal loss. The effectiveness of this approach is demonstrated with NMR as well as imaging experiments.

This three-pulse coherence transfer filter is schematically depicted in the Figure 6.1. It consists of a sequence of three pulses characterized by the same flip angle, θ, and phases φ_1, φ_2, φ_3. The delays τ_1 and τ_2 following the first and second pulses allow the creation of third order coherences, and their propagation, respectively. Those coherences are converted in measurable, transversal magnetization by the last pulse. The presence of the B_0 inhomogeneities is described

in terms of the parameter δ, defined as the deviation of the applied RF, ω, from Larmor frequency, ω_0,

$$\delta = \omega - \gamma B_0 . \tag{6.1}$$

Without loss of generality, we will assume for the remainder of this section that the inhomogeneity parameter is constant across the sample volume (when this is not the case a B_0 map can be used to obtain the value of this parameter at every voxel on the imaged volume).

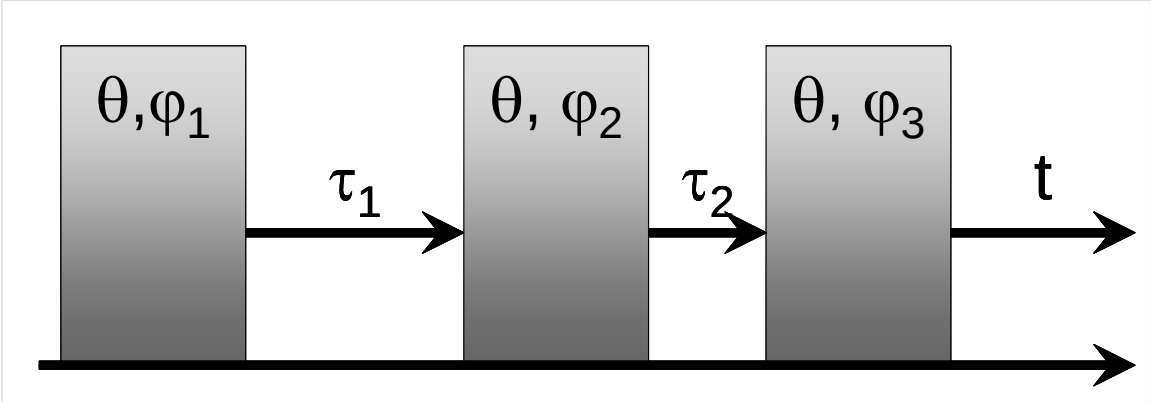

Figure 6.1 The schematic representation of the three-pulse sequence.

In a voxel characterized by a given value of B_0 inhomogeneity parameter, δ, the recorded NMR signal at the time t, $S_\delta(t)$ can be represented as a sum over coherence pathways, where the contribution of each coherence is a complex signal [34]. Because a pathway is completely characterized by the intermediate magnetic quantum numbers m_1, m_2, the total signal is given by a sum of twenty-one complex signals, with time dependent amplitudes $A_{mn}(t)$ and time independent phases Ψ_{mn} [35]

$$S_\delta(t) = \sum_{m_1=-1}^{1} \sum_{m_2=-3}^{3} \exp\left(-i\Psi_{m_1 m_2}\right) A_{m_1 m_2} \, \mathrm{e}^{-i\delta t} . \tag{6.2}$$

Apart of their dependence on the acquisition time, the amplitudes A_{mn}, are functions of the flip angles and time delays, while the phases Ψ_{mn} are functions of time delays, pulses phases, receiver phase, and main magnetic field inhomogeneity

$$\begin{aligned} A_{mn} &\equiv A_{mn}\left(t;\tau_1,\tau_2,\theta\right) \\ \Psi_{mn} &\equiv \Psi_{mn}\left(\tau_1,\tau_2,\varphi_1,\varphi_2,\varphi_3,\psi,\delta\right) \end{aligned}. \tag{6.3}$$

In the case of three identical RF pulses (*i.e.*, same RF width and amplitude, but different phases), the four relevant amplitudes contributing to the triple quantum signal are given below (up to a normalization factor)

$$\begin{pmatrix} A_{-1,-3}(t) \\ A_{-1,3}(t) \\ A_{1,-3}(t) \\ A_{1,3}(t) \end{pmatrix} = u_{31}^{1}(\tau_1)\,u_{33}^{3}(\tau_2)\,u_{31}^{1}(t)\sin^5\theta \begin{pmatrix} -\cos^2(\theta/2)\sin^2(\theta/2) \\ -\cos^2(\theta/2)\sin^2(\theta/2) \\ \cos^4(\theta/2) \\ \sin^4(\theta/2) \end{pmatrix}. \tag{6.4}$$

For ions experiencing a biexponential relaxation behavior, in which the short and long T_2 relaxation times are T_S respectively T_L, the relaxation functions $u_{mn}^{k}(t)$ are given by

$$u_{31}^{1}(t) = \left(\mathrm{e}^{-t/T_S} - \mathrm{e}^{-t/T_L}\right) \text{ and } u_{33}^{3}(t) = \mathrm{e}^{-t/T_L}. \tag{6.5}$$

The phases associated with a given coherence pathway can be further decomposed as the sum of two terms,

$$\Psi_{m_1m_2}\left(\tau_1,\tau_2,\varphi_1,\varphi_2,\varphi_3,\psi,\delta\right) = \Phi_{m_1m_2}\left(\varphi_1,\varphi_2,\varphi_3,\psi\right) + \Delta_{m_1m_2}\left(\tau_1,\tau_2,\delta\right). \tag{6.6}$$

The first term, Φ_{mn}, is defined by the receiver phase ψ and the pulse phases, φ_i,

$$\Phi_{m_1m_2}\left(\varphi_1,\varphi_2,\varphi_3,\psi\right) = -\psi + \left(m_1\varphi_1 + \left(m_2 - m_1\right)\varphi_2 + \left(1 - m_2\right)\varphi_3\right), \tag{6.7}$$

while the second term describes the phase accumulation during the off-resonance propagation along the given coherence pathway, and is defined by the off-resonance parameter δ,

$$\Delta_{m_1m_2}\left(\tau_1,\tau_2,\delta\right) = (m_1\tau_1 + m_2\tau_2)\delta. \tag{6.8}$$

The phase cycling [3] is performed by adding the signals from N repetitions with different RF and receiver phases. The resulting signal, when acquired on-the-fly (*i.e.*, automatically accumulated over each phase cycle by the scanner), can be written at any acquisition moment of time t as the sum

$$S_{\delta}^{TQ}(t) = \sum_{\varphi_1,\varphi_2,\varphi_3,\psi} S_{\delta}(t), \tag{6.9}$$

where the summation is performed over all combinations of RF phases φ_i and receiver phases ψ. By changing the order of summation in the last equation, an expression similar to Eq(6.2) can be obtained, namely

$$S_{\delta}^{TQ}(t) = \sum_{m_1=-1}^{1} \sum_{m_2=-3}^{3} \mathrm{e}^{-i\delta t} A_{m_1 m_2}(t) \mathrm{e}^{-i\Delta_{m_1 m_2}} f_{m_1 m_2} . \tag{6.10}$$

In this last expression, the extra-coefficients f_{mn} are sums over the RF phases

$$f_{m_1 m_2} = \sum_{\varphi_1,\varphi_2,\varphi_3,\psi} \mathrm{e}^{-i\Phi_{m_1 m_2}} \tag{6.11}$$

If the sign of the amplitudes $A_{mn}(t)$ are time independent, a phase cycling scheme can be designed such that

$$f_{m_1 m_2} = \begin{cases} 0 & \text{if } |m_2| \neq 3 \text{ or } m_1 = 0 \\ N \operatorname{sign}\left(A_{m_1 m_2}\right) & \text{if } |m_2| = 3 \text{ and } m_1 \neq 0 \end{cases}, \tag{6.12}$$

which brings the filtered signal in the form,

$$S_{\delta}^{TQ}(t) = N \sum_{m_1=\pm 1, m_2=\pm 3} \left|A_{m_1 m_2}(t)\right| \mathrm{e}^{-i\delta t} \mathrm{e}^{-i\Delta_{m_1 m_2}} , \tag{6.13}$$

effectively filtering out the contributions from unwanted coherence pathways. The requirement of a time independent sign of amplitudes is satisfied for the system considered here, *i.e.* ions in isotropic slow fluctuating environment, as it can be easily seen from their expression.

Such a phase cycling design is attractive since it has the property of producing the maximum on-resonance (*i.e.* when δ=0) signal:

$$S_{\delta=0}^{TQ}(t)=\left|A_{1-3}(t)\right|+\left|A_{13}(t)\right|+\left|A_{-1-3}(t)\right|+\left|A_{-13}(t)\right|. \tag{6.14}$$

One particular implementation of this approach is the six-phase scheme used frequently in the literature [31]. This scheme corresponds to the following choices for the receiver (ψ) and RF (φ_i) phases

$$\varphi_1=\alpha_1+\frac{\pi}{3}k \quad \varphi_2=\alpha_2+\frac{\pi}{3}k \quad \varphi_3=0 \quad \psi=k\pi \quad k=0,...,5. \tag{6.15}$$

Using the filtering from Eq(6.15), the corresponding coefficients f evaluate to expressions depending only on the starting phases of the cycle (α_1, α_2),

$$f_{m_1m_2}(\alpha_1,\alpha_2)=\begin{cases}6e^{-i\left(m_1\alpha_1+(m_2-m_1)\alpha_2\right)} & \text{if } |m_1|=1,|m_2|=3\\ 0 & \text{otherwise}\end{cases}. \tag{6.16}$$

Finally, by choosing $\alpha_1=\pi/6$, $\alpha_2=2\pi/3$, the scheme fulfills the requirements of Eq(6.12).

It has to be noted that this filtering scheme allows a residual signal, due to longitudinal recovery magnetization during the delay τ_1, to pass through the filter. In most imaging applications, the residual component is negligible because τ_1 is small compared with the longitudinal relaxation time T_1. Whenever this signal cannot be ignored (for example, in those 2D NMR experiments in which variable delays are used), the supplementation of the cycle with another six phases

$$\varphi_1=\alpha_1+\pi+\frac{\pi}{3}k \quad \varphi_2=\alpha_2+\frac{\pi}{3}k \quad \varphi_3=0 \quad \psi=\pi+k\pi \quad k=0,...,5, \tag{6.17}$$

cancels the T_1 contributions. For the sake of simplicity, we will assume these contributions to be negligible for the reminder of this section (*i.e.*, it is assumed that τ_1 is much smaller than T_1).

In the off-resonance case, the presence of Δ_{mn} phases in Eq(6.13) leads to destructive interference between components associated with different coherence pathways. By combining the equations (6.16) and (6.10) an analytic result is obtained for an arbitrary flip angles and inhomogeneity parameter

$$\begin{aligned} S^{\mathrm{TQ}}\left(\theta,\delta,\tau_1,\tau_2,t\right) &= \mathrm{e}^{-i\delta t}\, S^{\mathrm{TQ}}_{\mathrm{ideal}}\left(\tau_1,\tau_2;t\right) F\left(\tau_1,\tau_2;\theta,\delta\right), \\ S^{TQ}_{\mathrm{ideal}}\left(\tau_1,\tau_2,t\right) &= u^1_{31}\left(\tau_1\right) u^3_{33}\left(\tau_2\right) u^1_{31}\left(t\right), \\ F\left(\tau_1,\tau_2,\theta,\delta\right) &= \sin^5\theta \times \left\{\cos\delta\tau_1 \cos 3\delta\tau_2 - \cos\theta \sin\delta\tau_1 \sin 3\delta\tau_2 - \right. \\ &\qquad \left. i\cos\theta\left(\cos\delta\tau_1 \sin 3\delta\tau_2 + \cos\theta \sin\delta\tau_1 \cos 3\delta\tau_2\right)\right\}. \end{aligned} \tag{6.18}$$

From this expression, it is apparent that a reduction of the TQ signal from its maximum value to zero occurs for the offset parameter in the range $|\delta| \approx \pi/(2\tau_1)$ (in MRI applications τ_2 is much smaller than τ_1). For typical *in vivo* applications, the delay τ_1 is set to values maximizing the $u^1_{31}\left(\tau_1\right)$ functions, which usually leads to values around 5.0 milliseconds. Therefore, variations in B_0 of the order of 50 Hz could destroy the TQ signal. Unfortunately, those variations are common during MRI *in vivo* applications, due to variations in tissue susceptibility that lead to B_0 inhomogeneities, which are difficult to compensate through shim optimization in a reliable and timely fashion.

A simple approach to correct for the signal variations described by Eq(6.18) would be to experimentally determine θ and δ (which for MRI applications imply the acquisition of a B_1 map and a B_0 map) and use their values to compute the ideal signal. When the signal measurements are corrupted by noise (denoted η), Eq(6.18) reads

$$S^{\mathrm{TQ}}\left(\theta,\delta,\tau_1,\tau_2,t\right) = \mathrm{e}^{-i\delta t}\, S^{\mathrm{TQ}}_{\mathrm{ideal}}\left(\tau_1,\tau_2;t\right) F\left(\tau_1,\tau_2;\theta,\delta\right) + \eta\left(t\right), \tag{6.19}$$

and the corrected signal, $S^{\mathrm{TQ}}_{\mathrm{estimate}}$ would take the two term form

$$S_{\text{estimate}}^{\text{TQ}}\left(\delta,\tau_1,\tau_2;t\right)=\mathrm{e}^{-i\delta t}\,S_{\text{ideal}}^{\text{TQ}}\left(\theta,\delta,\tau_1,\tau_2,t\right)+\frac{1}{F\left(\tau_1,\tau_2;\theta,\delta\right)}\eta\left(t\right). \tag{6.20}$$

Because the correction factor is less than one, $|F(\tau_1,\tau_2;\theta,\delta)|\leq 1$, this signal correction approach is not desirable since it decreases the signal-to-noise ratio (SNR) and also, in extreme cases when total signal cancellation occurs, F vanishes, therefore (6.20) cannot be used to recover the ideal signal.

The effects of signal cancellation can be better compensated for by noting that the vanishing of the TQ signal under conditions of non-zero δ is not related to the intrinsic physics of the problem, but rather to the use of an inappropriate approach for the measurement of the TQ coherences. In other words, rather than correcting the effects at a data processing stage, a better approach would be to acquire the TQ signal under conditions that avoid the destructive interference between the coherence pathways. This new approach is presented in the text below.

From Eq(6.2) and Eq(6.6), it is clear that, once the off-resonance parameter is fixed, for any choice of the RF and receiver phases, the measured signal is a linear combination of twelve complex quantities, $B_{m_1m_2}\left(t\right)=\exp\left(-i\Delta_{m_1m_2}\right)A_{m_1m_2}\,\mathrm{e}^{-i\delta t}$, with time independent coefficients, *i.e.*,

$$S_{\delta}\left(t\right)=\sum_{m_1=-1}^{1}\sum_{m_2=-3}^{3}\exp\left(-i\Phi_{m_1m_2}\right)B_{m_1m_2}\left(t\right). \tag{6.21}$$

If several measurements are performed using different settings for the receiver and RF phases, and these signals are stored independently (*i.e.*, not added in real time by the scanner), Eq(6.21) generates a linear system in the unknowns B_{mn}. By solving this linear system, the ideal TQ signal, as defined by Eq(6.14), can then be obtained using the expression:

$$S^{TQ}\equiv\mathrm{e}^{i\delta t}\left(\mathrm{e}^{i\Delta_{-1,-3}}\,B_{-1,-3}+\mathrm{e}^{i\Delta_{1,-3}}\,B_{1,-3}+\mathrm{e}^{i\Delta_{-1,3}}\,B_{-1,3}+\mathrm{e}^{i\Delta_{1,3}}\,B_{1,3}\right) \tag{6.22}$$

Because the number of unknown complex quantities in Eq(6.21) is twelve, twenty-four different acquisitions have to be performed to for determining all of the complex amplitudes B_{nm}. Under these conditions, use of an optimal acquisition scheme involves the proper choice of twenty-four sets of phases (φ_1,φ_2,φ_3,ψ) such that the associated linear system can be solved for the complex amplitudes B_{mn}.

One possible choice of phase cycling that allows the solution of the system mentioned above would be to repeat the phase cycles from Eq(6.15) four times, each time with different starting phases $\left(\alpha_1^j, \alpha_2^j\right)$, $j = 1,2,3,4$. By using this acquisition, four signals S_j are obtained that are linear combinations of TQ components only

$$S_j(t) = \sum_{m_1=-1,1} \sum_{m_1=-3,3} f_{m_1 m_2}\left(\alpha_1^j, \alpha_2^j\right) B_{m_1 m_2}(t) \quad j = 1,2,3,4. \tag{6.23}$$

This approach reduces the dimensionality of the problem from twenty-four to four while also reducing the number of phases from ninety-six to eight. The starting phases chosen in this section, together with the corresponding collected signals are displayed in the (6.24)

$$\begin{cases} \left(\alpha_1^1, \alpha_2^1\right) = (30°, 120°) \\ \left(\alpha_1^2, \alpha_2^2\right) = (0°, 0°) \\ \left(\alpha_1^3, \alpha_2^3\right) = (60°, 75°) \\ \left(\alpha_1^4, \alpha_2^4\right) = (45°, 90°) \end{cases} \Rightarrow \begin{pmatrix} S_1 \\ S_2 \\ S_3 \\ S_4 \end{pmatrix} = 6 \begin{pmatrix} 1 & 1 & 1 & 1 \\ -1 & 1 & -1 & 1 \\ i & -i & i & -i \\ \frac{(1+i)}{\sqrt{2}} & \frac{(1-i)}{\sqrt{2}} & \frac{(-1+i)}{\sqrt{2}} & \frac{-(1+i)}{\sqrt{2}} \end{pmatrix} \begin{pmatrix} B_{-1,-3} \\ B_{-1,+3} \\ B_{+1,-3} \\ B_{+1,+3} \end{pmatrix} \tag{6.24}$$

By solving the above system, the modified individual amplitudes B_{mn} are retrieved in the form of simple linear combinations of the measured signals,

$$\begin{pmatrix} B_{-1,-3} \\ B_{-1,+3} \\ B_{+1,-3} \\ B_{+1,+3} \end{pmatrix} = \frac{1}{8} \begin{pmatrix} 1-i & 3+i & 2(1+i) & \sqrt{2}(1-i) \\ -1 & 1 & -1 & 1 \\ i & -i & i & -i \\ \sqrt{2}(1-i) & \sqrt{2}(1-i) & \sqrt{2}(1-i) & \sqrt{2}(1-i) \end{pmatrix} \begin{pmatrix} S_1 \\ S_2 \\ S_3 \\ S_4 \end{pmatrix} \tag{6.25}$$

From this system, the corrected TQ signal is then obtained using

$$S^{TQ} \equiv \mathrm{e}^{i\delta t}\left(\mathrm{e}^{i\Delta_{-1,-3}}\, B_{-1,-3} + \mathrm{e}^{i\Delta_{1,-3}}\, B_{1,-3} + \mathrm{e}^{i\Delta_{-1,3}}\, B_{-1,3} + \mathrm{e}^{i\Delta_{1,3}}\, B_{1,3}\right), \tag{6.26}$$

where the quantities Δ contain the information about the off-resonance parameter δ. This is the approach proposed in this thesis. Note that for imaging experiments, the method above is easily generalized through the use of spatial maps for the field inhomogeneity by constructing the solution of the linear system above in a pixel-by-pixel fashion. The effectiveness of this approach is experimentally demonstrated in the sections below.

6.1. NMR experimental results

All NMR experiments were performed on a vertical bore, 7Tesla Bruker DMX300 spectrometer (Bruker AG, Germany). The NMR experiments presented here are aimed at emulating the signal originating from a single voxel in a MRI experiment. Because the off-resonance is one of the main experimental parameters, in order for those experiments to be meaningful, a high homogeneity of the B_0 field is required (the B_1 homogeneity is a less stringent requirement). In the light of those considerations, the sample was chosen as cylindrical in shape with a 10 mm diameter and a height of 4 cm (longer than the RF coil). For the purposes of shimming and calibration of the 90° pulse, one-pulse experiments (consisting of a RF pulse, 128μsec delay and acquisition with a sampling rate d_w=8μsec) were used.

The calibration of the 90° pulse is performed at constant power level and the length of the 90° pulse is determined by acquiring an array of one-pulse spectra with the pulse length incremented from zero to 64 microseconds. The 90° pulse was found to correspond to a length of 15.7 microseconds. The homogeneity of B_1 field, estimated from the shape of spectra array was found to be satisfactory [36].

The triple quantum experiments are performed with the pulse sequence depicted in Figure 6.1. Relevant data acquisition parameters are τ_1=5msec, τ_2=64μsec and the number of FID's accumulated N=150. The data are accumulated at a rate d_w=16μsec, with an original delay d_e=32μsec. The τ_1=5.msec value is close to the optimal value for the sample used; the maximum TQ signal should be obtained for the setting

$$\tau_{\text{optim}} = \frac{T_L T_S}{T_L - T_S} \log \frac{T_L}{T_S} \tag{6.27}$$

Figure 6.2 presents the measured conventional TQ FID data (dots) and its biexponential non-linear fit (solid line) to the formula

$$s(t) = A\left(e^{-t/T_L} - e^{-t/T_S}\right) + B \tag{6.28}$$

Prior to fitting, the FID was scaled to its maximum value and phase corrected to zero and first order. This procedure rotates the entire signal onto the real channel thereby improving the SNR (only noise is left on the imaginary component, as seen in the Figure 6.2). The baseline as returned by the fit, B = 0.003, is much smaller than the amplitude A, A=1.6, and proves that the signal is a good approximation to an ideal TQ signal (*i.e.*, negligible bias in the fit).

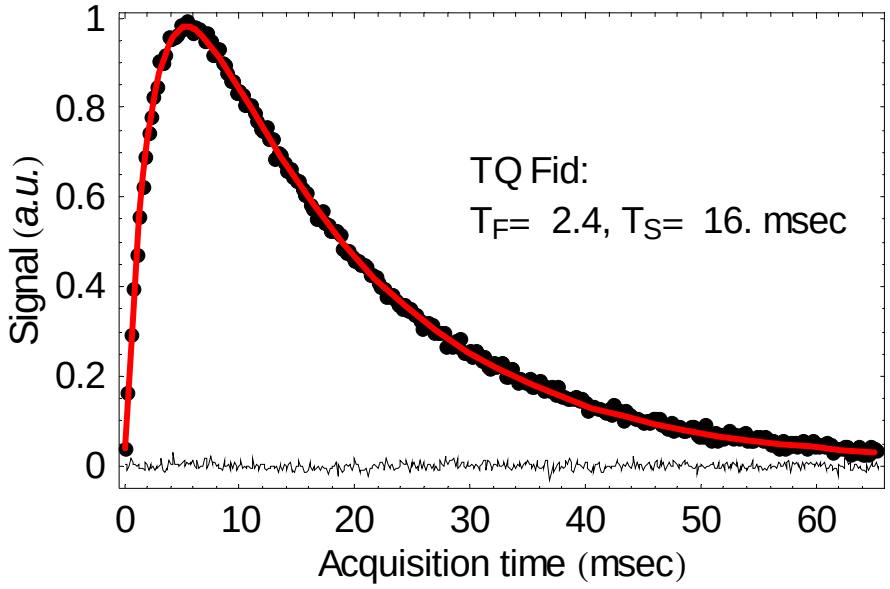

Figure 6.2 The conventional TQ filtered FID. The fit to a biexponential function (solid line) is presented together with the experimental real (dots) and imaginary (thin line) data points. The displayed data points are undersampled, to simplify the graph.

The effectiveness of the coherence pathways decomposition is demonstrated in Figure 6.3. The conventional TQ signal is shown together with the four individual contributions, associated with the different coherence pathways (the phase cycles required for their acquisition

are presented in Appendix 2). The individual signals are acquired with the same number of excitations, 150, and their sum is compared with the classical TQ signal. The agreement between the on-the fly filtered TQ signal and the sum of the four coherence illustrates the validity of coherence decomposition in Eq(6.13). The fact that all the components have the same shape demonstrates good B_0 homogeneity, while the equality of amplitudes confirms good B1 homogeneity. Those facts are another justification for considering the signal in Figure 6.2 as resembling a single voxel signal.

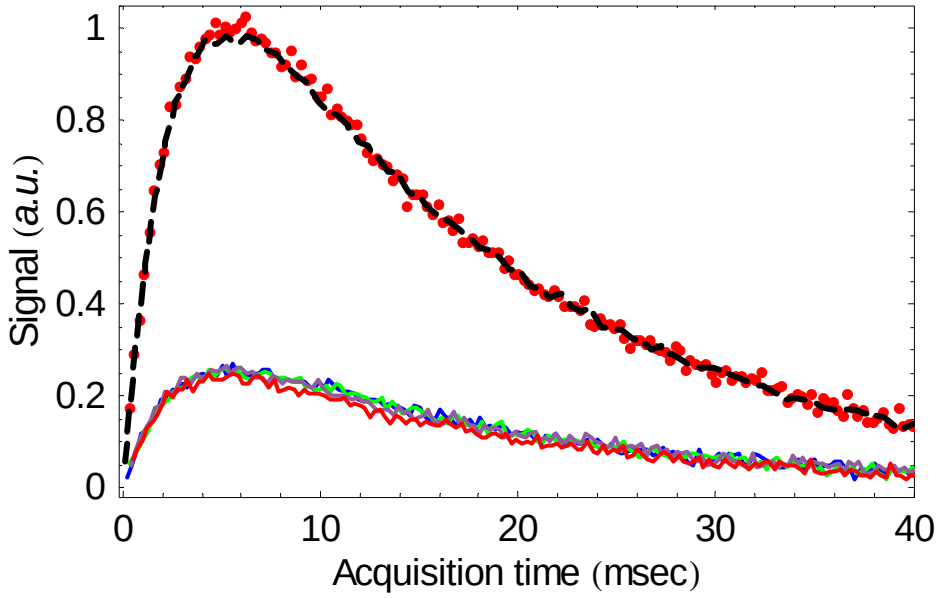

Figure 6.3 The on-resonance conventional TQ signal (dashed line) compared with signals originating from individual coherence pathways (solid lines) and their sum (dots).

The effect of off-resonance is graphically illustrated in Figure 6.4, where the conventional TQ signal is acquired on-resonance and with offsets of 32 Hz, 40 Hz and 56 Hz. The signals are phase corrected to 0^{th} and 1^{st} order, as described before. The normalization factor is the same for all the plots, in other words the relative amplitudes are preserved.

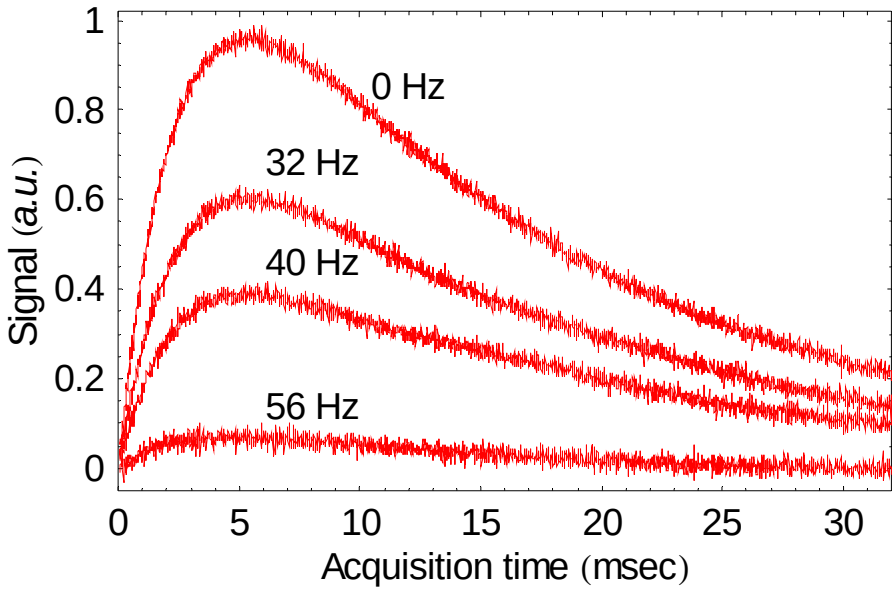

Figure 6.4 the conventional TQ signal for four different settings of the off-resonance parameters (0, 32, 40, and 56 Hz). Each signal is phase corrected to 0^{th} and 1^{st} orders. As expected, the TQ intensity is significantly diminished as the off-resonance increases.

In order to demonstrate the reconstruction of the TQ signal using the modified scheme introduced in Eq(6.24), the RF frequency in the previous TQ experiment was set 50Hz off-resonance. The signals acquired with each of the four phasing cycles are presented in Figure 6.5.

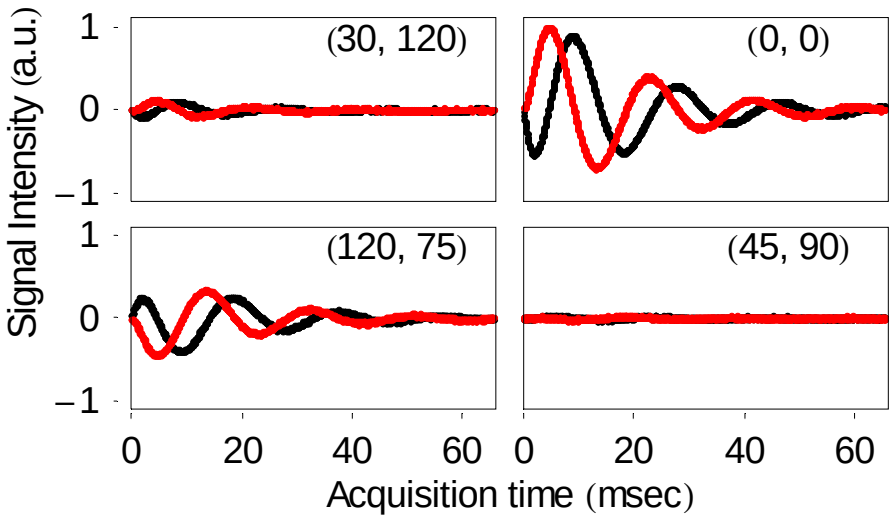

Figure 6.5 the four TQ filtered FID's acquired with different starting phases. Each plot displays the real (black line) and imaginary (red line) parts of the corresponding FID.

The solution (the determination of the B_{mn}'s) from Eq(6.25) is then computed for each data point. The demodulated amplitudes, $|A_{mn}|$ are displayed in Figure 6.6 together with their sum. The fact that the $|A_{mn}|$ functions are equal, together with the fact that their sum reproduces the on-resonance signal, demonstrates the effectiveness of the modified acquisition scheme, even in the presence of severe off-resonance.

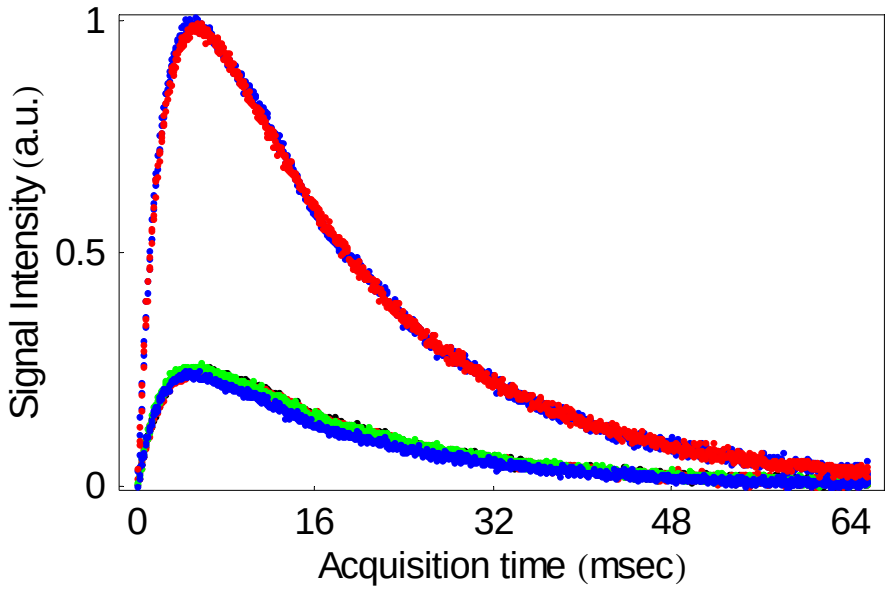

Figure 6.6 the four individual components (the overlapping, low amplitude FID's) are displayed together with the reconstructed and on-resonance signals (the overlapping, high amplitude FID's).

For an MRI experiment, the off-resonance parameter varies across the volume of interest. In order to verify the accuracy of the modified TQ acquisition scheme, four NMR experiments were performed in a 2D fashion, for each of the starting phase choice. In each experiment, the RF frequency was incremented from -120Hz to 120 Hz in 8Hz steps. For every frequency setting, the TQ fid was acquired using the same settings as in the 1D experiment. The number of FID's averaged was reduced from 150 to 60, in order to shorten the total experiment time. The dependence of conventional TQ signal as a function of the applied RF frequency is presented in Figure 6.7. Since a rough surface is harder to visualize, the surface was smoothed with a running average algorithm.

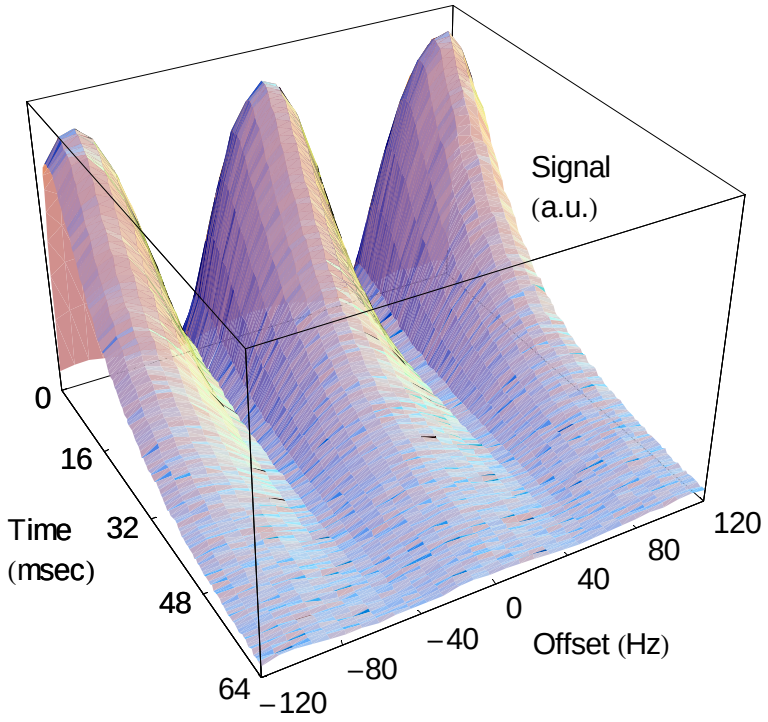

Figure 6.7 the acquired TQ FID magnitudes are displayed as a function of acquisition time and the off-resonance parameter. The vanishing of the TQ signal is expected around δ=±50Hz lines and it is well demonstrated by the plot.

To evaluate the efficiency of the modified scheme, the integrals of the demodulated TQ signals are presented in Figure 6.8, as a function of frequency. The crosses correspond to conventional acquisition scheme. They are following well the dependency ($\cos\delta\tau_1 \cos 3\delta\tau_2$), displayed as solid line. The boxes correspond to the modified acquisition scheme. The more benign variation of TQ intensity of the off-resonance parameter for the modified acquisition scheme makes this scheme suitable for imaging applications.

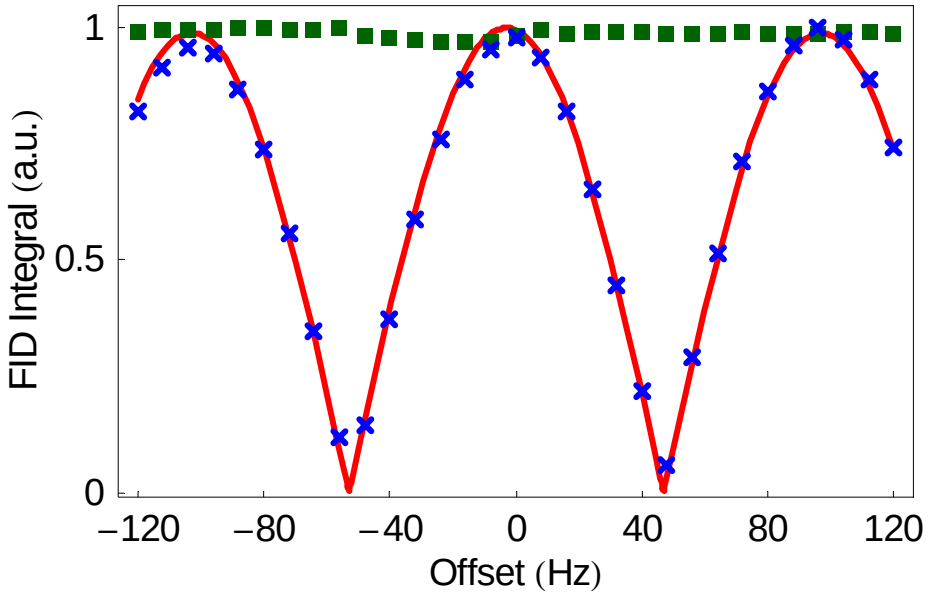

Figure 6.8 integral of the conventional TQ FID as a function of the off resonance parameter (crosses). The theoretical function (solid line) agrees well with experimental data. The modified TQ acquisition data (boxes) shows less variation with the off-resonance parameter.

6.2. Triple Quantum imaging in B_0 inhomogeneous fields

The imaging experiments were performed on a whole-body, 3 Tesla, MRI scanner (GEMS) using a custom-built sodium RF coil and a Twisted Projection Imaging (TPI) sequence. [35]. A cylindrical shaped (length L=12 cm, diameter ∅=12 cm), homogenous phantom filled with 10% agar gel, was used.

The first step in our procedure is the determination of the sample characteristic, accomplished by using the variable echo method. The results are presented in Figure 6.9. By simple examination, it is visible that is not possible to predict the relaxation parameters from none of the individual FID's. The simple approach in trying to predict the optimum delay (the point at which the TQ signal is maxim) fails, too. The maximum of a single FID coincides with the point of largest signal, only in the case in which the optimum delay is used.

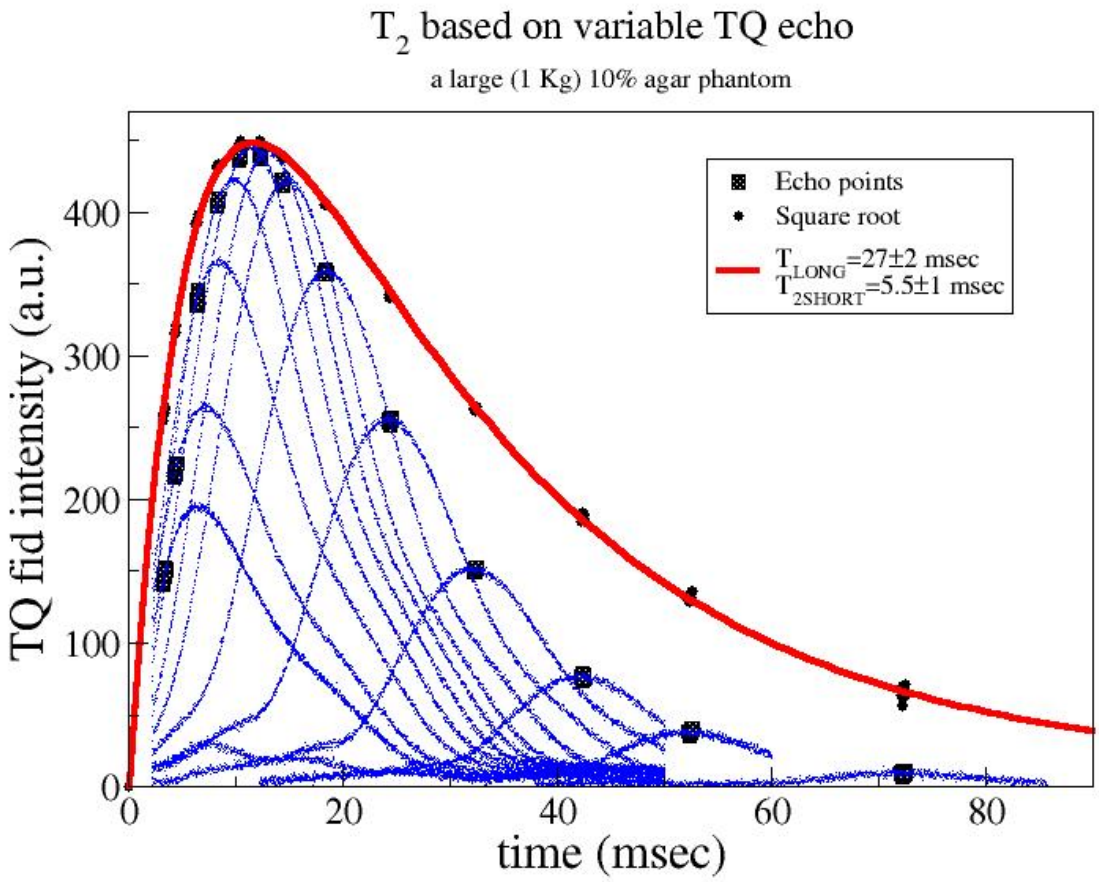

Figure 6.9 Variable echo experiment, the sample used, described in the text, is characterized by large B_0 inhomogeneities, therefore the indivifual FID's are distorted from the biexponential form. Selecting only the echo amplitudes and representing their square root values (bullets) the biexponential form is obtained with the T_{LONG} of 27 milliseconds and T_{SHORT} 5.5 milliseconds.

Two single quantum (SQ) data sets were obtained by exciting the sample with hard pulses (pulse width p_w=400μsec) and using echo times (the delay from the end of the pulse to the beginning of acquisition period) T_{E1}=10.msec and T_{E2}=11.5msec. The reconstructed images, obtained by using a regridding algorithm, are 64x64x64 complex matrices of complex values. Using the two SQ images, the off-resonance parameter δ, for each voxel, was obtained from the phases of SQ images, to generate a phase map

$$\delta = \frac{\phi_2 - \phi_1}{T_{E2} - T_{E1}} \tag{6.29}$$

with ϕ_1, ϕ_2 being the phases, in that voxel, of the reconstructed images corresponding to the echo times T_{E1} and T_{E2}, respectively. Phase unwrapping was not necessary, as the phase variation from one pixel to another are typically small. To speed up the analysis, an image mask (with a threshold set at 30% of the maximum SQ image intensity) was generated from the SQ image so that the solution of the linear system described above was not performed in areas of zero signals. Triple quantum (TQ) images are acquired with a modification of TPI sequence, as presented in. [29]. The separations between pulses were τ_1=7.0msec and τ_2=0.5msec. The echo time is T_E=10.0msec. Those values correspond to the highest TQ signal for the phantom used. Four different experiments, corresponding to the four phase cycles from Eq(6.24), were performed. Image reconstruction was performed using the same algorithm, with the same parameter settings as used for SQ images..

Figure 6.10 and Figure 6.11 present the SQ image for the first echo times and the B_0 map obtained from the collected SQ images. The presence of large inhomogeneities in the middle of phantom is clearly illustrated in this map. This B_0 map hast the expected shape for a finite cylinder, placed in uniform magnetic field.

In Figure 6.12 the conventional TQ images is presented. As expected from the phase map, the TQ signal is diminished in the center of the phantom. In Figure 6.13, the images obtained from modified TQ acquisition are presented. The artifacts due to the B_0 inhomogeneities have been largely removed.

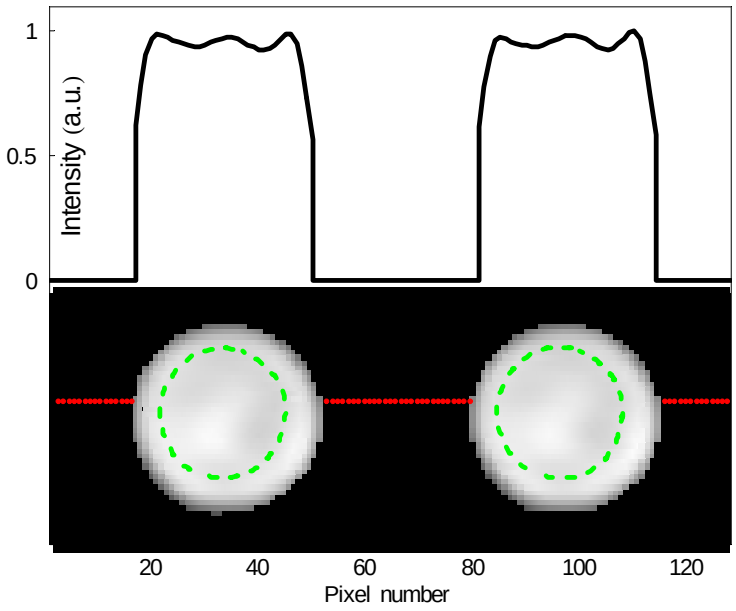

Figure 6.10 Selected partitions from the 3D SQ image of a cylindrical phantom.

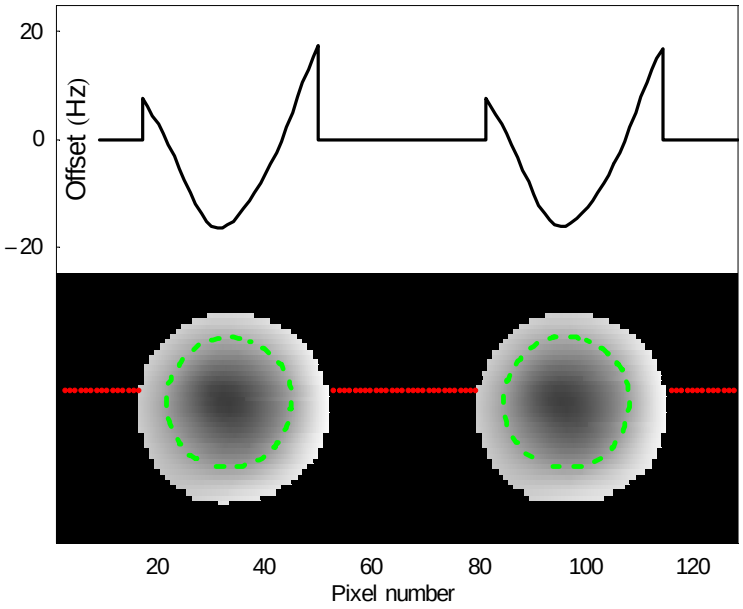

Figure 6.11 Selected partitions from the 3D B_0 maps from a cylindrical phantom.

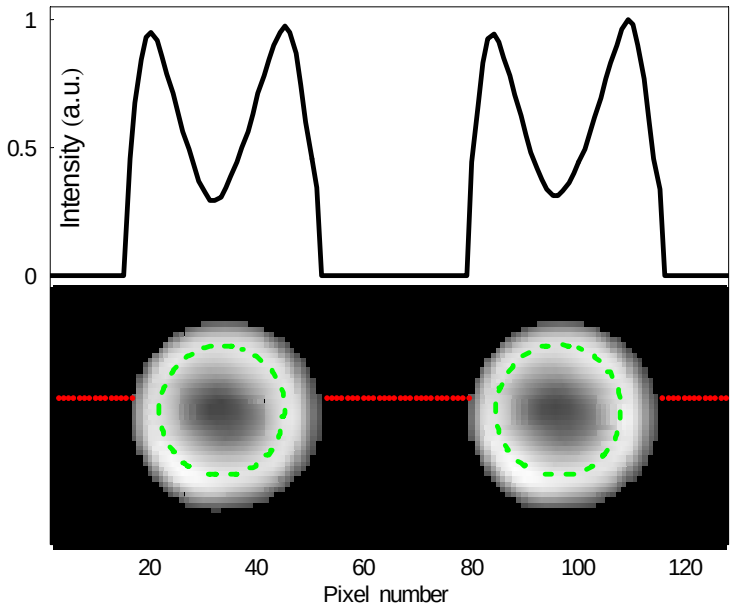

Figure 6.12 The TQ image of the cylindrical phantom. The effect of the off-resonance is visible as a low intensity area, in the center of image

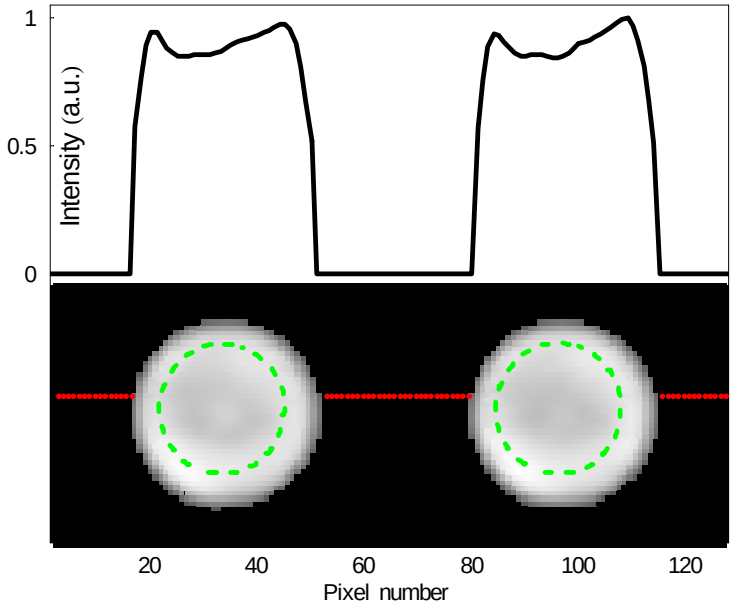

Figure 6.13 The TQ image acquired with the modified sequence. The hole in the center of image disappeared.

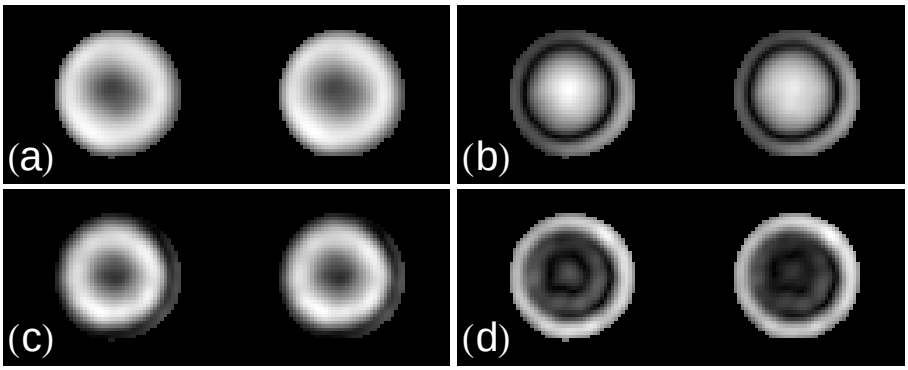

Figure 6.14 The TQ images of the cylindrical phantoms acquired with the four different starting phases, as described in text.

In Figure 6.15 a 1D illustration of the differences between the conventional and modified TQ results is given. The data were sampled along the dotted lines presented in each picture.

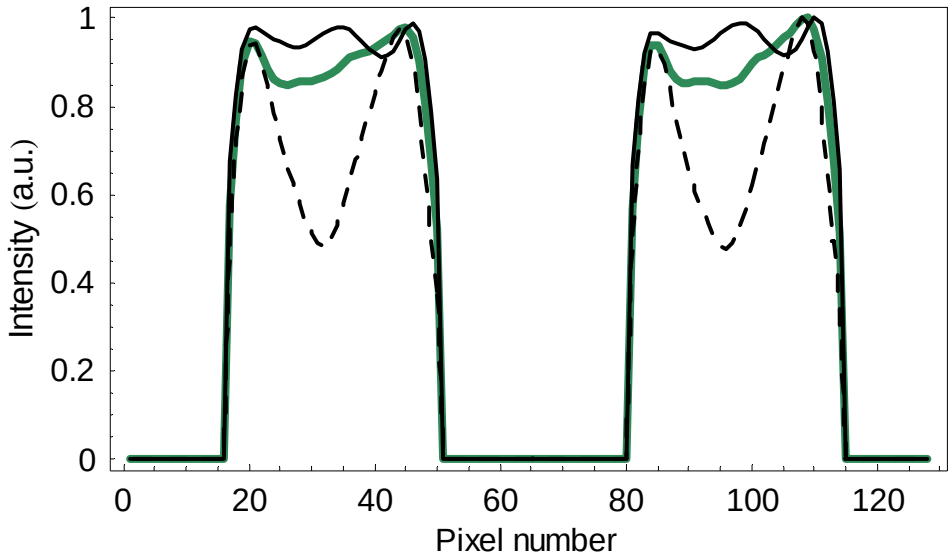

Figure 6.15 The conventional TQ profile (dashing) and modified TQ (thick solid line), together with the SQ profile (thin solid line). The variation in the reconstructed intensity observed in the corrected TQ image is due to the presence of B_1 inhomogeneity, ringing and intravoxel dephasing. However, a significant source of variation has been removed by using modified TQ scheme

A description of the effects of B_0 inhomogeneities on TQ filtered sodium MRI using a three-pulse coherence transfer filter has been presented. We have demonstrated that in the presence of large B_0 inhomogeneities significant signal loss arises due to destructive interference between the different coherence pathways. We have also shown that this effect can be eliminated through the separate acquisition of the TQ coherences followed by their addition after B_0 correction with the aid of a B_0 map. Our results demonstrate that this approach is well suited for TQ sodium MRI experiments using clinical MRI scanners.

6.3. TQ sodium imaging of human brain

The applications of TQ techniques for humans imaging encounter supplementary difficulties, as opposed to "phantom" experiments. First, the duration of the experiments can not exceed acceptable limits (30 minutes). This fact reduces the maximum attainable signal to noise ratio. Second, in order to avoid the harming of subjects, there are limits imposed on physical parameters. The RF power limitations are the most restrictive. The fast relaxation of sodium would allow high repetition rates in imaging experiments. During the experiments presented in this section, the repetition rate was decided not based on the relaxation properties but rather on the RF power limitation considerations.

In order to effectively implement the procedure described in the last section the first information necessary is the estimation of relaxation times in human brain. While the procedure, demonstrated on agar phantom and in vitro, can be applied in this situation, the limitations in the total scanning time restrict us from acquiring the full T_2 decay curve.

By selecting the (-1,-3) echo alone, three TQ filtered FID's have been collected with three different preparation times τ_1=3.5, 5 and 8 milliseconds. The sequence is characterized by

τ_2=0.5 milliseconds and the pulse width is p_w=0.4 milliseconds. The position of the echo is computed according to

$$\tau_{ECHO} = \tau_1 + 3\tau_2 + 7\frac{2}{\pi} p_w \tag{6.30}$$

Only 420 FID's were averaged, in order to keep this procedure as short as possible, the results are displayed in Figure 6.16. From this measurement, the optimum preparation time was decided as 3.5 milliseconds.

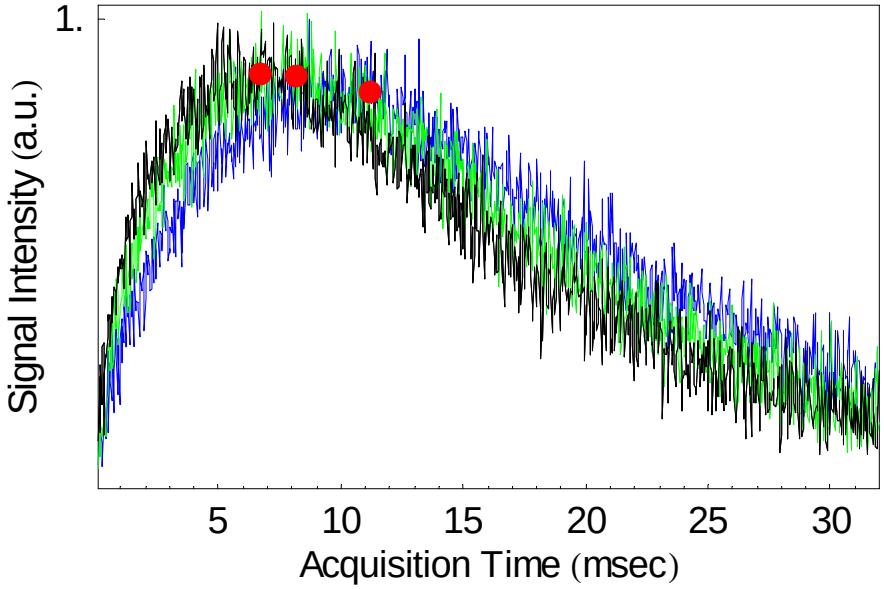

Figure 6.16 Three TQ FID, acquired with the filtering scheme TQ$^-$, the preparation time is τ_1=3.5, 5, and 8 milliseconds. The dots correspond to the echo positions.

Using a different, less efficient coil, not capable of achieving a 90° pulse, similar data were recorded, with preparation times, .5, 1, 2, 4 and 6 milliseconds. All five FID's are presented in Figure 6.17. The position of the echo was predicted with the previous formula (6.30). The amplitude at the echo is obtained by averaging nearby data points. Varying the span of the averaged data, no change in the ordering of the echo amplitudes is noticed.

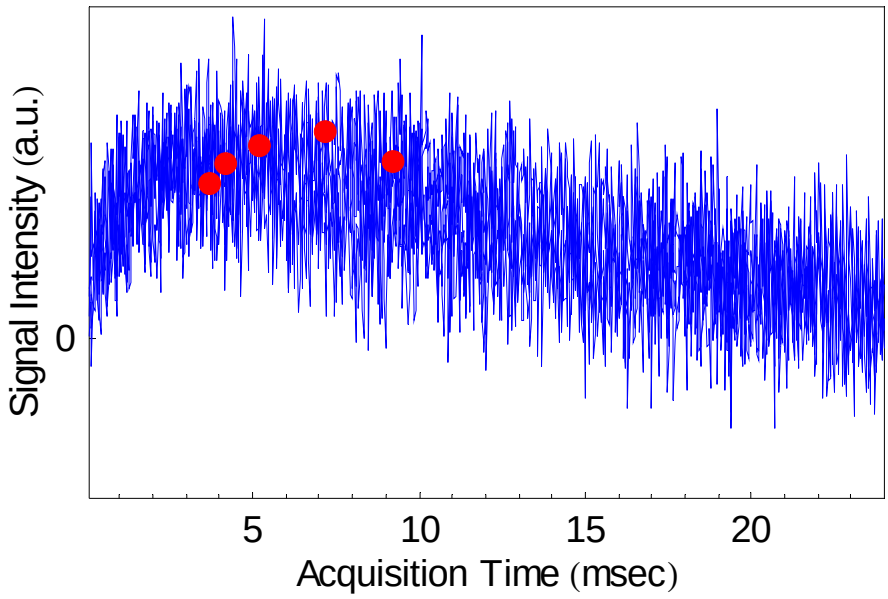

Figure 6.17 Five TQ variable echo experiment using a very inefficient coil. The flip angle was kept far from the 90, in an attempt to reduce the deposited power. The individual FID's are kept hard to visualize, to prove the point that the experimental determination of the optimum preparation time is possible even when the SNR is low. In obtaining the echo amplitudes (dots), the ordering does not change as we change the number involved in averaging between 50 and 100.

The application of the B_0 compensating method follows step by step the procedure presented in the previous section. The images are presented in the Figure 6.18, Figure 6.19, Figure 6.20, and Figure 6.21.

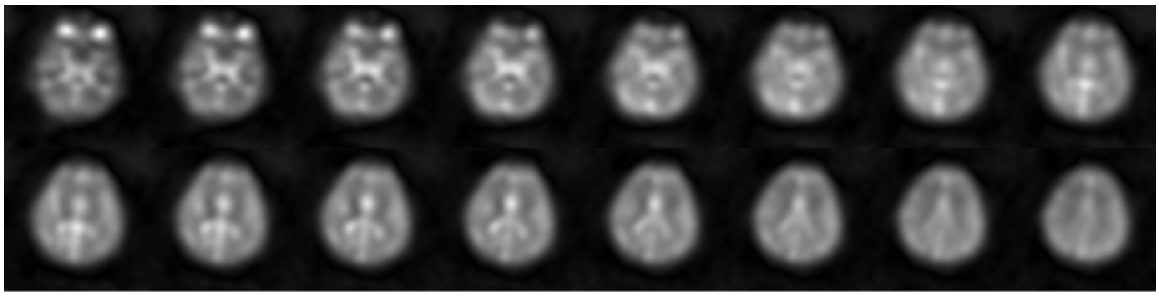

Figure 6.18 Selected slices from single quantum image, acquired with an echo time 100 μseconds.

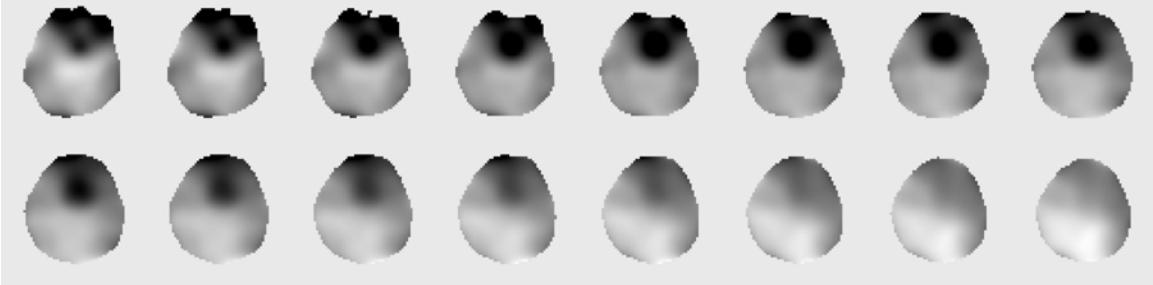

Figure 6.19 the phase map obtained from two SQ images. The sinuses area is the region in which the B_0 inhomogeneities have the maximum values.

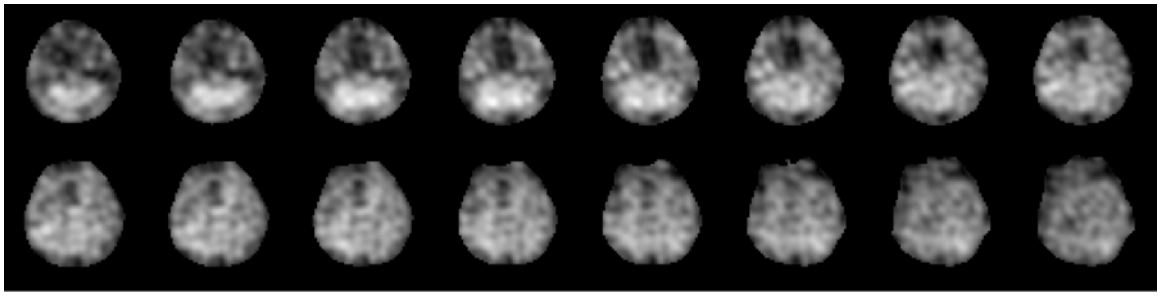

Figure 6.20 Standard TQ. acquisition. In the region of large B_0 inhomogeneities, the image intensity has an artificial low intensity (visualized as a dark hole)

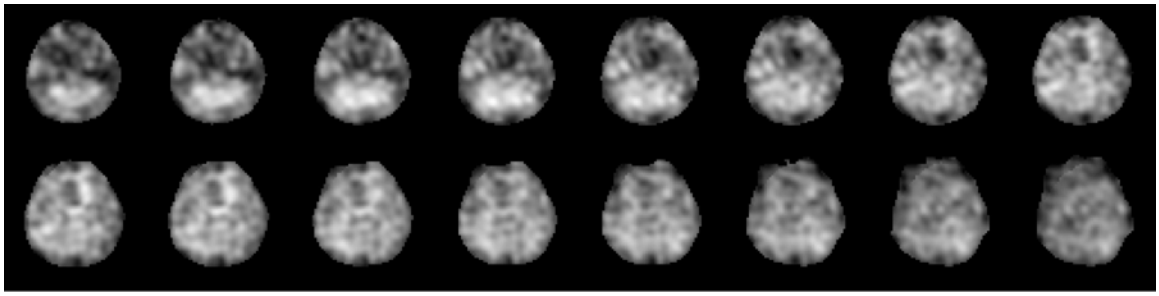

Figure 6.21 B_0 corrected TQ, acquired with the presented methodology. Partially, the B_0 effects have been removed.

The quest for quantitative sodium MRI has to overcome difficulties associated with field inhomogeneities. The B_0 field inhomogeneities, mainly due to variations in tissues susceptibility, manifest in variety of modalities. T_2^* effects and the distortion of k-space trajectories are the major difficulties encountered in MRI and they receive constant attention in the scientific literature. Atop of these manifestations, a source of significant variations in MQF MRI has been analyzed in this section. The source resides in the way that various coherence pathways add up to create the measured signal; the B_0 inhomogeneity introduces phase differences between such coherence pathways, effectively diminishing the signal. The problem is demonstrated for sodium TQ experiments, but it can manifest for any nuclei, in any experiment involving multiple RF pulses.

The obvious solution (which consists in designing the filtering scheme in such a way that only one coherence path contribution is allowed to pass the filter) lowers the SNR too much. In an attempt to preserve the SNR of the experiment, while avoiding the cancellation, a different scheme of acquisition is introduced. The main idea is that while acquiring all components, a supplementary encoding would allow their separation, later in the processing stage.

The way this idea is followed in this thesis, as four different TQ filtered acquisition, while demonstrated as being correct, it may be not optimal. For example, in the ideal case of perfect B_0 homogeneity, on-resonance, the second and fourth acquisitions retrieve only noise. This observation is not a critique of the method itself; it just emphasizes the fact that prior knowledge about the B_0 could be used to design a better acquisition scheme, for that specific situation. In itself, the design of the best acquisition scheme for acquiring TQ images, by taking in consideration the B_0 inhomogeneities, is a new problem. The current work proves that this approach is possible, and it would be developed in a future work.

APPENDIX A Linear Algebra

The canonical basis in C^N consist of N vectors, e_n, n=1,…,N whose elements satisfy $(e_n)_k = \delta_{nk}$. Whenever the k-th element of a canonical basis vector is to be referenced, the Kronecker delta function will be used instead. In the situation in which the dimension of the vectorial space is not clear from the context, the notation $e_n(N)$ is used to denote the n-th basis vector in the N-dimensional space.

A mxn matrix is defined as a matrix with m rows and n columns. The matrix can be considered either as a row of columns or as a column of rows

$$A = \left[col(A,1), \cdots, col(A,n) \right] = \begin{bmatrix} row(A,1) \\ \vdots \\ row(A,m) \end{bmatrix} \tag{7.1}$$

In the situation in which the orthonormal system b_j is given, satisfying

$$b_j^{\dagger} \cdot b_k = \delta_{jk}, \tag{7.2}$$

the column and row of a linear operator, in respect with the basis b_j are defined by the scalar products,

$$\begin{aligned} col(A,k) &= A \cdot b_k \\ row(A,k) &= b_k^{\dagger} \cdot A \end{aligned} \tag{7.3}$$

and the following relations are a consequences of the linear nature of the operator

$$\begin{aligned} A \cdot X &= \sum_k row(A,k) \cdot X \\ X \cdot A &= \sum_k X \cdot col(A,k) \end{aligned} \tag{7.4}$$

The space of the linear operators over C^n with values in C^m is, itself, a linear space, allowing the identification of such operators with vectors in a mn dimensional space (superspace). Such embedding could be realized in a variety of ways, most of which reduces to the choice of a proper labeling of the matrix elements associated with the original operator, in a given basis. The most natural choice is realized by defining the 'column stacking' operation

$$A \in C^{m\times n} \quad \text{cvec}(A) = \begin{bmatrix} \text{col}(A,1) \\ \vdots \\ \text{col}(A,n) \end{bmatrix}. \tag{7.5}$$

The matrix element at row i and column j, A_{ij}, is found in cvec(A) at position m (j-1)+i. The operation such defined preserves the natural scalar product in the operator space

$$\text{Tr}\left\{A^\dagger \cdot B\right\} = \left(\text{cvec}\left(A\right)\right)^\dagger \cdot \text{cvec}\left(B\right). \tag{7.6}$$

The relationship between the c-vector associated with the matrix and the one associated with the transpose is not trivial. In terms of the perfect shuffle matrix

$$\text{cvec}\left(A^T\right) = S_{m,n}\, \text{cvec}\left(A\right) S_{n,m} \tag{7.7}$$

The Kronecker product of two matrices $A \in C^{m\times n}$ and $B \in C^{p\times q}$ is defined as the $\left(mp\right)\times\left(nq\right)$ matrix obtained by replacing each element of a_{ij} with the block $a_{ij}B$

$$A \otimes B = \begin{pmatrix} a_{11}B & \cdots & a_{1n}B \\ \vdots & \ddots & \\ a_{m1}B & & a_{mn}B \end{pmatrix} \tag{7.8}$$

The following properties are well-known

$$\begin{aligned} \left(B\otimes C\right)^\dagger &= B^\dagger \otimes C^\dagger \\ \left(B\otimes C\right)\left(F\otimes G\right) &= BF \otimes CG \end{aligned} \tag{7.9}$$

One of the main advantages offered by Kronecker product is the transformation of the matriceal relations in (super) vectorial correspondents

$$\mathrm{cvec}\left(AXB\right)=\left(B^{T}\otimes A\right)\mathrm{cvec}\left(X\right). \tag{7.10}$$

The superoperators are defined as acting linearly on the regular operators. For any operator, A, one can define the left and right superoperators acting on an arbitrary operator B as the product to the left and, respectively, to the right

$$\begin{aligned}\mathbf{A}^{L}B&\equiv AB\\ \mathbf{A}^{R}B&\equiv BA\end{aligned}. \tag{7.11}$$

Using the Kronecker representation one could easily notice

$$\begin{aligned}\mathbf{A}^{L}&=1_{m}\otimes A\\ \mathbf{A}^{R}&=A\otimes 1_{n}\end{aligned} \tag{7.12}$$

The following commutation relation, becomes trivial, using this formalism

$$\mathbf{A}^{L}\mathbf{B}^{R}=\mathbf{B}^{R}\mathbf{A}^{L} \tag{7.13}$$

allowing one to express the exponential of a sum of left and right superoperators in a simple form

$$\begin{aligned}\exp\left(\mathbf{A}^{L}+\mathbf{B}^{R}\right)&=\exp\left(\mathbf{A}^{L}\right)\exp\left(\mathbf{B}^{R}\right)\\ \exp\left(\mathbf{A}^{L}+\mathbf{B}^{R}\right)&=\exp\left(\mathbf{A}^{L}\right)\exp\left(\mathbf{B}^{R}\right)\end{aligned} \tag{7.14}$$

APPENDIX B Superspace description of spin 1/2 systems

For a single, spin 1/2 particle a pure state is described by a 2 dimensional column of complex numbers.(ket)

$$|\psi\rangle = \begin{pmatrix} \alpha \\ \beta \end{pmatrix} = \alpha \begin{pmatrix} 1 \\ 0 \end{pmatrix} + \beta \begin{pmatrix} 0 \\ 1 \end{pmatrix} = \alpha |\chi^{+}\rangle + \beta |\chi^{-}\rangle \tag{8.1}$$

The adjoint (bra) is defined as transpose and conjugate

$$\langle\psi| = (\alpha^{*}, \beta^{*}) = \alpha^{*} \langle\chi^{+}| + \beta^{*} \langle\chi^{-}| \tag{8.2}$$

The state has to satisfy (a QM principle) the normalization condition

$$\langle\psi|\psi\rangle = 1 \quad \Leftrightarrow \quad |\alpha|^2 + |\beta|^2 = 1 \tag{8.3}$$

The parameterization (at this moment just a parameterization) of a general state is given by

$$|\psi\rangle = \begin{pmatrix} \cos\dfrac{\theta}{2} \\ e^{i\phi} \sin\dfrac{\theta}{2} \end{pmatrix}. \tag{8.4}$$

The results of a measurement for the physical quantity are the eigenvalues of the associated operator.

$$\begin{aligned} \hat{A}|a\rangle &= a|a\rangle \\ \langle a|a\rangle &= 1 \end{aligned} \tag{8.5}$$

The measurement has a statistic character. The (conditional) probability to obtain a given value "a" while the system is in a given state $|\psi\rangle$ is given by

$$p(\psi;a)=\left|\langle a|\psi\rangle\right|^2=\langle\psi|a\rangle\langle a|\psi\rangle=\langle\psi|\hat{P}_a|\psi\rangle \text{ with } \hat{P}_a\equiv|a\rangle\langle a| \tag{8.6}$$

The expectation value for observable A when the system is in the state ψ is the average of the possible outcomes, weighted with their probabilities

$$\left\langle\hat{A}\right\rangle_\psi=\sum_a p(\psi;a)\,a=\sum_a\langle\psi|\left(a\hat{P}_a\right)|\psi\rangle=\langle\psi|\hat{A}|\psi\rangle \tag{8.7}$$

Angular momentum operators are represented in terms of Pauli matrices

$$\hat{J}_x=\frac{1}{2}\begin{pmatrix}0&1\\1&0\end{pmatrix}=\frac{1}{2}\hat{\sigma}_x\quad \hat{J}_y=\frac{1}{2}\begin{pmatrix}0&-i\\i&0\end{pmatrix}=\frac{1}{2}\hat{\sigma}_y\quad \hat{J}_z=\frac{1}{2}\begin{pmatrix}1&0\\0&-1\end{pmatrix}=\frac{1}{2}\hat{\sigma}_z \tag{8.8}$$

The basic properties of Pauli matrices are expressed by the product law composition

$$\begin{array}{lll}\hat{\sigma}_x^2=\hat{1} & \hat{\sigma}_y^2=\hat{1} & \hat{\sigma}_z^2=\hat{1}\\ \hat{\sigma}_y\hat{\sigma}_z=i\hat{\sigma}_x & \hat{\sigma}_z\hat{\sigma}_x=i\hat{\sigma}_y & \hat{\sigma}_x\hat{\sigma}_y=i\hat{\sigma}_z\\ \hat{\sigma}_z\hat{\sigma}_y=-i\hat{\sigma}_x & \hat{\sigma}_x\hat{\sigma}_z=-i\hat{\sigma}_y & \hat{\sigma}_y\hat{\sigma}_x=-i\hat{\sigma}_z\end{array}, \tag{8.9}$$

and orthogonality,

$$\mathrm{Tr}\left\{\sigma_i\sigma_j\right\}=2\delta_{ij} \tag{8.10}$$

In short, one could write for the vector of Pauli matrices

$$\vec{\sigma}\times\vec{\sigma}=i\vec{\sigma} \tag{8.11}$$

The angular momentum projection along a direction (θ,ϕ) is given in spherical coordinates by

$$\hat{J}_{\theta,\phi}=\sin\theta\cos\phi\hat{J}_x+\sin\theta\sin\phi\hat{J}_y+\cos\theta\hat{J}_z\,. \tag{8.12}$$

The eigenvalues of this operator are $\pm\frac{1}{2}$, with the corresponding eigenvectors

$$\left|+\frac{1}{2}\right\rangle=\begin{pmatrix}\cos\frac{\theta}{2}\\ e^{i\phi}\sin\frac{\theta}{2}\end{pmatrix}\quad\left|-\frac{1}{2}\right\rangle=\begin{pmatrix}-e^{-i\phi}\sin\frac{\theta}{2}\\ \cos\frac{\theta}{2}\end{pmatrix} \tag{8.13}$$

In a general state parameterized by (8.4) the expectation values of the angular momentum components are found by simple matrix multiplications

$$\left\langle \hat{J}_x \right\rangle_\psi = \frac{1}{2}\cos\phi\sin\theta \quad \left\langle \hat{J}_y \right\rangle_\psi = \frac{1}{2}\sin\phi\sin\theta \quad \left\langle \hat{J}_z \right\rangle_\psi = \frac{1}{2}\cos\theta\,, \tag{8.14}$$

or, in vectorial notation

$$\left\langle \vec{J} \right\rangle_\psi = \frac{1}{2}\left(\sin\theta\cos\phi \quad \sin\theta\sin\phi \quad \cos\theta\right). \tag{8.15}$$

The polarization vector is defined as having components given the expectation values of Pauli matrices

$$\vec{P}_\psi \equiv \left\langle \vec{\sigma} \right\rangle_\psi = 2\left\langle \vec{J} \right\rangle_\psi \tag{8.16}$$

therefore,

$$\vec{P} = \underbrace{\left(\sin\theta\cos\phi \quad \sin\theta\sin\phi \quad \cos\theta\right)}_{\text{Unit versor pointing in } \theta,\phi \text{ direction}} = \vec{u}\left(\theta,\phi\right). \tag{8.17}$$

In such state the angular momentum points in direction given by the polar angles θ and ϕ. The system is aligned, and oriented along the direction $\vec{u}\left(\theta,\phi\right)$. For one single particle, the description through a state vector is sufficient. For a system of N (non-interacting) particles, the quantum state described by a single vector, pure state, is a special particular case of a physical state. This corresponds to a complete knowledge of the individual states of each particle. This implies that we have to be able to prepare such a state, and the information about the state is available. In general, there is available only a partial information about the system, namely the distribution of the individual particles among a sub-set of pure states

$$N = \sum N_j \quad N_j = \text{number of particles in the state } \left|\psi_j\right\rangle \tag{8.18}$$

For large N, the state of an ensemble of particles, could be described as a superposition of pure states with statistical weights $w_j=N_j/N$. The measurement for a physical (additive) quantity, A gives the result expressible in terms of the density matrix

$$A_{meas} = \sum N_j \sum p\left(\psi_j; a\right) a = N \sum_j w_j \left\langle \psi_j \middle| \hat{A} \middle| \psi_j \right\rangle = N \sum_j w_j \operatorname{Tr}\left\{ \left(\left| \psi_j \right\rangle \left\langle \psi_j \right| \right) \hat{A} \right\} = N \operatorname{Tr}\left\{ \hat{\rho} \hat{A} \right\} \quad (8.19)$$

For a particle in a pure state (or a system of particles prepared in identical states), the density matrix is just the projector

$$\hat{\rho}_\psi = \left| \psi \right\rangle \left\langle \psi \right| \quad (8.20)$$

In matriceal form

$$\hat{\rho}_\psi = \begin{pmatrix} a \\ b \end{pmatrix} \begin{pmatrix} a^* & b^* \end{pmatrix} = \begin{pmatrix} |a|^2 & ab^* \\ a^* b & |b|^2 \end{pmatrix} \quad (8.21)$$

The last equality holds only for pure states. For a pure state in which the angular momentum is aligned to a direction (θ,ϕ), the density matrix is completely determined by the polarization vector

$$\left| \psi \right\rangle = \begin{pmatrix} \cos\dfrac{\theta}{2} \\ e^{i\phi} \sin\dfrac{\theta}{2} \end{pmatrix} \qquad \hat{\rho} = \frac{1}{2}\left(1 + \vec{P}\vec{\sigma}\right) = \frac{1}{2}\left(1 + \vec{u}\left(\theta,\phi\right)\vec{\sigma}\right) \quad (8.22)$$

The last expression shows that the density matrix for a pure state decomposes in a trivial scalar component and a vectorial component. For a mixed state the density matrix is obtained as sum over projectors

$$\hat{\rho} = \sum_j w_j \left| \psi_j \right\rangle \left\langle \psi_j \right| = \sum_j w_j \hat{\rho}_j \quad (8.23)$$

In terms of polarization vectors (individuals, and the average polarization vector)

$$\hat{\rho} = \frac{1}{2}\left(1 + \left(\sum_j w_j \vec{P}_j\right)\vec{\sigma}\right) = \frac{1}{2}\left(1 + \vec{P}\vec{\sigma}\right) \tag{8.24}$$

The density matrix decomposes in a trivial scalar component and a vectorial component, this time characterized by a vector with norm less than one.

$$\vec{M}^2 = \left(\sum_j w_j \vec{P}_j\right)^2 \leq 1 \tag{8.25}$$

In general, any operator can be decomposed

$$\hat{A} = a_0 \hat{1} + \vec{a}\vec{\sigma} \quad a_0 = \mathrm{Tr}\left\{\hat{A}\right\} \quad a_i = \mathrm{Tr}\left\{\hat{A}\hat{\sigma}_i\right\}, \tag{8.26}$$

theefore, the expectation value in a general state described by the polarization $\vec{P}$ is given by

$$\begin{aligned} \left\langle \hat{A} \right\rangle &= \mathrm{Tr}\left\{\frac{1}{2}\left(a_0 \hat{1} + \vec{a}\vec{\sigma}\right)\left(\hat{1} + \vec{P}\vec{\sigma}\right)\right\} \\ &= \mathrm{Tr}\left\{\frac{1}{2}\left(a_0 \hat{1} + \left(\vec{a}\vec{\sigma}\right)\left(\vec{P}\vec{\sigma}\right)\right)\right\} = a_0 + \vec{a}\vec{P} \end{aligned} \tag{8.27}$$

In the particular case of the angular momentum operator

$$\left\langle J_i \right\rangle = \mathrm{Tr}\left\{\frac{1}{2}\left(\frac{1}{2}\vec{e}_i\vec{\sigma}\right)\left(1 + P_i\vec{\sigma}\right)\right\} = \frac{1}{2}P_i \tag{8.28}$$

In other words, a general state could be completely described by the expectation value of the angular momentum (which, up to a constant factor is the magnetization).

$$\hat{\rho} = \frac{1}{2}\left(\hat{1} + \vec{P}\hat{\vec{\sigma}}\right) = \frac{1}{2}\left(\hat{1} + 2\left\langle \vec{J} \right\rangle \vec{\sigma}\right) = \frac{1}{2}\hat{1} + \left\langle \vec{J} \right\rangle \vec{\sigma} \tag{8.29}$$

The Schroedinger equation governs the pure state evolution

$$i\frac{d}{dt}\left|\psi\right\rangle = \hat{H}\left|\psi\right\rangle \tag{8.30}$$

The density matrix evolves according to the equation

$$i\frac{d}{dt}\hat{\rho}=i\frac{d}{dt}\sum w_i\left|\psi_i\right\rangle\left\langle\psi_i\right|=\sum w_i\hat{H}\left|\psi_i\right\rangle\left\langle\psi_i\right|-\sum w_i\left|\psi_i\right\rangle\left\langle\psi_i\right|\hat{H} \tag{8.31}$$

which is the Liouville - von Neumann equation

$$i\frac{d}{dt}\hat{\rho}=\left[\hat{H},\hat{\rho}\right] \tag{8.32}$$

The Hamiltonian decompose according to the general rule

$$\hat{H}=h_0\hat{1}+\vec{h}\hat{\sigma}=\begin{pmatrix}h_0 & 0\\ 0 & h_0\end{pmatrix}+\begin{pmatrix}h_3 & h_1-ih_2\\ h_1+ih_2 & -h_3\end{pmatrix} \tag{8.33}$$

The h_0 contribution gives no dynamics; the identity matrix commutes any other matrix

$$\left[\hat{1},\hat{\rho}\right]=0 \tag{8.34}$$

The expression of density matrix in terms of polarization vector

$$\hat{\rho}=\frac{1}{2}\left(\hat{1}+\vec{P}\hat{\sigma}\right)\quad i\frac{d}{dt}\vec{P}\vec{\sigma}=\left[\vec{h}\vec{\sigma},\vec{P}\vec{\sigma}\right] \tag{8.35}$$

Using the algebra of Pauli matrices

$$\frac{d}{dt}\vec{P}=-i\vec{h}\times\vec{P} \tag{8.36}$$

This equation is a 3×3 differential equation, and could be written in explicit form

$$\frac{d}{dt}\begin{pmatrix}P_1\\ P_2\\ P_3\end{pmatrix}=-i\begin{pmatrix}0 & h_3 & -h_2\\ -h_3 & 0 & h_1\\ h_2 & -h_1 & 0\end{pmatrix}\begin{pmatrix}P_1\\ P_2\\ P_3\end{pmatrix}=-i\Omega\begin{pmatrix}P_1\\ P_2\\ P_3\end{pmatrix} \tag{8.37}$$

If the interaction is time independent, the solution could be expressed in terms of the exponential

$$P\left(t\right)=\exp\left\{-i\Omega t\right\}P\left(0\right) \tag{8.38}$$

The 3×3 matrix has the special structure

$$\Omega=h_1L_1+h_2L_2+h_3L_3 \tag{8.39}$$

If

$$\vec{h} = \vec{h}_0 = -\omega \vec{e}_z \tag{8.40}$$

The corresponding matrix is

$$\Omega = -i \begin{pmatrix} 0 & -\omega & 0 \\ \omega & 0 & 0 \\ 0 & 0 & 0 \end{pmatrix} = -i\omega L_z \tag{8.41}$$

the evolution is given by

$$P(t) = e^{-it\omega L_z} P(0) = \begin{pmatrix} \cos\omega t & \sin\omega t & 0 \\ -\sin\omega t & \cos\omega t & 0 \\ 0 & 0 & 1 \end{pmatrix} \begin{pmatrix} P_1(0) \\ P_2(0) \\ P_3(0) \end{pmatrix} \tag{8.42}$$

which is nothing else but the Larmor precession, rotation with angular velocity "–ω"

Interaction representation

$$\frac{d}{dt} \begin{pmatrix} P_1 \\ P_2 \\ P_3 \end{pmatrix} = -i \begin{pmatrix} 0 & h_3 & -h_2 \\ -h_3 & 0 & h_1 \\ h_2 & -h_1 & 0 \end{pmatrix} \begin{pmatrix} P_1 \\ P_2 \\ P_3 \end{pmatrix} = -i\Omega \begin{pmatrix} P_1 \\ P_2 \\ P_3 \end{pmatrix} \tag{8.43}$$

In the MRI case the interaction is given by the sum of terms describing interaction with main static magnetic field, interaction with a small fluctuating magnetic field

$$\vec{h} = -\omega \vec{e}_z + \vec{f}(t) \quad \Omega = -i\omega L_z + iF(t) \tag{8.44}$$

The solution is of the general form

$$P(t) = e^{-i\omega t L_z} I(t) \tag{8.45}$$

$$\frac{d}{dt} I(t) = i e^{i\omega t L_z} F(t) e^{-i\omega t L_z} I(t) = i F^I(t) I(t) \tag{8.46}$$

This equation has, now, a small random driving term. A second order integral equation can be written

$$I(t) = I(0) + i\int_0^t dt' F^I(t') I(0) - \int_0^t dt' F^I(t') \int_0^{t'} dt'' F^I(t'') I(t'') \tag{8.47}$$

After the average over fluctuations is performed

$$\langle I(t) \rangle = \langle I(0) \rangle + i\int_0^t dt' \langle F^I(t') I(0) \rangle - \int_0^t dt' \int_0^{t'} dt'' \langle F^I(t') F^I(t'') I(t'') \rangle \tag{8.48}$$

Using the standard assumptions about the fluctuations

$$\frac{d}{dt}\langle I(t) \rangle = -\int_0^t dt'' \langle F^I(t) F^I(t'') I(t) \rangle \tag{8.49}$$

Going back to the original variable, the polarization vector, P

$$\frac{d}{dt}\langle P(t) \rangle = -i\omega L_z \langle P(t) \rangle - \int_0^t dt'' \langle F(t) e^{i\omega(t''-t)L_z} F(t'') e^{-i\omega(t''-t)L_z} P(t) \rangle \tag{8.50}$$

After a change of variables

$$\frac{d}{dt}\langle P(t) \rangle = -i\omega L_z \langle P(t) \rangle - \int_0^t d\tau L_\alpha e^{-i\omega\tau L_z} L_\beta e^{i\omega\tau L_z} \langle f_\alpha(t) f_\beta(t-\tau) P(t) \rangle \tag{8.51}$$

Semiclassical theory of relaxation together with short-history assumption is obtained in three steps:

$$\frac{d}{dt}\langle P(t) \rangle = -i\omega L_z \langle P(t) \rangle - \int_0^t d\tau L_\alpha e^{-i\omega\tau L_z} L_\beta e^{i\omega\tau L_z} \langle f_\alpha(t) f_\beta(t-\tau) P(t) \rangle$$

$$\frac{d}{dt}\langle P(t) \rangle = -i\omega L_z \langle P(t) \rangle - \int_0^t d\tau L_\alpha e^{-i\omega\tau L_z} L_\alpha e^{i\omega\tau L_z} \langle f_\alpha(0) f_\alpha(\tau) \rangle \langle P(t) \rangle \tag{8.52}$$

$$\frac{d}{dt}\langle P(t) \rangle = -i\omega L_z \langle P(t) \rangle \underbrace{- \int_0^\infty d\tau L_\alpha e^{-i\omega\tau L_z} L_\alpha e^{i\omega\tau L_z} \langle f_\alpha(0) f_\alpha(\tau) \rangle}_{\text{Semi-classical Relaxation Matrix}} \langle P(t) \rangle$$

Finally, the evolution of the polarization is given by the vectorial equation, the master equation for spin 1/2

$$\frac{d}{dt}\langle P(t)\rangle = -(i\omega L_z + R)\langle P(t)\rangle \tag{8.53}$$

As a remedy of lack of approach to equilibrium, the existence of thermal equilibrium is imposed by modifying the master equation

$$\frac{d}{dt}\langle P(t)\rangle = -i\omega L_z \langle P(t)\rangle - R\left(\langle P(t)\rangle - \langle P\rangle_{eq}\right) \tag{8.54}$$

BIBLIOGRAPHY

1. Fano, U., *Description of States in Quantum Mechanics by Density Matrix and Operator Techniques.* Rev. Mod. Phys., 1957. **29**(1): p. 74-93.
2. Primas, v.H., *Eine verllagemeinerte Storrungstheorie fur quantenmechanische Mehrteilchenprobleme.* Helv. Phys. Acta, 1960. **34**: p. 330-351.
3. Loan, C.V., *The Ubiquitous Kronecker product*. J. Comp. Appl. Math., 2000. **123**: p. 85-100.
4. Mukamel, S.U., *Superoperator representation of nonlinear response: Unifying quantum field and mode coupling theories.* Phys. Rev. E, 2003. **68**(2): p. 1-60.
5. Baranger, M., *Simplified quantum-mechanical theory of pressure broadening.* Phys. Rev., 1958. **111**(2): p. 481-493.
6. Gabriel, H., *Theory of the Influence of Environment on the Angular Distribution of Nuclear Radiation.* Phys. Rev., 1969. **181**(2): p. 506-521.
7. Hioe, F.T., *Analytic solutions of density-matrix evolutions with the use of Racah tensorial decompositions.* Phys. Rev. A, 1984. **30**(6): p. 3097-3106.
8. Ben-Reuven, A., *Symmetry considerations in pressure-broadening theory.* Phys. Rev., 1966. **141**(1): p. 34-40.
9. Slichter, C.P., *Principles of magnetic resonance*. 3 ed. Springer Series in Solid State Sciences. 1996: Springer. 655.
10. Hubbard, P., *Nonexponential nuclear magnetic relaxation by quadrupole interactions.* J Chem Phys, 1970. **53**: p. 985-987.
11. Woessner, D. and N. Bansal, *Temporal characteristics of NMR signals from spin 3/2 nuclei of incompletely disordered systems.* J Magn Res, 1998. **133**: p. 21-35.
12. Bowden, G.J., W.D. Hutchinson, and J. Khachan, *Tensor operator formalism for multiple-quantum NMR. Spins 3/2, 2 and 5/2 and general I.* J. Magn. Res., 1986. **67**: p. 415-437.
13. Freed, D.E., M.D. Hurlimann, and U.M.U.-h.w.s.c.s.a.B.W.-W.B.-V.f.b.f.f.f.b.a.d. Scheven, *The equivalence between off-resonance and on-resonance pulse sequences and its application to steady-state free precession with diffusion in inhomogeneous fields.* Journal Of Magnetic Resonance (San Diego, Calif.: 1997), 2003. **162**(2): p. 328-335.
14. Balucani, U., M. Howard Lee, and V.U.--. Tognetti, *Dynamical correlations.* Physics Reports, 2003. **373**(6): p. 409-492.
15. Cao, J., *A phase-space study of Bloch-Redfield theory.* J. Chem. Phys., 1997. **107**(8): p. 3204.
16. Royer, A., *Combining projection superoperators and cumulant expansions in open quantum dynamics with initial correlations and fluctuating Hamiltonians and environments.* Physics Letters A, 2003. **315**(5): p. 335-351.

17. Redfield, A.G., *On the Theory of Relaxation Processes.* IBM Journal of Research and Development, 1957. **1**: p. 19-31.
18. Hubbard, P.S., *Quantum-Mechanical and Semiclassical Forms of the Density Operator Theory of Relaxation.* Rev. Mod. Phys., 1961. **33**(2): p. 249-264.
19. Van Kampen, N.G., *A cumulant expansion for stochastic linear differential equations. I.* Physica, 1974. **74**(2): p. 215-238.
20. Van Kampen, N.G., *A cumulant expansion for stochastic linear differential equations. II.* Physica, 1974. **74**(2): p. 239-247.
21. Hubbard, P., *Some Properties of Correlation Functions of Irreducible Tensor Operators.* Phys Rev, 1970. **180**(1): p. 319-326.
22. Dinesen, T.R.J. and S.B. C., *Relaxation of anisotropically oriented I=3/2 nuclei in multipole basis: Evolution of second rank tensors in the double quantum filtered nuclear magnetic resonance experiment.* J Chem Phys, 1994. **101**(9): p. 7372-7380.
23. Smith S. A., Palke W. E., and G.J. T., *Superoperator Propagators in Simulations of NMR Spectra.* Journal of Magnetic Resonance, Series A, 1994. **106**(1): p. 57-64.
24. Bodenhausen, G., H. Kogler, and R.R. Ernst, *Selection of Coherence-Transfer Pathways in NMR Pulse Experiments.* J. Magn. Reson., 1984. **58**(3): p. 370-388.
25. Kim, M. and S. Lee, *Spin Echoes after Arbitrary N Pulses.* Journal of Magnetic Resonance, 1997. **125**(1): p. 114-119.
26. Brown, S.P. and S. Wimperis, *NMR measurement of spin-3/2 transverse relaxation in an inhomogeneous B1 field.* Chemical Physics Letters, 1994. **224**(5-6): p. 508-516.
27. Bansal, N., *et al.*, *In vivo Na-23 MR Imaging and Spectroscopy of Rat Brain during TMDOTP5- Infusion.* J Magn Reson Imaging, 1992. **2**: p. 385-391.
28. Schepkin, V.D., *et al.*, *Sodium TQF NMR and intracellular sodium in isolated crystalloid perfused rat heart.* Magn Reson Med, 1998. **39**(4): p. 557-63.
29. Hancu, I., F.E. Boada, and G.X. Shen, *Three-dimensional triple-quantum-filtered Na imaging of in vivo human brain.* Magnetic Resonance in Medicine, 1999. **42**(6): p. 1146-1154.
30. Reddy, R., *et al.*, *Multiple-Quantum Filters of Spin-3/2 with Pulses of Arbitrary Flip Angle.* J. Magn. Res. Series B, 1994. **104**: p. 148-152.
31. Hancu, I., *et al. In vivo single and triple quantum filtered ^{23}Na MRI of brain neoplasms*. in *8-th Sci Meeting ISMRM*. 2000. Denver.
32. Tanase, C. and F. Boada. *Robust measurement of spin 3/2 transverse relaxation in the presence of both B_0 and B_1 inhomogeneities*. in *Experimental Nuclear Magnetic Resonance Conference*. 2004. Asilomar, USA.
33. Tanase, C. and F. Boada, *Algebraic description of spin 3/2 dynamics in NMR experiments (in publishing).* J Magn Res, 2004.
34. Keifer, P.A., *90 Pulse Width Calibrations: How to Read a Pulse Width Array.* Concepts in Magnetic Resonance, 1999. **11**(3): p. 165-180.
35. Boada, F.E., *et al.*, *Fast three dimensional sodium imaging.* Magnetic Resonance in Medicine, 1997. **37**(5): p. 706-715.
1. Lauterbur, P.C., *Image Formation by Induced Local Interactions: Examples Employing Nuclear Magnetic Resonance.* Nature, 1973. **242**: p. 190-191.
2. Fano, U., *Description of States in Quantum Mechanics by Density Matrix and Operator Techniques.* Rev. Mod. Phys., 1957. **29**(1): p. 74-93.

3. Primas, v.H., *Eine verllagemeinerte Storrungstheorie fur quantenmechanische Mehrteilchenprobleme.* Helv. Phys. Acta, 1960. **34**: p. 330-351.
4. Loan, C.V., *The Ubiquitous Kronecker product*. J. Comp. Appl. Math., 2000. **123**: p. 85-100.
5. Mukamel, S.U., *Superoperator representation of nonlinear response: Unifying quantum field and mode coupling theories.* Phys. Rev. E, 2003. **68**(2): p. 1-60.
6. Baranger, M., *Simplified quantum-mechanical theory of pressure broadening.* Phys. Rev., 1958. **111**(2): p. 481-493.
7. Gabriel, H., *Theory of the Influence of Environment on the Angular Distribution of Nuclear Radiation.* Phys. Rev., 1969. **181**(2): p. 506-521.
8. Hioe, F.T., *Analytic solutions of density-matrix evolutions with the use of Racah tensorial decompositions.* Phys. Rev. A, 1984. **30**(6): p. 3097-3106.
9. Ben-Reuven, A., *Symmetry considerations in pressure-broadening theory.* Phys. Rev., 1966. **141**(1): p. 34-40.
10. Slichter, C.P., *Principles of magnetic resonance*. 3 ed. Springer Series in Solid State Sciences. 1996: Springer. 655.
11. Hubbard, P., *Nonexponential nuclear magnetic relaxation by quadrupole interactions.* J Chem Phys, 1970. **53**: p. 985-987.
12. Woessner, D. and N. Bansal, *Temporal characteristics of NMR signals from spin 3/2 nuclei of incompletely disordered systems.* J Magn Res, 1998. **133**: p. 21-35.
13. Bowden, G.J., W.D. Hutchinson, and J. Khachan, *Tensor operator formalism for multiple-quantum NMR. Spins 3/2, 2 and 5/2 and general I.* J. Magn. Res., 1986. **67**: p. 415-437.
14. Freed, D.E., M.D. Hurlimann, and U.M.U.-h.w.s.c.s.a.B.W.-W.B.-V.f.b.f.f.f.b.a.d. Scheven, *The equivalence between off-resonance and on-resonance pulse sequences and its application to steady-state free precession with diffusion in inhomogeneous fields.* Journal Of Magnetic Resonance (San Diego, Calif.: 1997), 2003. **162**(2): p. 328-335.
15. Balucani, U., M. Howard Lee, and V.U.--. Tognetti, *Dynamical correlations.* Physics Reports, 2003. **373**(6): p. 409-492.
16. Cao, J., *A phase-space study of Bloch-Redfield theory.* J. Chem. Phys., 1997. **107**(8): p. 3204.
17. Royer, A., *Combining projection superoperators and cumulant expansions in open quantum dynamics with initial correlations and fluctuating Hamiltonians and environments.* Physics Letters A, 2003. **315**(5): p. 335-351.
18. Redfield, A.G., *On the Theory of Relaxation Processes.* IBM Journal of Research and Development, 1957. **1**: p. 19-31.
19. Hubbard, P.S., *Quantum-Mechanical and Semiclassical Forms of the Density Operator Theory of Relaxation.* Rev. Mod. Phys., 1961. **33**(2): p. 249-264.
20. Van Kampen, N.G., *A cumulant expansion for stochastic linear differential equations. I.* Physica, 1974. **74**(2): p. 215-238.
21. Van Kampen, N.G., *A cumulant expansion for stochastic linear differential equations. II.* Physica, 1974. **74**(2): p. 239-247.
22. Hubbard, P., *Some Properties of Correlation Functions of Irreducible Tensor Operators.* Phys Rev, 1970. **180**(1): p. 319-326.

23. Dinesen, T.R.J. and S.B. C., *Relaxation of anisotropically oriented I=3/2 nuclei in multipole basis: Evolution of second rank tensors in the double quantum filtered nuclear magnetic resonance experiment.* J Chem Phys, 1994. **101**(9): p. 7372-7380.
24. Smith S. A., Palke W. E., and G.J. T., *Superoperator Propagators in Simulations of NMR Spectra.* Journal of Magnetic Resonance, Series A, 1994. **106**(1): p. 57-64.
25. Bodenhausen, G., H. Kogler, and R.R. Ernst, *Selection of Coherence-Transfer Pathways in NMR Pulse Experiments.* J. Magn. Reson., 1984. **58**(3): p. 370-388.
26. Kim, M. and S. Lee, *Spin Echoes after Arbitrary N Pulses.* Journal of Magnetic Resonance, 1997. **125**(1): p. 114-119.
27. Brown, S.P. and S. Wimperis, *NMR measurement of spin-3/2 transverse relaxation in an inhomogeneous B1 field.* Chemical Physics Letters, 1994. **224**(5-6): p. 508-516.
28. Lindon, J.C. and A.G. Ferrige, *Digitisation and data processing in Fourier transform NMR.* Progress in Nuclear Magnetic Resonance Spectroscopy, 1980. **14**(1): p. 27-66.
29. Bansal, N., *et al.*, *In vivo Na-23 MR Imaging and Spectroscopy of Rat Brain during TMDOTP5- Infusion.* J Magn Reson Imaging, 1992. **2**: p. 385-391.
30. Schepkin, V.D., *et al.*, *Sodium TQF NMR and intracellular sodium in isolated crystalloid perfused rat heart.* Magn Reson Med, 1998. **39**(4): p. 557-63.
31. Hancu, I., F.E. Boada, and G.X. Shen, *Three-dimensional triple-quantum-filtered Na imaging of in vivo human brain.* Magnetic Resonance in Medicine, 1999. **42**(6): p. 1146-1154.
32. Reddy, R., *et al.*, *Multiple-Quantum Filters of Spin-3/2 with Pulses of Arbitrary Flip Angle.* J. Magn. Res. Series B, 1994. **104**: p. 148-152.
33. Hancu, I., *et al. In vivo single and triple quantum filtered ^{23}Na MRI of brain neoplasms*. in *8-th Sci Meeting ISMRM*. 2000. Denver.
34. Tanase, C. and F. Boada. *Robust measurement of spin 3/2 transverse relaxation in the presence of both B_0 and B_1 inhomogeneities*. in *Experimental Nuclear Magnetic Resonance Conference*. 2004. Asilomar, USA.
35. Tanase, C. and F. Boada, *Algebraic description of spin 3/2 dynamics in NMR experiments (in publishing).* J Magn Res, 2004.
36. Keifer, P.A., *90 Pulse Width Calibrations: How to Read a Pulse Width Array.* Concepts in Magnetic Resonance, 1999. **11**(3): p. 165-180.